

DISS. ETH NO. 25893

Soft-Sensing, Automation, and Diagnosis for Nitrification

A thesis submitted to attain the degree of
DOCTOR OF SCIENCES of ETH ZURICH

presented by

CHRISTIAN MARC THÜRLIMANN

MSc ETH in Environmental Engineering

born January 24th 1987

citizen of Häggenschwil (SG) and Wuppenau (TG)

accepted on the recommendation of
Prof. Dr. Eberhard Morgenroth, examiner
Prof. Dr. Bengt Carlsson, co-examiner
Prof. Dr. Kai Udert, co-examiner
Dr. Kris Villez, co-examiner

2019

**You can have data without information,
but you cannot have information without data.**

Daniel Keys Moran

Abstract

Nitrification of wastewater requires control for the purposes of efficiency and of stability. However, first, the highly complex microbial community in wastewater treatment plants and very different compositions of wastewaters impede a complete understanding of nitrification. Second, the determination of the states of the process is seldom exact because sensors are subject to a high level of wear and tear. Consequently, instrumentation, control, and automation (ICA) of nitrification processes are a challenge. I hypothesize that soft-sensors - based on the signals of robust, physical sensors - and specially designed control loops, which do not need redundant information to correct for drift, can reduce the maintenance needs for the control of nitrification. Consequently, the economical application range for ICA of nitrification processes can be extended.

A large part of this thesis is dedicated to the stabilisation of urine nitrification as a pre-treatment for nutrient recovery. To this end, an online nitrite detection and an according control of the process are required. Furthermore, the thesis comprises an ammonia aeration controller, which is based on pH signals, to be used in municipal wastewater. The four chapters of the thesis focus on the following topics.

The first chapter investigates calibration experiments for in-line UV-Vis sensors. Such sensors can serve as soft-sensors for numerous substances. With differently designed experiments, data for the calibration of UV-Vis based nitrite models in high strength wastewater was recorded. Online experiments executed in-situ allow calibrating similarly exact models like experiments which are conducted by spiking additional nitrite. The good performance of the models being based on online experiments is explained by the correlation of other light-absorbing substances in the process with nitrite.

The second chapter evaluates the potential of a stoichiometry-based soft-sensor for nitrite. The stoichiometry of nitrification theoretically allows distinguishing the ammonia and the nitrite oxidation rates by means of the derivatives of the dissolved oxygen and of the pH signal and in turn detecting nitrite accumulations. We show that under relatively ideal conditions the dynamics in the ratio of the two derivatives show similarities with the dynamics in the nitrite concentration. Factors that deteriorate this information quality are identified.

The third part of this thesis investigates how drifting sensor signals can be used as an input for a feedback controller without relying on redundant information to correct this

drift. The controller shall prevent uncontrolled nitrite accumulation in a urine nitrification system. To this end, the controller does not use the absolute value of the nitrite signal, but its 1st and 2nd derivative as inputs. By controlled accumulation and degradation of nitrite, the controller can keep the derivatives continuously informative. The switch from substrate inhibition to substrate limitation of the nitrite oxidising bacteria can be identified by means of the inflection point in the signal. The developed controller is tested successfully on a lab-scale reactor.

The fourth chapter of this thesis describes an ammonia based aeration controller. These controllers usually require maintenance intensive instrumentation. Therefore a new ammonia soft sensor for continuously operated municipal wastewater treatment plants is developed. It relies on the 1st derivative of a pH difference measured over the aerated zone. This soft sensor is successfully tested in a controller deployed on various municipal wastewater treatment plants. The controller was designed to increase its robustness towards drift in the pH signals.

Zusammenfassung

Für die Nitrifikation von Abwässern ist aus Effizienz- und Stabilitätsgründen eine automatisierte Regelung notwendig. Jedoch erschweren erstens die hohe Komplexität des Nitrifikations-Prozesses und die verschiedensten Abwassertypen das Prozessverständnis. Zweitens ist die Erhebung des Prozesszustands mittels Sensoren wegen deren hohen Verschleiss im Abwasser selten exakt. Folglich ist die Anwendung von Regelungs- und Messtechnik in Nitrifikationsreaktoren erschwert. Die Hypothese dieser Dissertation ist, dass virtuelle Sensoren basierend auf Signalen von robusten physischen Sensoren und speziell ausgelegte Regler, welche keine redundanten Informationen zur Korrektur von Drift in den Signalen benötigen, den Wartungsaufwand für die Messtechnik im Regelkreis reduzieren können. Dies erweitert den ökonomischen Anwendungsbereich von Regelungstechnik.

Der Fokus meiner Dissertation liegt auf der Stabilisierung der Urinnitrifikation als vorbehandelnder Schritt für die Nährstoffrückgewinnung. Zu diesem Zweck wird eine online Detektion des Nitrits benötigt, welche dann als Eingangssignal für einen Regler dient. Des Weiteren wird ein Ammoniumregler für kommunales Abwasser basierend auf pH Signalen präsentiert.

Im ersten Teil der Arbeit werden Kalibrationsexperimente für In-Line UV-Vis Sonden untersucht. Solche Sensoren können als virtuelle Sensoren (Softsensoren) für unzählige Substanzen dienen. Mit verschiedenen Versuchsanordnungen wurden Daten für ein UV-Vis basierendes Nitritmodell in hochbelastetem Abwasser (nitrifizierter Urin) erhoben. Direkt im Prozess durchgeführte Online-Experimente erlauben es ähnlich exakte Modelle zu kalibrieren, wie dies bei Experimenten mit künstlicher Zugabe von Nitrit möglich ist. Die gute Leistung, der auf Online-Experimenten basierenden Modellen kann unter anderem durch die Korrelation von Nitrit mit anderen absorbierenden Substanzen in den Online-Experimenten erklärt werden.

Im zweiten Teil der Arbeit wird das Potential eines stöchiometrischen Softsensors für Nitrit untersucht. Die Stöchiometrie der Nitrifikation erlaubt es theoretisch mittels Ableitungen des Sauerstoffkonzentrations-Signals und des pH-Signals die Ammonium- und die Nitritoxidationsraten zu trennen und somit Nitrit zu detektieren. Wir zeigen, dass unter einer relativ idealen Versuchsanordnungen die Dynamik des Verhältnisses der beiden Ableitungen Ähnlichkeit mit der Nitritkonzentrations-Dynamik aufweist. Faktoren welche die Informationsqualität verringern, werden identifiziert.

Der dritte Teil der Arbeit untersucht wie man driftende Signale als Eingangssignal für Regler verwenden kann, ohne redundante Informationen für dessen Korrektur zu verwenden. Der Regler soll unkontrollierte Nitritakkumulationen in der Urinnitrifikation verhindern. Der Regler nutzt statt des absoluten Werts des Nitritsignals als Eingangssignal dessen 1. und 2. Ableitungen. Durch die gezielte Akkumulation und den Abbau von Nitrit durch den Regler bleiben die Ableitungen des Signals informativ. Der Übergang der nitritoxidierenden Bakterien von Substrathemmung zu Substratlimitierung kann auf Grund von Wendepunkten im Signal identifiziert werden. Der Regler wurde erfolgreich auf einem Laborreaktor getestet.

Das vierte Kapitel der Arbeit beschreibt einen Ammoniumregler, welcher die Belüftungsintensität anhand der Ammoniumkonzentration optimiert. Solche Regler benötigen normalerweise wartungsintensive Sensoren. Deshalb wird ein neuer virtueller Ammoniumsensor für kontinuierlich bewirtschaftete Reaktoren entwickelt. Der Regler basiert auf der 1. Ableitung einer pH-Differenz, welche in der belüfteten Zone gemessen wird. Der Regler ist so konzipiert, dass er Drift in den pH-Signalen toleriert. Er ist auf mehreren kommunalen Kläranlagen erfolgreich getestet.

Acknowledgments

The time of a PhD is an enlightening, troublesome, and joyful process. Great support is inevitable to manage all the tasks, successes and fails, and emotions. Therefore, this page is meant to thank all of you, who contributed to this piece of work.

First of all, I would like to thank my supervisor Kris Villez. He has an impressive, very strategic view on all problems, or as he would say challenges, and he taught me how to think about the relevant questions. The inspiring, structured and unstructured discussions with Kris, and his inputs were very expedient and motivating. I thank him for all his confidence in me.

I am also very grateful to my supervising professor, Eberhard Morgenroth for his guiding advice, his constructive critique and his feedback - from the overall, strategic level down to important details. Being part of Eberhard's group during my years at the Eawag was a great opportunity to interact with others, to stay open-minded and to think about problems outside of my thesis.

I also want to thank Kai Udert who gave me a lot of advice and input from the "yellow" side. His motivating personality inspired me with lot of ideas.

I am also thankful to my external co-examiner Bengt Carlsson for critically reviewing this thesis.

A special thanks goes to Kito Ohmura. He was a big help when it came to my experiments and running my reactor.

My research did not only involve fruitful discussions and data interpretation. Behind the scenes, a lot of brainpower, software, and hardware was involved: Thank you Adriano, Richi, and Marco for the big effort you put into helping me to set-up my reactor and keeping it running all these years. I am also very grateful to our lab technicians Claudia, Karin, and Sylvia for the analysis of my samples. Thanks also to the master students, who conducted research for me, Benjamin, Qie, and Katja.

Furthermore, I want to thank the UWE and VUNA team for the numerous reunions and seminars, in which I learned a lot about all kind of urine treatment, modelling, data processing and science in general.

A big thank you goes to all former and current PhDs in the ENG department; namely Hampi, Alexandra, Johny, Basil, Michele, Ann-Kathrin, Peter, Jonas, Angelika, Isabel, Manu, Wenzel, Damian, and Bruno for being at the same time such a diverse but unified

group. I will miss the conversations and discussions about serious and less serious subjects and the many fun events we had after our seminars. Discussing less research-relevant subjects was also the idea of the LMPFC lunch group: Thank you Lena, Mariane, Philipp, and Fridolin for the fun. I also want to thank the SWW PhD students Omar, Dorothee, Matthew, Natalia, and Sven for being good companions. I want to thank my numerous former and current office colleagues from the BU-C12. Marco, Chris, Luis, Theresa, Valentin, Matthew, Philipp, Antoine, and Andrea, you all made my office space a very pleasant and green place.

Moreover, I want to thank my friends Mischa, Stego, Pascal, Mätti, Ueli, Stephan, and Christoph for all the city trips, board games, sailing hours, hiking trips and bike tours we did.

I am also thankful to my parents and my sister and brother for giving me moral support, for having interest in the work I do and for taking such good care of my daughter Anouk in times of need. A thank you to my parents-in-law for all the hours of babysitting when I was busy finishing this piece of work.

Finally, I want to thank my wife Sabrina and my daughter Anouk for the immense mental and hands-on support they gave me during my PhD. Without the numerous encouraging words from Sabrina, the so relaxing and cheerful personality of Anouk, I might have not come to the point of writing these lines. I love you!

Publications

The following publications are included in this thesis:

- Thürlimann, C.M., Dürrenmatt, D.J., Villez, K., 2018 Soft-sensing with qualitative trend analysis for wastewater treatment plant control. *Control Engineering Practice* 70, 121–133.
- Thürlimann, C.M., Udert, K.M., Morgenroth, E., Villez, K., submitted, Comparison of four methods to obtain calibration data for online nitrite estimation by means of in-line UV-Vis spectrophotometry.
- Thürlimann, C.M., Udert, K.M., Morgenroth, E., Villez, K., submitted, Stabilizing control of a urine nitrification process in the presence of sensor drift.

The following conference abstracts are part of my PhD research and partly covered by this thesis:

- Mašić, A., Santos, A.T.L., Hess, A., Thürlimann, C.M., Etter, B., Udert, K.M., Villez, K., 2015. Nitrite estimation in nitrified urine by UV spectroscopy of weak nitrite/nitrate absorbance peaks, Presented at the 9th IWA Symposium on Systems Analysis and Integrated Assessment, Gold Coast, Australia.
- Mašić, A., Santos, A.T.L., Hess, A., Thürlimann, C.M., Etter, B., Udert, K.M., Villez, K., 2015. Estimation of nitrite concentration in a urine nitrification reactor by means of UV spectrophotometry, Presented at the IWA Nutrient Removal and Recovery Conference (NRR2015), Gdansk, Poland.
- Thürlimann, C.M., Dürrenmatt, D.J., Villez, K., 2015. Evaluation of Qualitative Trend Analysis as a Tool for Automation, in: *Computer Aided Chemical Engineering*. Presented at the 12th International Symposium on Process Systems Engineering and 25th European Symposium on Computer Aided Process Engineering, Elsevier, pp. 2531–2536.
- Thürlimann, C.M., Dürrenmatt, D.J., Villez, K., 2015. Qualitative Trend Analysis for pH based soft-sensing of ammonia in full scale continuous WWTPs. Presented at the 2nd IWA New Developments in IT & Water conference, Rotterdam, The Netherlands.

- Thürlimann, C.M., Villez, K., 2016. In-situ nitrite sensing in a urine nitrification reactor by means of UV-Vis spectrometry. Presented at the WEF/IWA Nutrient Removal and Recovery (NRR2016), Denver, USA.
- Thürlimann, C.M., Udert, K.M., Morgenroth, E., Villez, K., 2016. Nitrite sensing in urine nitrification reactor with in-situ UV-Vis spectrometry. Presented at the 3rd IWA New Developments in IT & Water conference, Telford, UK.
- Thürlimann, C.M., Udert, K.M., Morgenroth, E., Villez, K., 2017. Qualitative control for stable and efficient urine nitrification. Presented at the 12th IWA Specialized Conference on Instrumentation, Control and Automation (ICA2017), Quebec City, QC, Canada, pp. 287–290.
- Thürlimann, C.M., Udert, K.M., Morgenroth, E., Villez, K., 2018. Assessment of two qualitative trend analysis tools for process control. Presented at the 4th IWA Specialized International Conference “Ecotechnologies for Wastewater Treatment” (EcoSTP2018), London, ON, Canada.

The following publication and the following preprint are part of the research I conducted at Eawag in Dübendorf. However, they are not part of this thesis.

- Thürlimann, C.M., Dürrenmatt, D.J, Villez, K., 2015. Energy and process data processing and visualisation for optimising wastewater treatment plants. *Water Practice and Technology*, 10(1), 10-18.
- Thürlimann, C.M., Villez, K., 2017. Input estimation as a qualitative trend analysis problem. *Computers & Chemical Engineering*, 107, 333-342.
- Derlon, N., Thürlimann, C., Dürrenmatt, D., Villez, K., 2017. Batch settling curve registration via image data modeling, *Water Research*, 114, 327-337,
- Ohmura, K., Thürlimann, C.M., Kipf, M., Carbajal, J.P., Villez, K., 2018. Characterizing Long-term Wear and Tear of Ion-Selective pH Sensors [Preprint WWW Document]. doi:10.31224/osf.io/mv6tz¹

¹ At the time of submitting this thesis this preprint has also been submitted to a journal.

Contents

I	Introduction	1
II	Research Papers	21
1	UV-Vis Calibration	23
1.1	Introduction	24
1.2	Material and Methods	25
1.2.1	Measurement principle of UV-Vis spectrophotometers	25
1.2.2	Reactor setup and operation	27
1.2.3	General experimental design	28
1.2.4	Modelling	33
1.3	Results	36
1.3.1	Model calibration and linear design correction results	36
1.3.2	Model test results	36
1.3.3	Intermediate conclusions	38
1.3.4	Detailed inspections	39
1.4	Discussion	42
1.4.1	Influence of solids and visible wavelength range	42
1.4.2	In-situ calibration performance	42
1.4.3	Bias reduction by linear correction	43
1.5	Conclusions	44
2	Oxygen uptake rate and proton production rate in urine nitrification: What do they tell us about nitrite concentrations?	45
2.1	Introduction	46
2.2	Material and methods	48
2.2.1	Reactor setup and operation	48
2.2.2	Experimental design	49
2.2.3	Theoretical steady state calculations	49

2.2.4	From pH to proton concentration	49
2.2.5	Rate calculations	50
2.3	Results	50
2.3.1	Relation between OURs of AOB, NOB, and HET	50
2.3.2	Relation of theoretical AOB PPR and measured PPR	52
2.3.3	Experimental Data	52
2.3.4	AOB driven nitrite dynamics	54
2.4	Discussion	56
2.4.1	Theoretical OUR fractions	56
2.4.2	Empirical relation of PPR2OUR with nitrite	57
2.4.3	PPR2OUR dependency on temperature and pH	57
2.4.4	Further analysis	57
2.5	Conclusion	58

3 Stabilising control of a urine nitrification process in the presence of sensor drift **59**

3.1	Introduction	60
3.2	Material and Methods	61
3.2.1	Conceptual model of the control problem	61
3.2.2	Basic Reactor set-up and operation	62
3.2.3	Stabilizing Nitrite Control	63
3.2.4	Identification of inflection point	65
3.2.5	Controller design	68
3.2.6	Unmeasured process disturbances	69
3.3	Results	70
3.3.1	Control behaviour	70
3.3.2	Controller performance	72
3.3.3	Unmeasured process disturbances	74
3.4	Discussion	76
3.4.1	General controller performance	76
3.4.2	Unmeasured Disturbances	76
3.4.3	Extension of controller	77
3.4.4	Linking to control theory	78
3.5	Conclusion	78

4	Soft-sensing with qualitative trend analysis for control in full-scale wastewater treatment plants	81
4.1	Introduction	82
4.2	Material and Methods	85
4.2.1	Work flow summary	85
4.2.2	Qualitative State Estimation algorithm	85
4.2.3	Hardware and Control strategy	89
4.2.4	Controller performance monitoring	94
4.2.5	Wastewater treatment plant characteristics	94
4.2.6	Oxygen slave controller	97
4.3	Results	97
4.3.1	Demonstration of Qualitative State Estimation algorithm	97
4.3.2	Demonstration of the control strategy	99
4.3.3	Performance evaluation	101
4.4	Discussion	102
4.4.1	Data sources	103
4.4.2	Kernel regression and hidden Markov model	103
4.4.3	Qualitative information	103
4.4.4	Implementation and fine-tuning	104
4.4.5	Energy savings and maintenance effort	104
4.4.6	Treatment technologies	105
4.4.7	Future work	105
4.5	Conclusion	106
III	Conclusions and Outlook	109
IV	Appendices	115
A	Appendix Chapter 1: UV-Vis Calibration	117
A.1	Mean squared error of cross-validation runs	118
B	Appendix: Chapter 2: Nitrite soft sensor based on OUR and PPR	123
B.1	Proton concentration and alkalinity consumption in a urine nitrification batch	124

C Appendix Chapter 3: Stabilizing nitrite control	125
C.1 Source-separated urine feed. Tank timeline, ammonium and chemical oxygen demand concentration.	126
D Appendix Chapter 4: Ammonia aeration control	127
D.1 Legal thresholds regarding nitrogen species	128
D.2 Dissolved oxygen setpoints ARA Hard	129
D.3 Parameter set for rule-based control and QSE at the three tested plants . .	130
D.4 Summary of routine lab analysis and hydraulic loading during controller test periods (n=26) and during reference periods (n=15)	131
D.5 Additional figures	134
V Bibliography	137
VI Curriculum Vitae	153

List of Figures

1.1	Schematic relations of species and their absorbance and measurements in nitrified urine	26
1.2	Overview of the generated data sets	29
1.3	Model calibration and model test procedure	35
1.4	Root mean squared error of model prediction	38
1.5	First four principal components of the four models	40
1.6	Residuals of Test 2 predictions with In-situ short-term original model . . .	41
1.7	Nitrite predictions of the nitrite corrected spectra from the-situ ST data .	41
2.1	Theoretical activity of bacteria at different levels of NOB inhibition	51
2.2	Nitrite spiking experiments	54
2.3	Low pH setpoint and net nitrite degradation	55
2.4	High pH setpoint and net nitrite accumulation	56
3.1	Conceptual model of urine nitrification	61
3.2	Control loops	64
3.3	Shape constrained spline model fitting	67
3.4	Schematic time-line of controller	69
3.5	Operational data from one control cycle	71
3.6	Nitrite <i>end of cycle concentrations</i> after identification of inflection point . .	72
3.7	Drift rate, nitrogen species concentrations and hydraulic residence time . .	73
3.8	Temperature high experiment	75
4.1	pH difference and $\text{NH}_4\text{-N}$ concentration	83
4.2	Preprocessing, QSE, control cascade and process response	85
4.3	Hardware setup	89
4.4	Evaluation procedure of the rule-based control	93
4.5	Mean and expected $\pm 3\sigma$ band characterising first derivative's distribution.	98
4.6	Positive derivative sign (upward trend) probability of the signal	98
4.7	Accepted maximum likelihood state of the signal	99
4.8	Rule evaluation and pH difference	100
4.9	Final resulting control decision with ammonia signal as a reference	101
4.10	Ammonia and nitrite concentration measured in 24h composite samples at the WWTP Hard, Winterthur	102

List of Tables

1.1	Experimental design for ex-situ calibration	30
1.2	Presence of variations in the experimental designs	32
1.3	Model characteristics for UV-Vis and UV models	37
2.1	States for three different levels of nitrite concentration	47
2.2	Comparison of calculated PPR with measured PPR	52
3.1	Thirteen primitives defined by the signs of derivatives	66
4.1	Thirteen primitives defined by the signs of derivatives	86
4.2	Pseudo code for Eco state	91
4.3	Pseudo code for Normal state	92
4.4	WWTP characteristics and performance evaluation	96

Acronyms

AOB	Ammonia oxidising bacteria
COD	Chemical oxygen demand
CSTR	Continuous flow stirred tank reactor
DO	Dissolved oxygen
ECC	End of cycle concentrations
EtN	Eco to Normal rules
Ex-Situ wBM	Ex-situ with biomass
Ex-Situ woBM	Ex-situ without biomass
HET	Heterotrophic bacteria
HMM	Hidden Markov model
HRT	Hydraulic retention time
ICA	Instrumentation, control, and automation
ICM	Intercept corrected model
In-Situ LT	In-situ long-term
In-Situ ST	In-situ short-term
ISCM	Intercept and slope corrected model
ISE	Ion selective electrode
LDC	Linear design correction
NOB	Nitrite oxidising bacteria
NtE	Normal to Eco rules
OM	Original model

ORP	Oxidation-reduction potential
OUR	Oxygen uptake rate
PPR	Proton production rate
PPR2OUR	Proton production rate to oxygen uptake rate ratio
QF	Qualitative feature
QPE	Qualitative path estimation
QS	Qualitative state
QSE	Qualitative state estimation
QTA	Qualitative trend analysis
SAC254	Spectral absorption coefficient at 254 nanometer wavelength
SBR	Sequencing batch reactor
SCADA	Supervisory control and data acquisition
SCS	Shape constrained splines
SPM	Spectrophotometer
SRT	Solid retention time
TOC	Total organic carbon
TSS	Total suspended solids
UV	Ultraviolet light
UV-Vis	Ultraviolet and visible light
WWTP	Wastewater treatment plant

Part I

Introduction

Introduction

Why we need wastewater treatment and why we want to control it

Excess of nitrogen and phosphorus in water can lead to algae blooms and hypoxia, which eventually curtails the ecological quality of these waters (Diaz and Rosenberg, 2008). Such quality losses can have severe consequences on economic activities connected with natural waters such as food production, drinking water production or tourism. Hence, nutrient discharge into natural waters should be minimised not only due to ecological but also economic and social reasons. By treating wastewater, one of the most important anthropogenic nitrogen point sources for the aquatic environment can be almost eliminated (Fowler et al., 2013). On a global level, wastewater treatment contributes only little to the total nitrogen turnover in the aquatic environment. In particular, the diffuse sources from agriculture account for the majority of the anthropogenic input. Nevertheless, on a local level, nutrient removal from wastewater can be the major driver to bring aquatic systems back to an oligotrophic state (Petri, 2006).

As any industrial process that is constrained (*i*) to be operated in an economically optimal state and (*ii*) by quality standards, wastewater treatment has a need for instrumentation and control. Moreover, automation plays an important role on wastewater treatment plants (WWTPs). The immense number of signals and actuators as well as the continuous operation of most wastewater treatment plants prohibits a solely manual operation.

Today, instrumentation, control, and automation (ICA) of wastewater treatment processes is almost entirely motivated by increasing cost efficiency of the treatment (i.e., costs for chemicals, energy, and labour). Furthermore, ICA can delay or prevent costly expansions of WWTPs. Olsson et al. (2005) states that with the use of ICA a capacity increase in the biological nutrient removal of up to 30% can be achieved.

The potential to save energy and chemicals is mainly given by the large centralised systems for collection and treatment of wastewater. Sewers and treatment plant are designed such that peak loads can be managed. In turn, this results in systems that are most of the time running below their capacity limit. Furthermore, most urban water system follow a very distinct diurnal pattern. Therefore, the pollution and hydraulic load arriving at the plant

is constantly changing. Consequently, implementing ICA to adapt the removal capacity to the current load automatically within minutes to hours is attractive. Due to the difference in growth rates between heterotrophic and nitrifying bacteria, it is commonly assumed that properly controlled nitrification implies adequate carbon removal.

In contrast to optimising control, stabilising control for aerobic wastewater treatment is neither widely applied in practice nor intensively studied in academia: Since plant capacities are designed for peak loads, nitrification is open loop stable meaning it could be operated with constant actuator settings. The recently developed urine nitrification as a pretreatment for nutrient recovery is an exception (Fumasoli-Hug, 2016). Nitrite accumulation and associated NOB losses is a common phenomenon that can be appear within hours. Constant actuator settings cannot prevent such accumulations. Consequently, the process requires either frequent manual interventions or automated control.

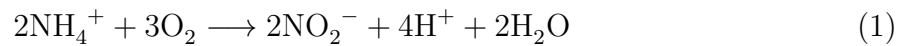
The remaining introduction is structured as follows: First, a general introduction into nitrification process and a detailed description of urine nitrification process and its challenges in terms of ICA is given. Second, the ICA of nitrification processes in general are discussed. Third, sensor faults and fault detection is introduced. In a fourth part, qualitative trend analysis (QTA) as a dominant family of methods in this thesis is presented. Finally, the aims of this thesis are stated and the research questions of the four research chapters are listed.

Nitrification: from nutrient removal to nutrient recovery

In the mid-20th century, scientist and engineers were shifting their attention from mechanical wastewater treatment and biological carbon removal to nitrogen and phosphorus removal (Lofrano and Brown, 2010). For phosphorus removal, operators have the choice between physico-chemical and biological treatment steps, which are both widely applied (Bunce et al., 2018). Also for nitrogen removal, operators can choose either to use a physico-chemical treatment such as ammonia stripping or a biological treatment. Due to its cost-advantage for low and mid-strength wastewater, biological treatment is predominant in practice (Mulder, 2003). Today, the most prominent biological pathway to remove nitrogen from wastewater is the autotrophic nitrification prior to heterotrophic denitrification. However, biological treatment systems also have disadvantages. Bacterial retention times are among the longest time constants in wastewater treatment. Therefore, the operation of biological processes is rather unresponsive. Consequently, process failures can be looming long before they are detected. Once biological processes fail, they also take a relatively long period for their full recovery (e.g., Jin et al., 2013). The same applies for the start-up of such

processes. Hence, preventing the irreversible loss of biological activity is one of the top priorities when operating biological reactors.

Nitrification is facilitated by two bacteria groups, first the ammonia oxidising bacteria (AOB) oxidise ammonia to nitrite and then the nitrite oxidising bacteria (NOB) oxidise nitrite to nitrate. (1) and (2) show the net reactions that are performed by AOB and NOB respectively. These are also referred to as nitritation (1) and nitrataion (2).



Both AOB and NOB are only collective terms for a vast number of single bacteria species that oxidise ammonia or nitrite respectively. Part of these species can also grow on other substrates than ammonia or nitrite. This leads, on the one hand, to very high variability of environments, in which these bacteria grow (Wagner et al., 2002). On the other hand, it impedes our full understanding of the nitrification as a whole (Kuypers et al., 2018). For the same reason, also the kinetics of the reactions are by far not determined and show high variability (Park and Bae, 2009). Therefore it is not surprising that Graham et al. (2007) was able to produce evidence that nitrification systems are inclined to behave chaotic in the sense that small changes in the initial conditions can develop into large differences once the system evolves. Additional evidence was produced by further studies such as Bürgmann et al. (2011) who observed after a massive performance increase in a partial nitritation/anammox reactor a sudden, unexpected, and irreversible regime-shift in the microbial community that led to a performance degradation. Thus, despite worldwide application of nitrification processes for the treatment of wastewater, the underlying microbial processes are far from completely understood. A more complete understanding would facilitate the use of models for controllers with predictive ability such as e.g., model predictive control (Rawlings and Mayne, 2009).

The increasing awareness of energy and resource scarcity since the 1970s has also been influencing the way scientist and engineers are looking at wastewater treatment. Despite the cost advantage over other ways of nitrogen removal, biological nitrification/denitrification is still an energy and resource intensive process. Ammonia is actually over oxidised to nitrate just to be reduced again to irrecoverable nitrogen gas using up valuable carbon (Siegrist et al., 2008) Thus, scientist and engineers have been studying how the conversion from ammonia to nitrogen gas can be engineered more efficiently. Partial nitritation/anammox is so far the most relevant short-cut of nitrification/denitrification in engineering practice (Strous et al., 1997). Short-cutting the nitrogen cycle in a pure autotrophic way has two

major advantages: First, less oxygen is required as only half of the ammonia is oxidised to nitrite. Second, no carbon is required as nitrite and ammonia are directly converted to nitrogen gas. Consequently, carbon can now be diverted to recovery. Even though partial nitrification/anammox increases the energy efficiency and frees up carbon for recovery, it does not improve the recovery of nutrients. However, since nutrients are usually heavily diluted when they arrive at the wastewater treatment plant (WWTP) end-of-pipe recovery is not very attractive.

Fortunately, for both nitrogen and phosphorus, the biggest single contributor in municipal wastewater is human urine (Larsen and Gujer, 1996). Human urine only accounts for less than 1% of the hydraulic volume of a typical municipal wastewater. Urine is therefore a highly concentrated nutrient solution and thus attractive to be used for nutrient recovery. The little volumes produced daily makes urine also manageable with off-grid transport solutions. Thus, regions lacking sewer systems are well suited for urine separation with a decentralised dry toilet system. However, also in locations serviced by sewer systems, separation of urine could reduce the nutrient load on plants (Wilsenach et al., 2005) and reduce carbon dosage or divert carbon now needed in denitrification to future recovery (Hernandez-Sancho and Sala-Garrido, 2008).

In rural areas urine is already today directly applied to crops. However, first, in densely populated urban areas this is not an option (Udert et al., 2014) and, second, the health risk entailed by the direct application is relatively high compared to urine that underwent some treatment (Höglund, 2001). One such treatment was presented by Randall et al. (2016). They studied a physico-chemical treatment to increase the pH such that the urea decomposition is prevented in the first place. If urine however, is not directly treated after its collection the fast decomposition of urea into ammonia increases the pH of stored urine to around 9 (Udert, 2002). At this pH, free ammonia volatilises leading to malodour and nitrogen loss. Once the urea decomposition took place biological nitrification of urine is another way to stabilise it. There are two effects responsible for the stabilising effect nitrification has. First, nitrification converts volatile ammonia into non-volatile nitrate. Second, the ammonia oxidation reduces the pH to around 6, which shifts the chemical equilibria from free ammonia to the non-volatile ammonium. Additionally, malodour disappears as the responsible volatile organics are oxidised. In contrast to other means of recovery such as struvite precipitation (e.g. Etter et al., 2011), urine nitrification coupled with distillation allow for full nutrient recovery and does not produce any liquid or solid waste-streams that require further treatment (Udert and Wächter, 2012). This makes this process suitable for long-term autonomous operation. Thus, even though Udert and Wächter (2012) found that their urine nitrification/distillation process consumes 2.5 times more energy than conventional nitrification/denitrification on a WWTP, the

direct recovery of the nutrients shows potential to make wastewater management more sustainable. However, the nitrification of urine is a very delicate process. The high salt concentration and low alkalinity challenge the smooth operation of the process (Fumasoli et al., 2016).

The most reported process failure is the accumulation of nitrite caused by an imbalance of AOB and NOB activity. Fumasoli et al. (2016) observed them in an moving bed bio-reactor, Sun et al. (2012) in a sequencing batch reactor (SBR) and a membrane bio reactor and Udert and Wächter (2012) in a membrane aerated bio-reactor. Once the accumulation started, they are theoretically self-accelerating due to the increasing NOB inhibition with increasing nitrite concentration. However, Fumasoli et al. (2016) reported that in one experiment nitrite accumulated up to $109 \text{ mg NO}_2^- \text{-N/L}$, which should have eventually led to a complete failure, but the nitrite was later degraded again despite no obvious changes in the operation of the reactor. In other cases, the same study reports that nitrite accumulated to the point that the process failed. Just as in the case of conventional low-strength nitrification processes, a complete understanding of this high-strength nitrification process and in turn the mechanisms leading to these accumulations is not yet developed. The limited alkalinity in urine further complicates the operation of urine nitrification. The alkalinity present in urine only allows for oxidising approximately 50% of the ammonia to nitrate. Hence, nitrified urine still contains ammonia and thus facilitates the growth of acid tolerant AOB that can drive the pH below 3 within a few hours to weeks if no urine is fed to the reactor (Fumasoli et al., 2015). Overcoming the alkalinity limitation with base addition has been studied by Jiang et al. (2011). These authors completely nitrified urine to achieve maximal nitrate concentration for in-sewer denitrification as a measure to prevent sewer corrosion. Apart from initial nitrite accumulation, Jiang et al. (2011) did not report process instabilities. This is also in line with initial test results obtained by myself (not reported). Thus, base addition seem to stabilise the process. However, base addition is costly, adds complexity to the management of decentralised urine treatment systems and is not necessary for the subsequent fertiliser production.

In contrast to the lower pH, the upper pH limit, which would cause free ammonia inhibition of the biomass, is not as relevant for the practical operation. So far nitrite accumulation have appeared before these high pH levels were reached. Furthermore, the acidification by the AOB reduces the pH if the inflow is stopped. Thus, only an immediate large jump in pH could lead to a complete inhibition of the AOB and make the process fail.

The use of the nitrified urine as a fertiliser requires to reduce the loss of nutrients during the process to minimise in order to keep the economic value of the fertiliser high. Udert and Wächter (2012) found that the nitrification led to a nitrogen loss of up to 24%. They identified denitrification of nitrite or nitrate to nitrogen gas as a main pathway for the

loss. The risk for denitrification is particularly high in the nitrification reactor itself as readily biodegradable COD as well as nitrate or nitrite are available. By keeping the oxygen concentration high denitrification can be suppressed. However, Udert and Wächter (2012) suspected that in biofilm system oxygen can still be limiting and cause the relevant losses. During the subsequent storage of nitrified urine denitrification can be limited by minimising the carbon content in the stored urine (e.g., remove biomass prior to storage).

Challenges in control of urine nitrification

So far, the loading rate was controlled by the pH (Udert et al., 2003). In other words, the AOB activity or the acidifying effect of the AOB activity respectively is monitored and used to control the loading rate. This control concept neglects the nitrite oxidation and can lead to process instabilities if the nitrite oxidation becomes the rate-limiting step of the nitrification process. Thus, for process stability it is essential to monitor both bacteria AOB and NOB and adapt the loading such that it matches the one oxidation process, ammonia or nitrite, that is rate-limiting. Ultimately, this means that in steady state the ammonia oxidation is always the rate-limiting step.

The two process stability issues regarding nitrite and limited alkalinity call for opposing actions: Nitrite can be again degraded by reducing the loading rate to the reactor, which reduces the pH, and in turn the ammonia oxidation rate allowing the NOB to oxidise the surplus nitrite. However, lowering loading rates to reduce the pH also increases the risk of growing in acid tolerant bacteria, which become critical once no fresh urine is available for feeding.

These considerations neglect completely the optimisation of the process performance. Even though first and foremost stability is a prerequisite to start with optimisation, the loading rate has to remain a degree of freedom for the latter.

Challenges in instrumentation of urine nitrification

Whereas control algorithms can be relatively complex, instrumentation of any process should be kept simple since instruments are usually the most maintenance intensive components in control loops. In particular, for urine nitrification, which is a technology that is intended to be operated in a decentralised manner in low-income countries, advanced instrumentation such as analysers or ISE ammonia or nitrate sensors are not a viable option. So far, the installed instrumentation consists of a pH sensor for feed control and a DO sensor for aeration monitoring or control. To monitor the NOB activity additional software or hardware sensor to detect nitrite are required. The options are however, limited. Ex-situ analysers are too costly and maintenance intensive for the given purpose. In-line

UV-Vis spectrophotometers are challenged by high concentrations of nitrate and organics that saturate the signal (Mašić et al., 2015). Nevertheless, UV-Vis sensors to determine nitrite are further studied in Chapter 1. Chapter 2 discusses a nitrite sensor based on the already obtained data from pH and DO sensors.

Instrumentation and control of nitrification processes

Soft-sensors

Sensors can be split into two types: Hardware sensors and software sensors. Software sensors are also known as virtual sensors and are further referred to as soft-sensors. In this thesis, a soft-sensor is defined as any software that produces an output signal, by means of a model, that has two or more inputs from other sensors. With this rather broad definition there are only a few sensors categorised as true hardware sensors (e.g., spectral absorption coefficient at the 254 nanometer wavelength, SAC254) while many commercially available sensors are defined as soft-sensors. For example, dissolved oxygen (DO), pH or oxidation-reduction potential (ORP) sensors correct their raw signals with temperature. Since these types of corrections are usually based on the law of physics they are offered as turnkey solutions embedded in hardware. Often such sensors allow tapping the raw measure quantity to build customised soft-sensor based on these raw signals (e.g., mV and temperature in a pH sensor). These customised soft-sensors are widely studied in literature. Commonly, these types of soft-sensors are advertised as sensing technologies for quantities, which are expensive or impossible to measure otherwise, or as diagnosis tools for the hardware embedded soft-sensors that measure the same quantities.

Models in soft-sensors can either be purely data driven (i.e., black-box models) (e.g. Haimi et al., 2013), be purely based on mechanistic knowledge such as physical laws (i.e., white-box models) or a combination of both (i.e., grey-box models) (e.g. Benazzi et al., 2007). Despite dedicated research about black-box soft-sensor in WWTPs their application in practice is very limited (Corominas et al., 2018). Corominas et al. (2018) named two major obstacles for a more broad application of data driven soft-sensors. First, the lack of clean datasets that represent meaningful periods impedes the calibration of representative models. Second, black-box soft-sensors often lack of intuitiveness and operators cannot trace back the signals just based on their expert knowledge. These obstacles are less of a concern for grey-box or white-box soft-sensors. Mechanistic models make them intuitive and require less or no historical data. Dürrenmatt and Gujer (2012) provided evidence that soft-sensors based on black-box models perform significantly worse when extrapolated in time than soft-sensors developed based on expert knowledge. Nevertheless, all soft-sensors

require a model, which is always an approximation of reality. Thus, they are always subject to error. In this thesis Chapter 1 and 2 deal with nitrite soft-sensors and Chapter 4 with an ammonia soft-sensor.

Instrumentation for nitrification

The main purpose of instrumentation in the biological reactors for wastewater treatment is to monitor nitrification. Carbon removal is less critical due to the higher growth rates of heterotrophic bacteria compared to nitrifying bacteria. However, on many smaller WWTPs, sensors are not installed at all or only used for monitoring. In turn, basic and advanced control loops are not implemented. Cornelissen et al. (2018) found that in Flanders, Belgium only a small number of industrial WWTP actually use advanced control loops. Similar results were found in an instrumentation survey on municipal WWTP in Finland by Haimi et al. (2013). In the following paragraphs, the most common types of online sensors used to monitor nitrification are briefly described. A more comprehensive overview can be found in Vanrolleghem and Lee (2003).

Dissolved oxygen

Providing sufficient oxygen is key to all aerobic processes. Thus, DO probes have been one of the first online in-situ sensors used on WWTP. DO is measured either electrochemically or more recently also by means of fluorescence. Newer processes such as simultaneous nitrification/denitrification (Zeng et al., 2004) or one-stage anammox systems (Laureni et al., 2016) increased the demand for accurate oxygen measurement. This goes even so far that Joss et al. (2011) suggested controlling the airflow in an anammox system not by a DO sensor but according to the NO_3^- concentration in the treated effluent. DO signals allow to obtain the oxygen uptake rate (Bocken et al., 1989), which is informative about the status and progression of nitrification (cf. Chapter 2).

pH

The ion-selective principle is used to measure pH. For nitrification, pH is essential since it determines the dissociation ratio of ammonium to free ammonia and thus can limit or inhibit the ammonia oxidation step (Fumasoli-Hug, 2016). In particular, when alkalinity is limiting pH monitoring is essential. Therefore, pH is also widely studied as a monitoring signal for nitrification (cf. Chapter 2). A recent study shows that drift is still an issue despite the maturity of this sensor type (Ohmura et al., 2018).

Oxidation-reduction potential

The oxidation-reduction potential (ORP) defines how likely a substance is accepting electrons and thus being reduced. Its measurement principle is similar to a pH sensor with two electrodes, a measuring one and a standard one. ORP is typically measured in mV. In general, the ORP of wastewater increases the more purified it gets. With knowledge about the present species in wastewater, one can derive relevant information about the end of certain oxidation-reduction reactions. Very prominent examples are the nitrate knee and the DO elbow/ammonia breakpoint (Olsson et al., 2005).

Conductivity

Conductivity or electrical conductivity measures the ability of a solution to conduct an electric current. It is measured in Siemens per meter. The higher the ion concentration in a solution the higher the conductivity. Thus, in general the conductivity of wastewater reduces with its purification. In high strength wastewater the ammonia concentration differences of influent and effluent can lead to significant changes in conductivity such that conductivity is proposed as a soft sensor for ammonia (e.g., Joss et al., 2009).

Ammonium and nitrate ion-selective electrodes

Ion-selective electrodes for ammonium and nitrate monitoring in water became commercially available in the early 2000s (Winkler et al., 2004). As the pH sensors, they are based on a potentiometric measurement principle. Their relatively low investment costs and their direct application in the media without the need of sample preparation promise the operators a relatively simple and cheap operation (Winkler et al., 2004). However, the in-situ application also increases the wear and tear on these types of sensors. Thus, even recent literature highlights that properly maintaining these types of sensors requires experience (Cecconi et al., 2019). Furthermore, the membrane is not exclusively selective for ammonium or nitrate respectively. Thus, for municipal wastewater often potassium and chloride compensation is necessary. Instead of measuring the ammonium ion, there are also electrodes that measure ammonia by means of amperometry (e.g., Crowley et al., 2008). A further alternative to these sensors with respect to ammonia controlled aeration is presented in Chapter 4.

UV-Vis

In-situ UV-Vis spectrophotometers measure the absorbance of light in a spectrum ranging from ultraviolet to visible light. The high frequency and high-resolution measurement allows determining multiple variables in parallel on a minute resolution scale. Nitrate,

nitrite, chemical oxygen demand (COD) and total suspended solids (TSS) are the most important concentrations in nitrification processes that can be estimated by means of UV-Vis absorbance measurements. In particular for nitrite, measurements are in need (Chapter 1 and Gujer, 2010) and cost effective alternatives are missing. Each light absorbing substance has a determined absorbance spectrum Spinelli et al. (2007). The Beer-Lambert law relates the measured absorbance with the concentration of the substance in the solution. However UV-Vis lacks of specificity making it challenging to use it in media such as wastewater that contains numerous species (Thomas and Burgess, 2017). There are also sensors available that only determine the absorbance at single or selected wavelengths within the UV or UV-Vis spectrum. Normally they are used to determine the concentration of single species e.g., single wavelength absorbance (SAC254), NO_3^- , or the lumped concentration of multiple species such as COD.

Total suspended solids

The total suspended solids concentration is a crucial parameter in wastewater treatment as it approximates the dryweight biomass present in the wastewater. Today, TSS is most often measured by optical methods. Depending on the solids concentration, back scattering, forward scattering, nephelometry or absorption (i.e, reciprocal value of transmission) can be used to estimate the TSS concentration.

Analysers

Analysers are the most expensive types of sensing technology used for wastewater treatment. Analysers take a small sample stream and analyse the sample for the desired species photometrically after a reaction with certain reagents to obtain a concentration value. Most typical quantities determined by analysers in wastewater treatment are phosphorus, nitrite, nitrate, ammonia, COD, and total organic carbon (TOC). Apart from high investments costs, the complexity in operation due to sampling, sample pre-treatment and the use of reagents hampers their application in mid-size and small plants. On larger plants, savings achieved through more exact monitoring or control can compensate the investment and operational costs.

Off-gas measurements

Off-gas measurements have been studied with respect to many quantities connected with nitrification (e.g. CO_2 production, O_2 consumption (Hellings et al., 1996), or N_2O production (Wunderlin et al., 2012)). Advantages of off-gas measurements include the ability to measure multiple compounds at once and the lack of sensitive pre-treatment

steps. Furthermore, unlike wastewater that is challenged by sedimentation and degradation processes when transported from the sampling site to a measurement station, gas behaves relatively inert once it is collected. The raising awareness to holistically reduce the greenhouse gas emission on WWTPs will most likely lead to more interest in this measurement principle in practice (Caniani et al., 2019).

In-situ nitrous oxide sensor

In-situ nitrous oxide sensors measure electrochemically nitrous oxide dissolved in the bulk liquid. Wunderlin et al. (2013) suggest that measuring nitrous oxide could be the next standard for controlling ammonia oxidation. Andalib et al. (2018) studied such a sensor in a control loop to optimise denitrification.

Control of nitrification process

Control of nitrification started with the implementation of nitrification processes on WWTPs. At that time, dissolved oxygen (DO) control was one of the first types of control loops implemented in full-scale plants. Since the determination of the actual process state in wastewater has always been difficult, indirectly informative signals have been used to control nitrification. DO signals are such an example of indirect information, which have proven to be mostly useful but still bare the risk of a misinterpretation. High values of the DO concentration can indicate either too high aeration intensities or too low oxygen consumption: The first is an optimisation problem, the latter means that no or little nutrients are oxidised. Consequently, only the combination of online signal and process knowledge allows extracting the actually required information from such indirect signals about the state of the desired process (i.e., sufficient bacterial activity). Olsson and Andrews (1978) analysed the profile of the DO signal along the reactor cascade together with the absolute values to control the aeration intensity.

Later on, instrumentation that actually measures ammonia was developed, which then facilitated the use of more direct information to control nitrification. This more direct information about the state of nitrification reduces the need to incorporate process knowledge into the control design. However, the ammonia measurement only offers an incomplete view on the nitrification process. The decrease of ammonia is a necessary but not a sufficient condition for a successful nitrification as it only confirms successful ammonia oxidation but does not inform about the nitrite oxidation step. For larger WWTPs ammonia based aeration control is today state of the art. Chapter 4 investigates an alternative ammonia soft-sensor to facilitate such control also in remote and smaller WWTPs. The controller in Chapter 3 goes one step further. The instabilities in the

urine nitrification is a prime example where the control of ammonia oxidation alone is insufficient to guarantee a complete nitrification. Thus, the nitrite oxidation step must be controlled as well.

Controllers can be characterised in different groups. One differentiation is whether the control action is dependent on the current process state or not. In other words if it has a feedback loop (i.e., closed loop) or not (e.g., time based control). A typical time based controller on a WWTP is the sludge wastage. Such controllers are simpler to implement as they do not require substantial instrumentation but cannot reject any disturbances. If the process behaves differently than expected the control action will be faulty. In the case of sludge wastage, concentration or volume changes will lead to change in the amount of wasted sludge. Consequently, such control is only applied in processes with time constants in the range of a few days, in which single executions of the control task are not significantly changing the system. If however, control actions have an almost immediate effect on the plant performance, automated closed loop control is needed to reach the optimal efficiency (e.g., aeration control). This differentiation is also related to the term automation. In both cases presented above the given task is executed automatically without a human intervention. However, in controllers without feedback, there is no automated selection of which task the controller should execute. Thus, in systems with irregular disturbances, frequent checks by a supervisor are needed. In a feedback controller, the selection of the task is automated to some extent and hence reduces the need for human interventions. The most typical controllers for nitrification are briefly described below. These single controllers can be cascaded to one large controller. Furthermore, there are specific controls for different reactor configurations such as sequencing batch reactors (SBR) (Villez et al., 2010) or alternating intermittent reactors (Battistoni et al., 2003). These controllers use the additional flexibility (e.g., determined phase lengths) these reactor configurations offer compared to continuous-flow reactors.

Dissolved Oxygen Control

Dissolved oxygen (DO) control regulates the aeration capacity such that it meets the oxygen uptake rate of the biomass. This can either be the speed of a surface aerator or the airflow to a fine bubble diffuser system. This is done by keeping a fixed DO concentration in the bulk media. The DO setpoint itself has again a feedback to the total oxygen uptake rate (OUR) of the process. By setting the DO setpoint into a specific concentration range an operator can already control various processes. Low DO concentrations reduce the total nitrification capacity (cf. Chapter 4). Furthermore, certain niches can be created that facilitate simultaneous nitrification/denitrification (e.g., Pochana and Keller, 1999) or bacteria can be out-competed (e.g., Laurenzi et al., 2016). In terms of controller type, DO

is often controlled with PI controllers. Such controllers either determine the airflow that is required, which is then fed to the flow rate controller or directly control the valve opening. To adjust for pressure changes in the pressurised air system, air pressure controllers are controlling the blower performance. Thus, DO control itself is already heavily cascaded and thus requires careful tuning. The DO setpoint itself is either manually adapted or is adapted with a closed loop control resulting in a further cascading of the aeration control.

Ammonia aeration control

Ammonia aeration control is used as a top layer controller for a DO control system. It adapts the nitrification capacity of the WWTP to the current ammonia load by adapting the DO setpoint of the DO control. Ammonia aeration controllers can be designed either as a feed-forward controller measuring the incoming ammonia or as a feedback controller measuring the ammonia in the effluent (Rieger et al., 2014). Feed-forward control requires detailed knowledge about the systems behaviour as the effluent ammonia concentration needs to be predicted. Rieger et al. (2014) reported that ammonia aeration control not only enhances energy efficiency but also leads to improvement of nitrification and denitrification efficiency. Ammonia aeration control can lead to higher electricity costs. The consumption is normally reduced but the peak consumption may increase. Depending on the tariff structure this can lead to increased costs (Aymerich et al., 2015). A comprehensive review of DO and ammonia aeration control was compiled by Åmand et al. (2013).

Sludge age control

When biomass is grown in suspension, sludge age control is required to achieve nitrification (Ekama, 2010). However, the large time constants do not require automated sludge age control. Municipal WWTPs in middle latitudes adjust the sludge age often with the seasons to adjust for the yearly temperature fluctuations. At higher temperatures, plants can be operated with lower sludge ages, without risking a biomass washout. To this end, hydraulic control is the easiest way to achieve the desired sludge age since it only requires a flow meter (Ekama, 2010). Selective sludge age control has become important in particular for partial nitritation/anammox. For these processes sludge age control has been identified as one way to achieve stable process performance. Either specific biomass such as anammox granules are specifically enriched (Wett et al., 2010) or hybrid systems that allow different retention times for different types of bacteria (Laureni et al., 2018).

Sensor faults

Faulty instrumentation is a major obstacle for automation on WWTPs and can lead to elevated operational costs (Steyer et al., 2006). Rosen et al. (2008) defined six abnormal sensor modes *(i)* calibration, *(ii)* shift, *(iii)* drift, *(iv)* fixed value, *(v)* complete failure, and *(vi)* wrong gain. Most sensor modes can be detected by existing fault detection methods. Sensor faults are either determined manually by comparing manually obtained reference measurements with online measurements (Thomann et al., 2002) or automatically with fault detection methods (Venkatasubramanian et al., 2003). For automated fault-detection, typically, faults are first detected, secondly isolated, then corrected for, and eventually the intended control performance is recovered. However, Corominas et al. (2011) stated that methods are limited, if they do not take into account expert knowledge in the form of process dynamics and actuator data. Carlsson and Zambrano (2016), for example showed, that with help of redundant information and expert knowledge about the system's behaviour the identification of sensor faults is even in close-loop control relatively simple. However, redundant information is rarely abundant or cheap. Moreover, the concept of using redundant information is challenged by the recent findings of Ohmura et al. (2018). They reported that all types of pH sensors they exposed to nitrified urine started to drift immediately after their installation. Thus, the assumption of having a well working sensor in a first period after installation, thereby producing data suited well as a reference to train a fault detection method, is at least questionable. Therefore, we hypothesize that drift should not be corrected for but instead should be accounted for in the control design (cf. Chapter 3 and 4). Information that is affected by drift such as the absolute sensor value should be avoided. Instead information which quality is not affected by drift, should be considered.

Derivatives and qualitative trend analysis

In this thesis the signs of the derivatives of different signals are used as a source of information that is only little affected by sensor drift. This assumes that the sensor drift is mainly induced by changes in the off-set and not by changes in the sensitivity of the sensor. This approach places high demands at the correct identification of the derivatives' signs. A correct identification is challenged by noise in the data. The basis for this noise is formed by random measurement errors and irrelevant process dynamics represented in the signal.

In this thesis two *qualitative trend analysis* (QTA) methods are applied to identify the signs in the derivatives. QTA stands for multiple methods that were developed since

the 1990s (e.g., Cheung and Stephanopoulos, 1990; Dash et al., 2004; Maurya et al., 2007; Rengaswamy and Venkatasubramanian, 1995; Villez et al., 2013). They all aim at subdividing data into *episodes* in which constant signs of the derivatives are assumed. By identifying points in which the signs of the derivatives changes maxima, minima, and inflection points can be identified.

The qualitative representation of trends is mainly motivated by the fact that expert knowledge is mainly stated in a qualitative manner. Quantitative expert knowledge in particular for nitrification is often associated with numerous boundary conditions that complicate the implementation into software and may even prevent the practical application. Hence, incorporation of such human knowledge into a software is simplified by the qualitative representation. Consequently, a qualitative representation also covers a more broad range of situations that are from an application perspective of similar nature but still result in different quantitative data. That is why we hypothesize that qualitative representation of sensor data makes the extracted information more robust towards small quantitative changes in the underlying signal.

Aim of this thesis

Control of nitrification is challenging due to lack of full process understanding and the harsh environment sensor are exposed to. Consequently, sensors require extensive maintenance. This thesis should reveal if the classical approach of ICA management that aims at reaching standardised quality levels for sensor signals based on absolute values (i.e., accuracy, precisions, sensitivity) (ISO Central Secretary, 1994, 2001) can be complemented with a novel approach. This novel approach does not require that a high quality sensor signal in the sense of classical notions of accuracy can be maintained, but takes faults, in particular drift, as inherent and irreducible properties of sensor signals. Precision and sensitivity remain relevant quality parameters. It is expected that with this novel approach the sensor maintenance frequency can be reduced, which in turn facilitates the use of ICA in applications that were so far excluded due to the relative high investment or maintenance costs. Consequently, this thesis soft-sensor and controllers are developed within the scope of this novel approach.

I hypothesize that advanced data analytic approaches can compensate sensor faults without redundant information and therefore facilitate control of nitrification processes with signals conventionally perceived as faulty and, with almost no exception, useless.

This main hypothesis gives guidance to the following four research questions answered within the four research chapters of this thesis:

- Chapter 1: What are relevant matrix effects that should be taken into account for the calibration of UV-Vis spectrophotometers?
- Chapter 2: To what extent can nitrite in high strength wastewater be detected by means of analysing pH and DO signals?
- Chapter 3: Can nitrite accumulation in urine nitrification reactors be prevented despite drifting controller input signals by identifying kinetic information in the derivatives of the input signal?
- Chapter 4: Does the pH difference over the aerated reactors of a continuously operated municipal WWTP inform about aeration requirements such that it can be used for advanced aeration control?

Thesis outline

The thesis includes two chapters about nitrite instrumentation in high strength wastewater and two chapters about feedback control of nitrification.

- Chapter 1 investigates experimental designs for nitrite calibration of in-line UV-Vis spectrophotometer in nitrified urine. Four experiments were designed, executed, and the resulting models were tested on two independent data sets.
- Chapter 2 presents results from an exploratory data analysis of the information content of pH and DO data in terms of nitrite concentration. The stoichiometry of nitrification allows in principle to distinguish oxygen uptake rate of ammonia oxidisers and nitrite oxidisers by putting the total oxygen uptake rate into a ratio with the measured proton production rate. Using the already needed DO and pH sensor signals to determine nitrite presence would prevent using an additional sensor for nitrite.
- In Chapter 3, we followed a stabilising nitrite controller that uses information that is contained in the first and second derivative of a UV-Vis based nitrite signal. Using qualitative knowledge about nitrite degradation behaviour in a nitrification system and qualitative trend analysis should allow determining if the nitrite oxidising bacteria are inhibited or limited by their substrate nitrite.

- In Chapter 4, a pH based ammonia soft-sensor is developed and tested on multiple municipal WWTPs. The pH difference over the aerated reactors informs about the mismatch of aeration requirement and aeration performance. The ratio of CO₂ stripping and acidification due to AOB activity influence the difference and thus allow feeding this information into an advanced aeration controller.

Part II
Research Papers

1 Comparison of four methods to obtain calibration data for online nitrite estimation by means of in-line UV-Vis spectrophotometry

This chapter is based on the following manuscript, submitted for publication:

Thürlimann, C. M.^{a,b,c,d,e}, Udert, K. M.^{a,e}, Morgenroth E.^{a,e}, Villez, K.^{a,c,e} Comparison of four methods to obtain calibration data for online nitrite estimation by means of in-line UV-Vis spectrophotometry.

^aStudy concept and design, ^bAcquisition and analysis of data, ^cInterpretation of data, ^dDrafting of chapter, ^eCritical revision.

1.1 Introduction

Nitrite is a key variable in the removal or recovery of nitrogen from wastewater. The recent focus on shortcuts in the nitrogen cycle in wastewater treatment processes increases the demand for reliable nitrite measurements - on one hand to achieve process stability (e.g., Bürgmann et al., 2011 for treatment of urine with anammox), on the other hand to achieve high process performance, (e.g., Lotti et al., 2012 for treatment of reject water with anammox granules). Even some conventional nitrification processes such as the one of source-separated urine were so far only successfully operated with close manual supervision to prevent nitrite accumulation (e.g., Fumasoli et al., 2016; Sun et al., 2012). Despite advancements, online nitrite measurement in wastewater remains a challenging task. To obtain high-quality and high-resolution nitrite data high-end automated colorimetric analysers are a logic choice. However, wastewater is a harsh medium making frequent maintenance from skilled staff necessary to keep the measurement quality high. A more cost-effective alternative consists of using an in-line ultraviolet-visible (UV-Vis) spectrophotometer (SPM). SPMs are robustly built and do not require sample preparation steps (i.e., filtering, potential toxic reagents). Consequently, SPMs require less maintenance, which facilitates use in remote and small-scale wastewater treatment units. Furthermore, SPMs are sensitive to many relevant species in wastewater and can therefore be used to monitor multiple variables at once without significant delay and at a high frequency ($< 1 \text{ min}^{-1}$). Nitrite estimation by UV-Vis SPMs have been reported by few studies (e.g., Rieger et al., 2004). However, saturation by nitrate and organics in the low UV range can challenge SPMs in high strength wastewaters. Mašić et al. (2015) successfully estimated spiked nitrite concentrations in nitrified urine by relying on the much weaker secondary nitrite absorbance peak around 355 nm (Spinelli et al., 2007).

In general, species are required to have specific molecular bonds, which absorb substantial fractions of light at certain wavelengths in order to be estimated by means of UV-Vis absorbance (Thomas et al., 2017). The broad multi-species sensitivity results unfortunately also in a lack of specificity of the absorbance measurements. This in turn requires one to obtain a model before using a UV-Vis SPMs to measure species concentrations. To get a model, one has to execute two steps: First, calibration data, which contain paired absorbance spectra and concentrations of the target species, have to be obtained in an experiment. This step is referred to as the *calibration experiment*. Second, a model is calibrated that relates the model input (i.e., absorbance measurement) and model output (i.e., nitrite measurement). This second step is further referred to as *model calibration*. Good statistical practice also recommend the use of an independent test data set, obtained through the *test experiment*, which has the same structure as the calibration data yet is exclusively used for model performance evaluation. The calibration and test experiments, specifically the collection of high-quality target species concentration measurements, are the most expensive steps in most practical cases.

The causes for the high costs for the calibration experiment are twofold. First, the concentrations of the target species and non-target species should be as decorrelated as possible in the calibration data set to cover all potential system states in a representative manner. Second, the concentration range of the target species as well as all non-target species should be represented in the calibration set to avoid strong extrapolation. So far, ex-situ calibration design is the preferred approach for single target species. To this end, site specific samples are spiked with the target species (e.g., Rieger et al., 2004) or standards for the specific species are measured to obtain a model (e.g., Sutherland-Stacey et al., 2008). In-situ calibration design is less common but has two potential advantages: (i) the experimental effort can be reduced, especially as representative sampling and mixing steps are avoided, and (ii) the calibration might profit from the correlation between measurable effects and the concentration of the target species, which may be

a non-absorbing species (Etheridge et al., 2014). In the in-situ calibration experiment, coinciding grab samples are taken for laboratory analysis and paired with the corresponding absorbance measurements. Models for lumped species are often obtained with in-situ design, as there are no generally accepted standards available for the purpose of spiking. However, recently also for these parameters ex-situ designs have been studied Carré et al. (2017).

For the model calibration step a vast amount of chemometric approaches are available. A significant amount of studies focus on the selection of a good model structure (e.g., Lepot et al., 2016). Recent results suggest that the preference for any model structure is difficult to extrapolate from one data set to the next (e.g., Lepot et al., 2016). This problem has also been reported in other fields of spectroscopy (e.g., Anderson et al., 2011; Dyar et al., 2012). Fortunately, the selection of a predictive model structure is computationally efficient and straightforward to implement via cross-validation. In contrast, and rather unfortunately, much less attention has been paid to good experimental design in order to enhance model performance.

To counter the lack of information concerning calibration experiment design, this work compares four different experimental designs for obtaining a UV-Vis calibration data set in practical laboratory conditions. All four sets are then used to obtain a model to predict nitrite in a biological nitrification process of source-separated urine. Two different ex-situ and two different in-situ designs are chosen for the calibration experiments. The designs differ in terms of the most relevant sources of variation in the absorbance that are expected in the nitrification of source-separated urine (Fig. 1.1). All data sets are generated based on media from the same reactor.

Furthermore, the test predictions of these four different models will be linearly corrected with a *linear design correction* (LDC). The principle is the same as the one of the *local calibration* (Caradot et al., 2015). A subtle distinction is that LDC is applied to compensate the errors caused by the difference in experimental design between the calibration experiments and test experiments whereas local calibration is applied to compensate errors associated with extrapolation in the presence of variations between measurement sites.

The assessment of the different model performances reveals the most important factors one should consider when designing a calibration experiment. The following three hypotheses will be tested:

- Hypothesis #1: In-situ calibrated models profit from correlations caused by indirect effects the target species induces in the media.
- Hypothesis #2: Slow variations of the non-target species in the process should be captured in the data to obtain more accurate models.
- Hypothesis #3: The removal of solids from the media leads to noise-reduced calibration data and therefore to a more accurate model.

1.2 Material and Methods

1.2.1 Measurement principle of UV-Vis spectrophotometers

For the absorbing species the relation of the absorbance and the concentration of a species is described linearly by the Beer-Lambert law. Eq. 1.1 shows the underlying principle of the law. The absorbance at each wavelength A_λ consists of a fraction α that is caused by the *target-species* (i.e., nitrite) and a

fraction that is the sum of all effects $\beta \cdot C$ caused by all other absorbing species C the *non-target species* (i.e., nitrate, solids (X) and organic compounds (OC_x)).

$$A_\lambda = \alpha \cdot C_{\text{NO}_2^-} + \sum_i \beta_i \cdot C_i \quad i = \{\text{NO}_3^-, X, \text{OC}_1, \text{OC}_2, \dots\} \quad (1.1)$$

Fig. 1.1 illustrates the relations of the species and solids in nitrified urine with the processes, the absorbance spectrum and the classical measurements in nitrified urine. The non-target absorbing species in nitrified urine are namely nitrate and absorbing organic molecules. Due to the high number of different organic molecules, they are commonly measured as chemical oxygen demand (COD). However, not all organic molecules in nitrified urine contribute to the absorbance spectrum. This means that the relationships between COD and absorbance measurements, as well as all other lumped concentrations, do not satisfy the Beer-Lambert law. SPMs can however be used to measure COD, when one assumes that the concentrations of all absorbing and all non-absorbing organic molecules contributing to the COD measurement exhibit a fixed correlation between each other (e.g., Rieger et al., 2004).

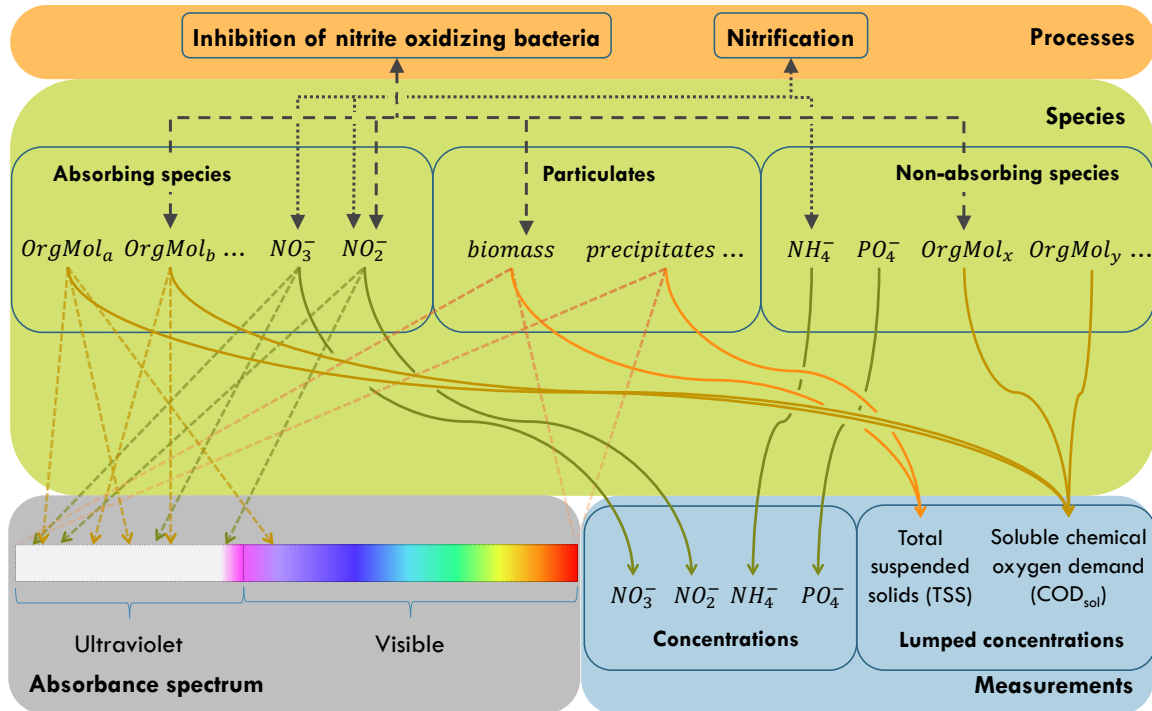


Figure 1.1: Schematic relations of species and their absorbance and measurements in nitrified urine. OrgMol stands for organic molecule. The full curved arrows show the relation of the species to the measurements; the dashed straight arrow from the species to the absorbance measurement; the dotted and dashed arrow potential correlations of a species caused by a process (not conclusive).

The second lumped concentration in nitrified urine are total suspended solids (TSS). It is known that solids (e.g., Berho et al., 2004) and bacteria (e.g., Park et al., 2012) will absorb in the UV as well as in the visible range of the spectrum. However, in contrast to COD, solids, and biomass cannot be separated into absorbing and non-absorbing parts but show gradual changes in their absorbance behaviour based on their size, shape, composition etc. Apart from absorbing the light, they also scatter it, which violates the Beer-Lambert law and in turn further complicates a calibration (e.g., Fu et al., 1998). Measuring

TSS with an SPM implicitly assumes that the absorbance and scattering behaviours of the particles and biomass have a stable correlation with the reference measurement for TSS.

Based on the assumption of stable correlation, one can even measure non-absorbing species. Etheridge et al. (2014) successfully estimated concentrations of phosphorus and salinity by in-line SPMs even though they do not absorb UV-Vis light. Their model takes advantage of the correlation between the concentrations of non-target absorbing species (i.e., organics, solids etc) with the concentrations of the non-absorbing target species (e.g., phosphorus). However, extrapolating such models in time and space comes with a significant risk that the correlation used in the model identification vanishes while the collected spectra remain within normal specifications.

A typical wastewater treatment process may also induce important correlations between the concentrations of absorbing species via a hidden latent variable. In contrast to the correlations that are necessary to estimate successfully lumped concentrations or even non-absorbing species as described above, these correlations are assumed to be actively caused by the presence of nitrite (i.e., causalities). These potential causalities between the concentrations of the target species nitrite and the concentrations of the other absorbing and non-absorbing non-target species are not studied well. However, it is highly likely that the elevated concentrations of nitrite also indirectly influences the concentrations of other absorbing components. Most prominent is nitrification that relates increasing nitrite concentrations with decreasing nitrate concentrations (Fig. 1.1 dotted arrow). Another potential factor net release of organics from nitrite oxidising bacteria (NOB) decay during nitrite inhibition, which in turn changes the absorbance characteristics of the COD fraction (Fig. 1.1 dashed arrow). Furthermore, this inhibition may also affect the biomass and its absorbance behaviour. Even though the detailed investigation of these causalities is not subject of this study, they are important when considering the collection of calibration data. The in-situ designs (cf. 1.2.3.1) intentionally leave correlations between species concentrations undisturbed while the ex-situ designs deliberately break correlations between target and non-target species concentrations (cf. 1.2.3.2).

In principle, one can separate the effects of as many species or lumped concentrations as the number of wavelengths selected for absorbance measurement. In wastewater, there are 1000s of species so that the number of wavelengths (e.g., 220 for the here used SPM) is too low to differentiate all species, even if noise-free measurements could be obtained. Despite this challenge, UV-Vis SPMs are commercially available and effectively operated in specific situations: *(i)* when there are no cost-effective alternatives, *(ii)* when the produced signal quality is acceptable, or *(iii)* when the variation in concentration of the non-target species during model application is similar to the variations captured during calibration experiment.

1.2.2 Reactor setup and operation

An intermittently fed and continuously stirred tank reactor with suspended biomass is used for the partial nitrification of source-separated urine. The reactor was seeded with activated sludge from a municipal wastewater treatment plant (Dübendorf, Switzerland) and concentrated biomass from the reactors described by Fumasoli et al. (2016) 29 weeks before the experiments started. The reactor influent for the reactor is source-separated male urine originating from the same collection system as in Fumasoli et al. (2016). Dissolved oxygen is provided with intermittent fine-bubble aeration. The reactor has two continuously operated bypasses. The first one feeds the UV-Vis spectrophotometer with a hydraulic retention time (HRT) of 10 sec. The second one is used to feed a pH sensor pack used in another study Ohmura et al. (2018) (HRT: 20 sec).

The pH is controlled similarly as in Udert et al. (2003) with an on-off controller. Each time the pH setpoint is reached approx. 15-25 ml of urine are fed leading to an increase of 0.05-0.1 pH units. During the experiment, the HRT of the reactor ranged from 10 to 30 days. No alkalinity is added and therefore only about 50% of the ammonia load is oxidised to nitrate. The airflow (6 L/min) is controlled with an on-off controller between 5.0 and 6.0 mg O₂/L to ensure full aerobic conditions in the reactor and the bypasses. Two dissolved oxygen sensors (COS61D, Endress&Hauser, Reinach, Switzerland) and two pH sensors (CPS11D, Endress&Hauser, Reinach, Switzerland) are installed to monitor the reactor. One of each is used for feedback control. Data from these sensors and from controlled aggregates of the reactor (e.g., air valve, inflow pump etc.) are published on a WAGO OPC server (WAGO CONTACT, Domdidier, Switzerland) and are recorded every 10 s.

1.2.2.1 Sample Preparation and Analysis

The concentrations of ammonia, nitrite, and nitrate were measured in every sample taken from the reactor. Concentrations of ammonia and COD were measured from samples of the inflow. The samples were filtered prior to the analysis with a 0.45 μm GF/PET filter (Art. Nr. 916 02, Macherey-Nagel, Oensingen, Switzerland). Dilutions were executed on a scale in grams to four decimal points. The concentrations of total ammonia were obtained with colorimetric LCK303 tests (as all LCK Tests, Hach-Lange GmbH, Rheineck, Switzerland) or an flow injection analyser (Foss FIA star 5000, Rellingen, Germany), or on the ion chromatograph (IC) (Compact IC 761, Metrohm, Herisau, Switzerland). Nitrate was analysed with LCK340 or on an IC, nitrite with LCK341 and COD with LCK314. A TSS measurement was conducted (van Loosdrecht et al., 2016) every week. The measurement error including the dilution procedure was estimated with a single triplicate of measurements: NO₂⁻ with LCK 341: 0.364 mg N/L NH₄⁺ with FIA: 14.434 mg N/L and NO₃⁻ with IC: 15.275 mg N/L. Due to the required dilution, nitrite concentrations below 2 mg N/L cannot be determined precisely. To determine very low concentrations prior to the corresponding experiments additional strip tests were used with a lower limit of 0.6 mg N/L (Art. Nr. 1.10007.0001, MQuant, Merck KGaA, 64271 Darmstadt, Germany). These strip test measurements were not used for calibration.

1.2.2.2 UV-Vis spectrophotometer

The in-line UV-Vis spectrophotometer (s::can spectro::lyser V1) has a 2 mm path-length, measuring wavelengths ranging from 200 nm to 750 nm with a resolution of 2.5 nm. The sensor was horizontally mounted in a flow cell (s::can F-445). The spectra were recorded on an s::can con::stat V1 (s::can Messtechnik GmbH, Vienna, Austria) with a one minute measuring and recording interval. The sensor was cleaned and tested at least every four weeks. The instrument offset was tested with distilled water. The instrument sensitivity was tested with a 500 mg NO₂⁻-N/L solution. Both tests did not indicate any measurable change in instrument performance during the whole experimental period.

1.2.3 General experimental design

Two in-situ and two ex-situ calibration experiments were executed. Each calibration data set consists of 16 samples. The obtained models were tested on two different test data sets. Furthermore, two linear correction models were obtained with the LDC data set. Fig. 1.2 gives an overview over all samples taken during the experimental period and the selected samples for the different calibration and test data sets (see below). The next three paragraphs describe the three main designs. All data sets were obtained with

one of these three designs: in-situ, ex-situ or nitrite degradation. In the in-situ and ex-situ designs two different versions were executed.

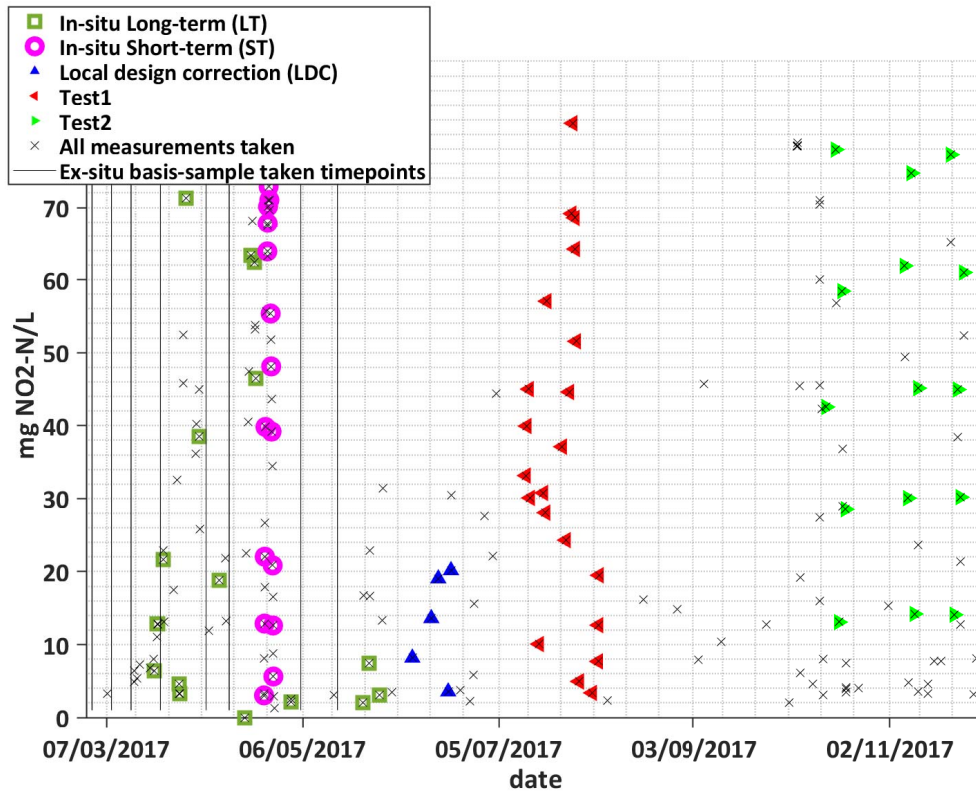


Figure 1.2: Overview of the generated data sets.

1.2.3.1 In-situ calibration and test experiments

The in-situ experimental design was chosen to obtain the following data sets: (i) a long-term (LT) calibration data set: (Fig. 1.2, green squares), (ii) a short-term (ST) calibration data set (magenta circles) (iii) a linear design correction data set (LDC) (blue triangle upward), and (iv) a test data set *Test 1* (red triangle leftward). To this end, the nitrite concentration was varied by manipulation of the pH setpoint of the influent pump control. With high pH setpoints (6.6-6.9) (i.e., high ammonia oxidizing bacteria (AOB) growth rates) nitrite concentration increases as the NOB cannot react fast enough to the increased nitrite concentration and start to get inhibited by nitrite Fumasoli et al. (2016). At lower pH setpoints (5.9-6.2) the AOB have a slower nitrogen turnover rate as the NOB resulting in net nitrite consumption. By repeated switching between high and low pH levels, the bulk nitrite concentration was varied effectively between 0 and 80 mg N/L. Each such increase and decrease in nitrite is further referred to as an *event*. It is important to note that in contrast to other in-situ designs, the variations of the target species is not driven by natural variations but instead induced by intentional manipulation of the pH setpoint.

The short-term (*In-situ ST*) calibration data were obtained within a single event, focusing on the short-term variations during one full event. 32 samples were taken (24.04.2017-27.04.2017). Only the 16 uneven indexed samples (1, 3, ..., 29, 31) were included in the In-situ ST calibration data set. The in-situ long-term (*In-situ LT*) calibration data set is obtained over multiple events thereby capturing slower

variations in the process in-between events. 42 samples were taken (21.03.2017- 29.05.2017 except in the event used to obtain the In-situ ST data). Out of the 42 samples, 16 samples were selected to simultaneously ensure a comparable nitrite concentration range and the coverage of the whole In-situ LT experimental period. This selection was executed before any calibration was executed. The LDC data set (5 samples, 08.06.17-20.06.17) and the Test 1 data (21 samples, 13.07.17-04.08.17) were obtained analogously to the In-situ LT experiment.

1.2.3.2 Ex-situ calibration experiments

The ex-situ experiments were executed with eight *basis-samples* taken from the reactor at the very same period as the In-situ LT was obtained (Fig. 1.2 black vertical lines). This selection aimed at representing the same slow variations of the non-target species as in the In-situ LT data set. One data set was collected with untreated reactor media (i.e., with biomass and particles (*Ex-situ wBM*)). The other data set was obtained with supernatant from the very same basis-samples after centrifugation (i.e., without biomass and particles (*Ex-situ woBM*)). Both experiments were conducted with the same 4x4 full-factorial design as shown in Table 1.1 covering different nitrite and nitrate levels.

Table 1.1: Experimental designs for ex-situ calibration data. The first digits and fill colours represent four fractional factorial designs of which each covers each nitrite and nitrate concentration once.

		additional nitrite [mg N/L]			
		0	25	50	75
additional nitrate [mg N/L]	0	S41	S22	S34	S13
	300	S23	S11	S43	S31
	600	S32	S44	S12	S24
	900	S14	S33	S21	S42

Each of the eight basis-samples was used to cover two of the sixteen grid-points in Table 1.1. (e.g., basis-sample 1 into S11 and S12, basis-sample 2 into S13 and S14 etc.). The first digit of the sample label represents a fractional factorial design. The full number represents the chronological order. To this end, each basis-sample was immediately split up into two subsamples of which one was centrifuged (3000 RPM for 3 min). The supernatant of the centrifuged subsample and the untreated subsamples were each again split to cover the two grid points (e.g., S11, S12). For each design and each grid point, 250 ml of media was used and constantly recirculated in a closed loop through the flow cell. Nitrate levels were elevated with 0, 300, 600, or 900 mg N/L by spiking 5ml NaNO₃-salt (1.06537.1000, Merck KGaA, Darmstadt, Germany) stock solution. Nitrite levels were elevated with 0, 25, 50, or 75 mg N/L by spiking 1 ml of NaNO₂-salt (8.22285.5000, Merck KGaA, Darmstadt, Germany) stock solution. To ensure comparable dilutions effect in the media, the volume of spiked stock solution or distilled water (for 0 mg N/L additions) was kept constant (5 ml for nitrate and 1 ml for nitrite) and the concentration level were adapted. The spiking of nitrite tries to break all potential correlations with the other absorbing non-target species. The spiking of nitrate breaks also all correlations with the other absorbing non-target species and enhances the contrast of nitrite to nitrate.

1.2.3.3 Nitrite degradation test experiment

The nitrite degradation test experiment (Fig. 1.2 green, left facing triangles) was executed by spiking nitrite in form of a NaNO_2 -salt (8.22285.5000, Merck KGaA, Darmstadt, Germany) stock solution into the continuously operated reactor with nitrite concentrations below 1 mg N/L at constant pH (5.9). Here the concentration of the stock solution was constant as the calculated dilution effects were marginal. After each spike of nitrite the NOB degraded the nitrite completely before the next nitrite addition. Three times the five concentrations (15, 30, 45, 60, and 75 mg N/L) were spiked in random order resulting in three sampling series (during 04.10.2017-24.11.2017). Only the samples taken shortly after the spiking of nitrite (i.e., 25 min later to ensure mixing) were considered for this test (Fig. 1.2 right/green triangle). If nitrite is only present in the reactor for only a short period of time it is assumed that indirect effects on the absorbance from the presence of nitrite are largely reduced. In-between the three series the reactor was operated as described in 1.2.3.1 with multiple nitrite events.

1.2.3.4 Analysis of effects

The presented experiments result in the four most relevant variations that are investigated in this study.

- (i) Slow variations are most likely dominated by dynamics in concentrations caused by variations in the influent composition (i.e., biomass adaptation, organics, nitrate). These are captured in all but the In-situ ST set. The Ex-situ woBM set will only capture slow variations of the soluble non-target species.
- (ii) Short-term variations of the non-target absorbing species are presumably dominated by processes correlated with a nitrite accumulation: Nitrate concentrations will likely decrease when nitrite is accumulated. Furthermore, concentrations of organics are likely to change when inhibition leads to an enhanced decay rate of the NOB population. They are specifically present in the In-situ ST data. The In-situ LT data will likely capture these effects as well. However, the design is not aimed at capturing them in a representative manner. The same applies for Test 1.
- (iii) The scattering and absorbance of biomass and other solids is present in all but the Ex-situ woBM set. Removal of solids might reduce the noise in the measurement and in turn improves the model calibration.
- (iv) Representing a contrast of nitrate and nitrite from all other non-target species prevalent in the nitrification process should avoid model deterioration by influent driven changes in the non-target species composition (i.e. decorrelation of species). Nitrate is the only full controllable non-target species.

The effects are present in the ex-situ data and partly in the Test 2 data. These effects are analysed based on the two test data sets. In Test 1, most of the effects can be already separated. Test 2 is focused on identifying if and how indirect effects in the spectrum caused by nitrite, affect the different models. Furthermore, the effects of LDC and the wavelength reduction on the different model performances were evaluated and may further inform about the relevant factors and supposedly also explain why the effects listed above are important or not.

Table 1.2: Presence of variations in the four different experimental designs for calibration and the experimental designs for the two test data sets.

Variations	Slow variations	Short-term variations	Scattering by solids & biomass	Nitrate contrast to all other species	Nitrite contrast to all other species
Data set					
Ex-situ with biomass	Yes	No	Yes	Yes	Yes
Ex-situ without biomass	Yes	No	No	Yes	Yes
In-situ long-term	Yes	No ^a	Yes	No	No
In-situ short-term	No	Yes	Yes	No	No
Test 1 (In-situ)	Yes	No	Yes	No	No
Test 2 (Nitrite degradation)	Yes	No	Yes	No	Yes

^a The design focuses on other variations that should dominate the data set. However, the design does not exclude these variations completely.

1.2.4 Modelling

1.2.4.1 Data

All data sets consist of pairs of a single nitrite species concentration measurement and six spectra. We refer to such a pair as a *sample*. The six spectra are considered as replicates of each other and were recorded three minutes before until two minutes after the sampling was executed. The six spectra are averaged prior to the analysis. Due to potential saturation effects in the low UV range, making the Beer-Lambert law inadmissible only wavelengths from 300 nm till 730nm are selected Mašić et al. (2015). The spectra were visually checked on outliers, which were removed prior to the analysis (only for Ex-situ woBM and LDC).

1.2.4.2 Model calibration

For an effective comparison across the different calibration data sets, the procedure illustrated in Fig. 1.3 is repeated with all four calibration data sets separately. First, the calibration data are used to obtain the original model (OM) with the spectra as the input data and the nitrite measurements as the output data. Then, the procedure makes use of a LDC data set, which is used to produce two additional models, the intercept-corrected model (ICM) and the intercept-and-slope-corrected model (ISCM). In a final step, the three resulting models per calibration data set are tested with independent test data sets.

The model identification step for the OMs consists of mean centring, PCA decomposition, and regression of the nitrite concentration measurements to the principal scores (in this order). To identify the relevant number of components the cross-validated (CV) mean squared error (MSE) for each number of principal components (PC) is computed with samples assigned evenly yet randomly to 4 folds.

$$MSE = \frac{\sum_i^N (y_{ref,i} - y_{pred,i})^2}{N} \quad (1.2)$$

As in Mašić et al. (2015), model selection is executed with the 1-standard-deviation rule (Hastie et al., 2009), i.e. selecting the least complex model producing an MSE within one standard deviation of the minimal MSE. For the detailed mathematical description of the practical implementation we refer to Appendix A of Mašić et al. (2015). The use of a 4-fold cross-validation (CV) rather than leave-one-out-CV constitutes the only difference from the method presented in Mašić et al. (2015). The LDC step consists of a simple linear regression of the OM output onto the six LDC samples. The obtained slope and/or intercept of the model function is then used to correct the predictions of the OMs. The model structure for the linear design correction is the following:

$$y_{pred,LDC} = a + b * x_{pred,OM} \quad (1.3)$$

The slope b and intercept a of the ISCM is calculated as follows. $x_{pred,OM}$ are the predictions of the OM based on the LDC spectra and $y_{ref,LDC}$ are the nitrite measurements of the LDC data set

$$b = \frac{\sum_i (x_{pred,OM,i} - \bar{x}_{pred,OM}) * (y_{ref,LDC,i} - \bar{y}_{ref,LDC})}{\sum_i (x_{pred,OM,i} - \bar{x}_{pred,OM})^2} \quad (1.4)$$

$$a = \bar{x}_{pred,OM} - b * \bar{y}_{ref,LDC} \quad (1.5)$$

For the ICM the value of b is assumed known and equal to 1 and a is then computed accordingly. Each model (OM, ICM, and ISCM) is characterised for each test data set by a root mean squared error (RMSE) of the predicted test nitrite concentrations in mg N/L as:

$$RMSE = \sqrt{\frac{\sum_i^N (y_{ref,i} - y_{pred,i})^2}{N}} \quad (1.6)$$

1.2.4.3 Modelling for result interpretation

Wavelength selection To further study the effect of non-target species in particular in the visible range, the modelling was repeated with the same underlying data but a reduced wavelength range. Wavelengths above 400 nm were discarded to remove the wavelengths which only contain information about organics and solids and in turn maximise the variation in the spectra that can be explained through variations of the nitrite concentrations. These models are further referred to as *UV-models*; the full wavelength range models as *UV-Vis models*.

Modelling for identification of indirect nitrite effects on absorbance The drastic difference in performance of the In-situ ST model between Test 1 and Test 2 (details below) gives rise to the question if missing indirect nitrite effects in Test 2 caused the poor performance of all the In-situ ST models. To test if such indirect nitrite effects are actually represented in the In-situ ST set another modelling exercise was executed in three steps: First the modelling was reversed in the sense that absorbance of each wavelength is regressed against the nitrite species measurements (Beer-Lambert law in Eq. 1.1). The Test 2 data set is used for this as it only contains direct nitrite information. Eq. 1.3 above shows the formula used to obtain the model. In this case, y is the absorbance measurement at one wavelength and x is the corresponding nitrite measurement. The 41 resulting linear models (i.e., one per wavelength) should ideally represent the direct nitrite effect on the absorbance measurements only. In a second step these models are then used to predict the spectra of the In-situ ST data set based on the nitrite measurements. These predicted spectra are then subtracted from the measure spectra to produce *residual spectra*. These residual spectra should not contain any direct nitrite effects anymore. In a third step, these residual spectra and the corresponding nitrite measurements are then used to calibrate a model with the same 4-fold cross-validated PCA/PCR steps as used for the original model calibration. If a model is found that explains the nitrite variations then it can be concluded that the residual spectra for the In-situ ST data set contain indirect information about the nitrite concentration.

Uncertainty of the RMSE To differentiate the influence of bias and variance on the RMSE, the uncertainty of the RMSE is evaluated. To this end, a 100'000-fold bootstrapping (*bootstrap* function in Matlab 2015a) is executed to estimate the standard deviation of the prediction errors. At 100'000 steps, a convergence of averaged standard deviation down to two decimal places was observed.

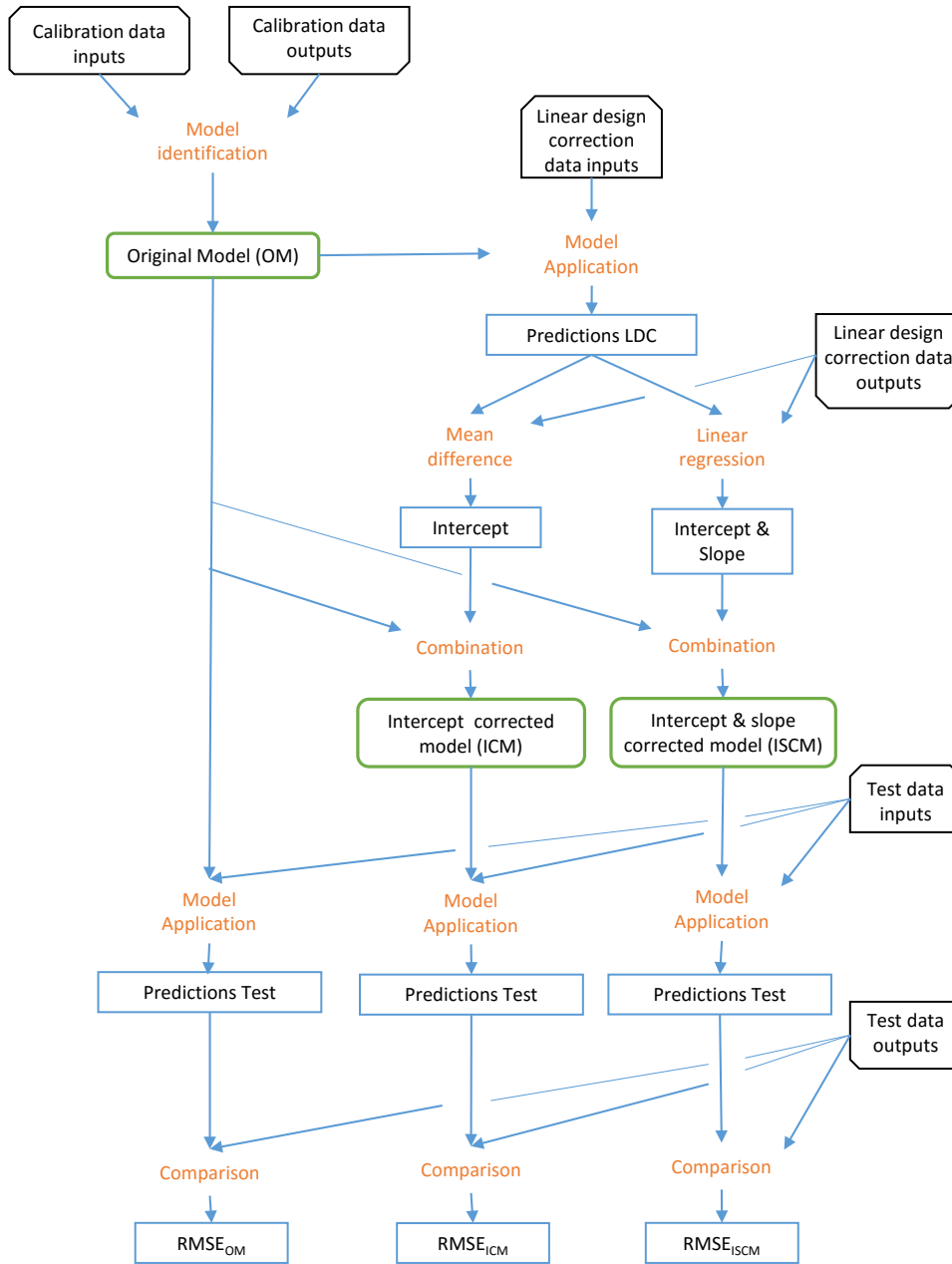


Figure 1.3: Model calibration and model test procedure. Black top edges cut rectangle: Data set inputs (spectra), Black bottom edges cut rectangle: Data set outputs (nitrite measurements), Unframed orange: Data processing, Rounded green boxes: Resulting models, Blue rectangle: Results.

1.3 Results

1.3.1 Model calibration and linear design correction results

For the UV and the UV-Vis case, the model with the lowest MSE in the cross-validation is the In-situ ST followed by Ex-situ wBM, the Ex-situ woBM and the In-situ LT. Figures showing the MSE as a function of the number of PCs for each data set in UV-Vis and UV can be found in the Appendix A.1. Table 1.3 shows the selected number of PCs (#PC): The in-situ models are less complex than the ex-situ models for the UV-Vis case. For the UV case, the in-situ models exhibit the same or an increased complexity while the ex-situ models have two PCs less than in the UV-Vis case.

Table 1.3 also lists the slope, intercept for ISCMs, and intercept for the ICMs. Ideally, the computed intercepts and slopes should be 0, respectively 1. Within the UV-Vis models, the effects of the intercept are most relevant for the Ex-situ woBM and the In-situ LT. The Ex-situ wBM ISCMs and the In-situ ST ISCMs exhibit a similar model performance change with the correction of the intercept as with the slope correction. For the UV case, the intercepts get closer to zero for all models while the slopes do not show a uniform change. The most substantial differences between the UV-Vis case and the UV case in terms of intercept and slope values exhibits the Ex-situ woBM model.

1.3.2 Model test results

For each test and calibration design three RMSE values in mg NO_2^- -N/L are plotted: For the original model (OM), for the intercept corrected model (ICM) and for the intercept and slope corrected model (ISCM). In Test 1 for the UV-Vis models (Fig. 1.4 left) the Ex-situ wBM ICM performs best with an RMSE of 5.14 mg NO_2^- -N/L. A similar performance have Ex-situ woBM ICM and In-situ ST ICM (RMSE < 8.6 mg NO_2^- -N/L). All other models have an RMSE larger than 10 mg NO_2^- -N/L. The worst performance is recorded for the Ex-situ woBM ISCM with an RMSE of 451 mg NO_2^- -N/L. This indicates a failure in the slope correction of Ex-situ woBM, which can be related to the large deviation of the slope from the ideal value (cf. Table 1.3). All In-Situ LT models have a high RMSE (>20 mg NO_2^- -N/L). Except for the Ex-situ woBM models, the best models are always the ICMs followed by the ISCMs and the OMs.

The reduction of wavelengths to the UV range has substantial effects on almost all models (Fig. 1.4 centre). The ICM Ex-situ wBM still performs best (RMSE: 4.78 mg NO_2^- -N/L). The most substantial improvements are however exhibited by the three Ex-situ woBM models. All In-situ LT models show a reduced RMSE compared to the UV-Vis case. For the In-situ ST and Ex-situ wBM models no clear tendency in the RMSE change is observed. This is not true anymore for Test 2 (Fig. 1.4 left). The Ex-situ wBM model still performs consistently well and even better in terms of the OM, while the In-situ ST prediction quality degrades in all models compared to Test 1. The Ex-situ woBM model performs worse than in Test 1 while the In-situ LT errors shows no uniform change.

Table 1.3: Model characteristics for UV-Vis and UV models. Number of principal components (#PC), slope and intercept from the linear fit of the original model predictions on the nitrite measurements from linear design correction data set (rounded numbers).

Range	300 nm -730 nm (UV-Vis)			300 nm -400 nm (UV)		
	Original model	Intercept and slope corrected model	Intercept corrected model	Original model	Intercept and slope corrected model	Intercept corrected model
Design	#PC	Intercept [mg N/L]	Slope [mg N/mg N]	Intercept [mg N/L]	Slope [mg N/mg N]	Intercept [mg N/L]
Ex-situ with biomass	7	-16.61	0.83	-18.82	0.74	-18.57
Ex-situ without biomass	6	81.32	0.19	70.51	0.49	-2.89
In-situ long-term	5	-35.92	0.77	-38.93	0.79	-18.47
In-situ short-term	3	-12.85	1.43	-7.14	1.09	0.9

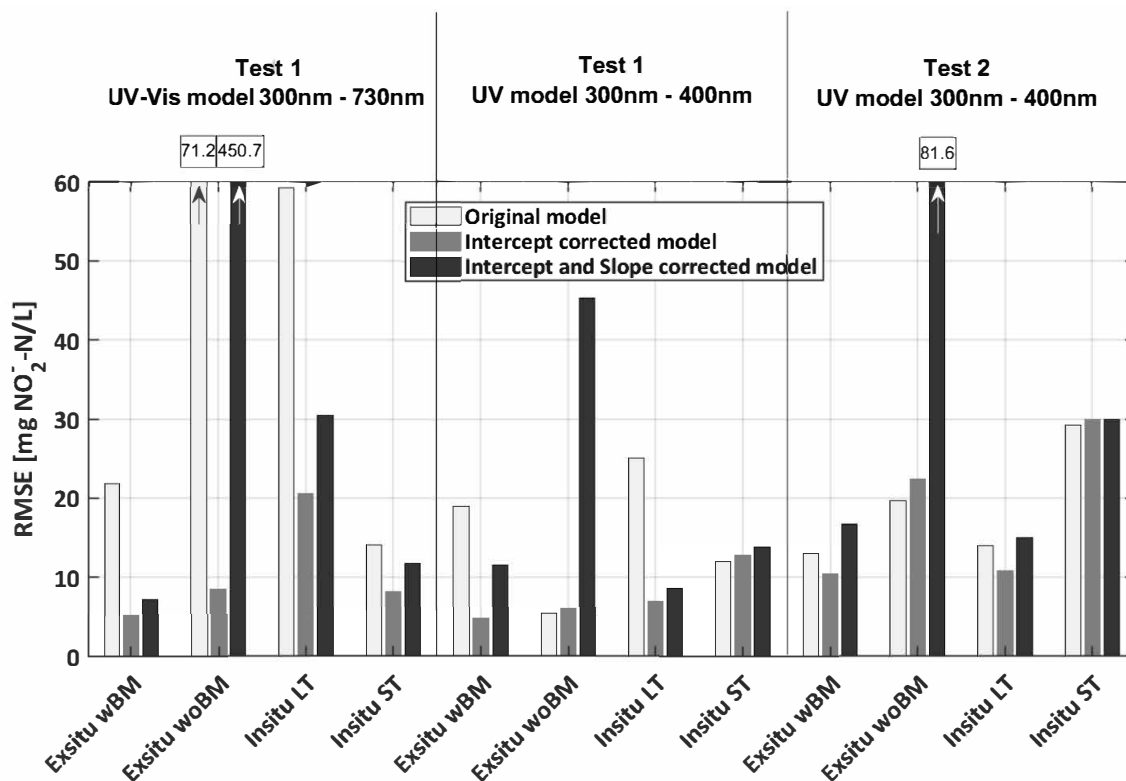


Figure 1.4: Root mean squared error of model prediction: left section UV-Vis models applied on Test 1. Centre section UV models applied to Test 1. Right part UV models applied on Test 2. Each design has three RMSEs, one from the original model (light grey), one from the intercept corrected model (grey) and one from the intercept and slope corrected model (dark grey).

1.3.3 Intermediate conclusions

To explain the analysis below, the following intermediate conclusions are drawn based on the result presented so far:

- (i) Capturing slow variations of nitrate, biomass, and organics is not crucial for the experimental design. The In-situ ST data set, which does not capture such variations, lead to similar or even better model performance compared to calibration experiments designed to capture these slow variations.
- (ii) Capturing the short-term dynamics of nitrite can lead to good model performance. The Ex-situ wBM results reveal that neglecting the short term dynamics can also lead to a good model performance. Thus, intentionally breaking the correlations of the target species concentration with other absorbing species concentrations results in similar performance as increasing the importance of such correlations by artificially induced process dynamics.
- (iii) Statement (ii) is closely related to another effect included in the ex-situ designs: The ex-situ models in which the nitrate concentration is maximally decorrelated from all other species concentration do not necessarily perform better than the in-situ models.
- (iv) Scattering and absorbance by solids is a relevant factor. The removal of solids during model identification in order to avoid scattering and have a less noisy signal is not recommended.

- (v) Correcting the offset of the predictions subsequent to the PCR calibration by LDC helps almost all models improving their performance. However, the wavelength selection can already remove many of the effects compensated by LDC and thus render the LDC useless.
- (vi) Wavelength selection prior to the modelling seems to be crucial to achieve best possible model performances. The conclusions (ii), (iii), (iv), and (v) are further investigated in the two following paragraphs.

1.3.4 Detailed inspections

1.3.4.1 Bias and variance in predictions

The improvement in Test 1 RMSEs when reducing the wavelength range has a dramatic effect on the performance of all models. This therefore deserves further inspection. The improvement of a model by discarding information in the calibration is counterintuitive as less information is available that the model can be built upon. Furthermore, one would also expect that the principal component regression would discard irrelevant, noisy information. As this clearly did not occur, this section presents results that can partly explain these phenomena.

The ICM seem to compensate a lot of the OMs error for the UV-Vis models. Thus, bias is the main driver for the large errors for some OMs. However, in the case of Ex-situ woBM the reduction of the RMSE by discarding the visible part of the spectrum goes beyond the improvements that are achieved by the ICM in the UV-Vis case. Thus, part of the error is caused by variance. Comparing the uncertainty of the OMs' RMSEs in the UV case shows reduced standard deviation for all but the Ex-situ wBM model (4.43 to 4.73 mg NO₂⁻-N/L). The In-situ ST (6.02 to 4.84 mg NO₂⁻-N/L) and the In-situ LT (4.06 to 2.60 mg NO₂⁻-N/L) improve their precision. The most substantial effect is found for the Ex-situ woBM model with a reduction of the standard deviation of the RMSE from 8.43 to 2.79 mg NO₂⁻-N/L. It has to be noted that even in the case of the Ex-situ woBM these numbers are still one order of magnitude lower than the error caused by bias. Nevertheless, the improvements are substantial looking at the remaining RMSEs of the UV models. To understand what factors cause this variance reduction in the UV models, the model structures of the UV-Vis models are investigated: In Fig. 1.5 the first four PCs of the UV-Vis models are shown.

The first and therefore most important eigenvector of the Ex-situ woBM differs from the other three models (Ex-situ wBM, In-situ LT, In-situ ST), which have similar eigenvectors. Thus, it is highly likely that the first eigenvector in these three models mainly represents the variance in the data sets caused by solids, in particular as the weighing is relatively uniform over the whole wavelength range. Furthermore, all components seem to be most sensitive in the UV range and to be less smooth in the visible range. The missing smoothness is counter-intuitive considering that neighbouring wavelengths are highly correlated, which should lead to a smooth weighing by the eigenvectors. Thus discarding these wavelengths also discard the effect that causes the non-smooth behaviour of the eigenvectors. One potential explanation for this non-smooth behaviour could be the correlated measurement errors of neighbouring wavelengths, which leads to non-linear effects in the data set. In such cases, models that do not assume independent measurement errors, such as maximum likelihood PCA Wentzell et al. (1997), could be used. This is considered out of scope for this study.

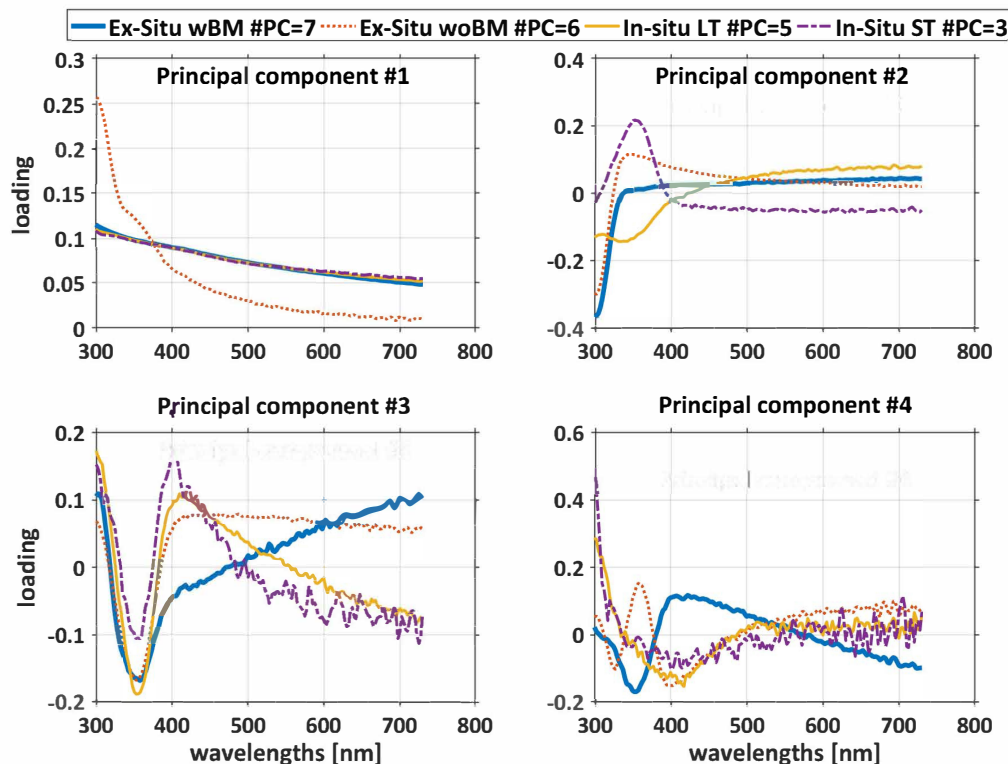


Figure 1.5: First four principal components of the four models plotted against the wavelengths. In-situ ST model only consists of three selected components. All models except Ex-situ woBM have almost completely overlapping first component (top left).

1.3.4.2 Correlation with nitrite affected non-target species

The In-situ ST performs well in Test 1 but fails to meet the same performance in Test 2. In Test 2 presumably only the direct effect of nitrite is represented in the absorbance spectra. The analysis of the residuals of In-situ ST OM in Test 2 (Fig. 1.6) reveals that the offset is increasing with time. More important is that the measurement errors within the three single series (five grouped measurements Fig. 1.6, right) are dependent on the actual concentrations (Fig. 1.6, left).

There were two phenomena observed during the Test 2 phase. First, the nitrate level became elevated most likely due to the surplus of nitrite that was oxidised during this experiment (from around 2250 to 2450 mg N/L). Nitrate has a major effect on the spectra and therefore may affect the model predictions. Second, the total suspended solids concentration was decreasing during this period. These two phenomena might explain why the offset of the measurement was increasing with time but they cannot explain why the residuals are correlated with the nitrite concentration. We hypothesize that the correlation of the residuals with nitrite comes from indirect nitrite effects, which were present in the In-situ ST design but do not appear in the Test 2 data set (section 2.3.3). As the samples for Test 2 were taken right after the spiking of nitrite there was no time for inducing such indirect effects in the process and in turn influence the spectrum accordingly. Thus, the information in the spectra about the nitrite concentration in this test experiment is only influenced by the direct absorbance effect of nitrite. In the In-situ ST data set, indirect effects such as correlation between the nitrite and nitrate concentrations, are likely more relevant. To this end, this hypothesis was further investigated as described in Section 1.2.4.3.

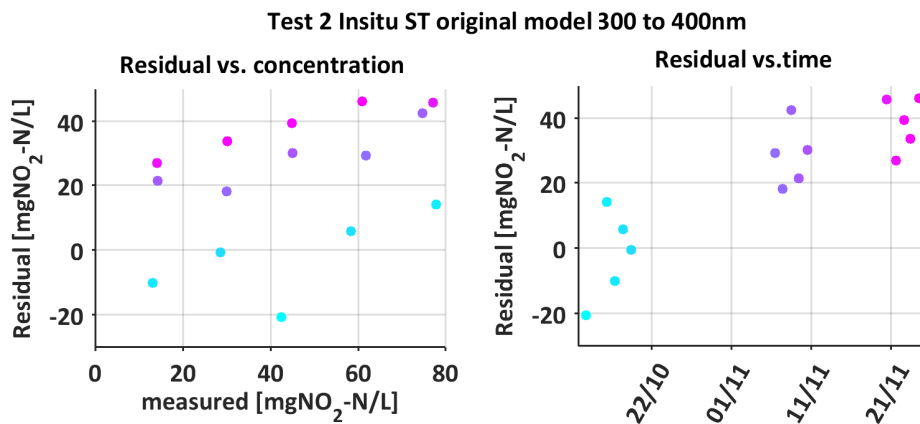


Figure 1.6: Residuals of Test 2 predictions with In-situ short-term original model. Right: Residuals plotted against nitrite measurement, Left: Residuals plotted against time. Colours indicate the time and group the predictions of the three single experimental series.

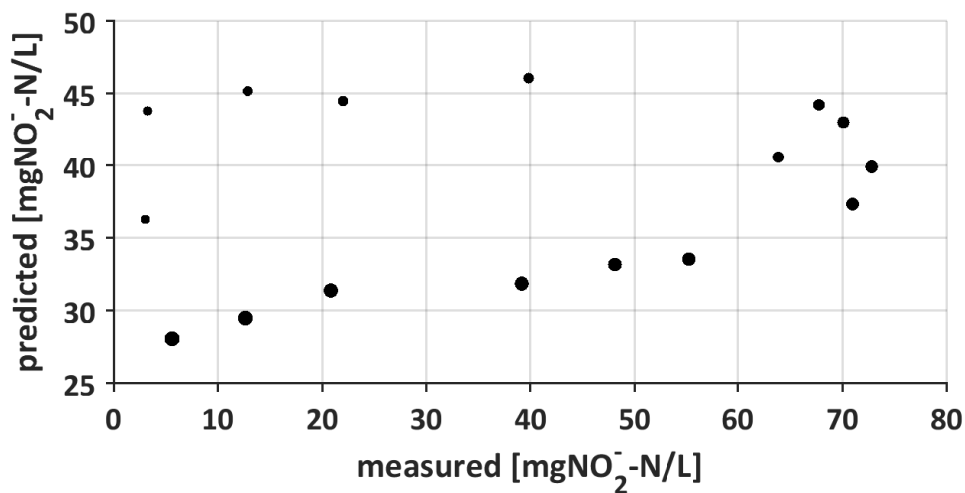


Figure 1.7: Nitrite predictions based on a PCA/PCR model with the residual spectra from the-situ ST data set that should not contain any information about nitrite. The size corresponds to timestamp of sample. Early samples are small, last samples are large.

Fig. 1.7 shows the predicted nitrite concentrations of the PCR model obtained with the residual spectra of In-situ ST data set, which should not contain any direct nitrite effects. In the first part of the event (smaller dots), the predictions do not follow the measured nitrite concentrations but the longer the nitrite has been present in elevated concentrations (bigger dots) the more the trend of the prediction follows the trend of the nitrite measurements. The results reveal that there are still some indirect nitrite effects in the residual spectrum present. Thus, it can be concluded that the In-situ ST also captures indirect nitrite effects. These modelled indirect effects likely make the model more robust in the case of Test 1 (same design as In-situ ST) but sensitive to changes in these indirect effects, as observed during Test 2.

1.4 Discussion

1.4.1 Influence of solids and visible wavelength range

Despite different calibration designs, all models considering solids and biomass have a surprisingly similar first (i.e., most important) principal component (PC). This PC presumably covers the variance caused by the solids. The rather uniform shape of the PC is also in line with knowledge that all wavelengths are absorbed and scattered by solids. At first sight, such a PC seems to be required even if not sufficient to have a representative model structure when solids are present.

The subsequent tests with the UV models show that the prediction performance improves when discarding wavelengths without direct nitrite information, especially for the Ex-situ woBM design. The bias and variance is reduced. Thus, there are two points to consider: First, the improvement of the prediction performances by discarding data that theoretically follows the linear Beer-Lambert law in the model calibration is counterintuitive. Given the principle of PCA/PCR one would assume that non-target related variance that is captured in the PCA step will be discarded in the PCR step. However, this is not the case. One potential reason could be the representation of non-linear effects (i.e., limit of detection, saturation) in the data set. Based on the results, it is recommended not only to fine-tune the number of PCs but also the selection of wavelengths. This step can be either based on expert knowledge (i.e., as presented here) or automatically executed. When done automatically, the wavelengths can be either selected prior to the model identification (e.g., bootstrapping) or by selecting a method for model calibration that includes regularization (e.g., sparse PCA-based regression (Zou et al., 2006) or LASSO regression (Tibshirani, 1996)).

Second, the scattering of light (Thomas et al., 2017) by solids and biomass might also play a role. The results suggest that there are two ways to deal with it: One way is to include solids and biomass in the design (all but Ex-situ woBM) and reach a relatively good accuracy either with ex-situ or in-situ designs. The other way is to account for the solids and biomass only in the UV range and neglect the visible range in which the scattering is much more dominant due to the low total absorbance. The current results with similar lowest RMSEs for both ways to handle biomass and solids indicate that the removal cannot be recommended as it requires more effort without guaranteeing enhanced model performance. This decision naturally also depends on the location of the absorbance spectra of target species.

1.4.2 In-situ calibration performance

The effects seen in the In-situ ST models in Test 1 reveal that it is possible to reach the same accuracy for in-line UV-Vis SPMs with a simple in-situ calibration experiment, despite neglecting the slow variations caused by the biomass fractions, organics, and nitrate. The In-situ ST calibration experiments have the fundamental advantage that the effort is reduced, as there is no need for laboratory work such as producing stock solution or installing additional equipment. Furthermore, the data generation happens at one point in time and does not require repeated sampling over a longer period as the executed ex-situ design. However, it can only be speculated if neglecting the slow variations by conducting the ex-situ experiment with only one basis-sample for all 16 data points would perform worse than the executed experiment with eight staggered basis-samples.

The In-situ ST design however, exhibits a poor performance under special circumstances. One such circumstance appears when the correlations between species concentrations present during the model

calibration are absent during model application and testing. In the case of nitrite estimation in urine nitrification, the risk of this phenomenon is relatively low. First, the source-separated urine fed to the reactor is relatively homogenous in its composition. This makes it easier to identify the nitrite dynamics as the accumulation of nitrite is a relatively large disruption to the process, which in turn strongly affects the absorbance spectra. Second, the target species nitrite is an intermediary product of the process in the system. Thus, correlations caused by the process are at least partly caused by a hidden latent variable (i.e., nitrite inhibition). For the same process set-up the causality should therefore be persistent over time. In general, one should evaluate two characteristics of the system aimed to monitor with the SPM, when considering in-situ design: First, how pronounced are the variations of the target species compared to other sources of variations (e.g., nitrite accumulation vs. inflow variations) and second, how many correlated groups of non-target species have to be ruled out (variations of medium composition). In a system with many such groups (e.g., municipal wastewater with different industrial dischargers), the in-situ design requires lot of samples to represent all sources of variations in the spectra. Thus, it may be better to break as much correlations as possible by picking an ex-situ design. In systems, which have a rather determined behaviour and pronounced variations of the target species (e.g., process product) in-situ design should be considered (e.g., side stream processes).

Comparison of the in-situ designs for calibration with each other indicates that a more controlled representative experimental design applied at one point in time is more promising than a less controlled sampling campaign over a longer period. One could expect that using the same method to elevate the nitrite concentrations and covering the same nitrite concentration range would lead to similar performances independent of the time range in which the data set is produced. However, it seems that the In-situ LT data apparently does not represent the relevant variations in the system as accurately as the In-situ ST data.

1.4.3 Bias reduction by linear correction

The intercept correction determined with a simple linear regression of the residuals of six independent samples (LDC) predicted by the OMs, improves the predictions of all models. This is less of a surprise for the ex-situ models in particularly the Ex-situ woBM. The ex-situ models were calibrated with very different experimental designs than the test data sets were obtained with, which makes most likely any kind of adaptation towards the test experiment designs favourable. However, for the in-situ models that were calibrated and tested within the very same reactor and experimental design, the effect is surprisingly strong. The UV model results, however, indicate that the in-situ models suffered as well from inclusion of the visible part of the spectrum. This might explain why also these models profited from a linear correction. The general improvements by LDC and by the wavelength selection indicate that an intelligent pre-processing of the data prior to the model calibration is an effective way to improve prediction quality. Consequently, the model calibration process should be complemented with a preceding automated or expert based wavelengths selection step. A systematic approach to select among the vast amount of feasible pre-processing steps (e.g., variable selection (Jolliffe et al., 2003), centring and scaling (Gurden et al., 2001), wavelet decomposition (Rosen and Lennox, 2001), functional analysis (Mears et al., 2016)) is however lacking today.

The slope correction was deteriorating almost all model predictions. This is most likely caused by the limited concentration range of the underlying LDC samples, which did not fully represent the application range and therefore led to extrapolation errors.

1.5 Conclusions

In this study, four different experimental designs to record calibration data sets for an in-line UV-Vis spectrophotometer (SPM) calibration were developed, executed, and tested on independent data sets. All four designs were executed with the same urine nitrification reactor. These are the conclusions:

- (i) Capturing the exact process variations expected during sensor use within the calibration data set proves very useful for in-situ model calibration. The benefits of this are explained by the presence of correlation between the concentrations of absorbing target and absorbing non-target species. Classic experimental designs break such correlations by spiking with standard solutions (corresponds to Hypothesis #1).
- (ii) Slow variations of the non-target species in the process can be neglected for systems in which the target species variations are the most dominant variation (corresponds to Hypothesis #2).
- (iii) The selection of wavelengths was identified as one way to compensate for effects of solids and biomass. Including or excluding solids in the experimental design has large impacts on predictions errors. These errors are largely explained as model bias. However, the inadvisable decision to exclude solids and biomass can also be corrected with a posteriori by wavelength selection or an additional (linear) correction of the predictions in the model application (corresponds to Hypothesis #3).
- (iv) The short-term in-situ experiment rather than in-situ long-term or ex-situ experiment is the favoured approach to collect calibration data for spectrophotometric monitoring of a urine nitrification process (corresponds to Hypothesis #1).

Acknowledgement

The authors want to thank Kito Ohmura and Marco Kipf for their assistance with the experiments and Claudia Bänninger, Karin Rotterman and Sylvia Richter for their assistance with the laboratory analysis. This research was made possible by the Swiss National Foundation (Project: 157097).

2 Oxygen uptake rate and proton production rate in urine nitrification: What do they tell us about nitrite concentrations?

This chapter has been authored by:

Thürlimann, C. M.^{a,b,c,d,e}, Udert, K. M.^{a,e}, Morgenroth E.^{a,e}, Villez, K.^{a,c,e}

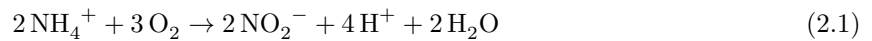
^aStudy concept and design, ^bAcquisition and analysis of data, ^cInterpretation of data, ^dDrafting of chapter, ^eCritical revision.

2.1 Introduction

Nitrite detection in nitrification is a key element for process stability (e.g., Gujer, 2010; Fumasoli et al., 2016). Measuring nitrite online is costly however. Thus, finding a robust and cheap nitrite soft-sensor is key to facilitate higher level of automation and deeper understanding for nitrification processes. In contrast to Chapter 1, where nitrite concentration estimates are derived from absorbance of ultraviolet light by nitrite directly, in this chapter, the potential of a nitrite soft-sensor based on stoichiometry in high strength wastewater is assessed.

For industrial bio-processes, stoichiometry based soft-sensors are widely studied (e.g. Luttmann et al., 2012), but there is little research in the field of wastewater treatment. Villez et al. (2019) mentioned the potential of *extents* (i.e., stoichiometric balance) for soft-sensors. Other balances such as mass balances have been studied as a method to obtain additional information (e.g. Villez et al., 2016).

Nitrite identification in nitrification processes based on stoichiometry requires separating ammonia oxidising bacteria (AOB) activity Eq. 2.1 and nitrite oxidising bacteria (NOB) activity Eq. 2.2.



The equations show that both bacteria AOB and NOB consume oxygen and thus contribute to the oxygen uptake rate (OUR). The higher their activities, the higher the OUR. However, only the AOB produce protons when they oxidise ammonia to nitrite. This influences in turn the pH. It has to be noted that this approach considers exclusively the catabolic processes and neglects the anabolic processes required to maintain the nitrification activity.

If the AOB activity remains constant and the NOB activity changes, we expect changes in the OUR but not in the PPR. If however, the AOB activity changes and the NOB activity remains stable, we expect dynamics in both PPR and OUR. Consequently, we hypothesize that the ratio of proton production rate (PPR) (i.e., pH signal derivative shortly before a new feeding) over the OUR (i.e., DO signal derivative in non-aerated phases) allows monitoring the ratio of AOB activity to the sum of the AOB and the NOB activity. This in turn informs about mismatches between the activities of the two bacteria groups and thus should allow to derive information about nitrite concentrations. The ratio of PPR to OUR is further referred to PPR2OUR (Eq. 2.3).

$$PPR2OUR = \frac{PPR}{OUR} \quad (2.3)$$

Since decades, online pH and DO signals and their first derivative have been used to characterise and control nitrification processes. OUR is a key variable to determine kinetics of single bacterial groups (e.g. Spanjers and Vanrolleghem, 1995). In such cases, the absolute values are relevant and thus high precision is required. OUR has also been used to monitor the completion of nutrient removal in aerobic treatment of wastewater in sequencing batch reactors (e.g. Jaramillo et al., 2018). In this case, the trend in the OUR is of interest.

PPR has also been widely studied for control of nitrification (e.g. Won and Ra, 2011). For both OUR and PPR the literature focuses mainly on sequenced processes (e.g., sequencing batch reactors) within which short-term signal dynamics are easier to interpret than in continuous processes. An example of using pH for nitrification control in a continuous system is given in Chapter 4.

OUR and PPR are normally determined in phases in which disturbances on the raw sensor signal by irrelevant effects are minimised. For OUR calculation, non-aerated phases where DO concentration is solely influenced by oxygen consumption are considered. The PPR is determined in phases in which the proton balance is almost solely influenced by the AOB growth. Interestingly, also for the PPR active aeration is a disturbance due to the CO_2 that is stripped then. Thus, intermittent feeding and aeration are considered the simplest way of deliberately inducing these conditions.

However, in practice, neither PPR nor OUR are exclusively determined by AOB and NOB activity. Buffer systems act as a source or sink for the protons based on their acid dissociation constant K_a and the pH in the bulk. Consequently, not all protons produced by AOB end up in the bulk and in turn are also not accounted for in the pH signal. For source-separated urine, Udert (2002) reported that the most relevant buffer systems in urine are bicarbonate and ammonia. Despite these buffer systems, the AOB population can be successfully controlled by pH controlled feeding (e.g., Udert et al., 2003; Sun et al., 2012). Thus, it is safe to assume that the proton production rate (PPR) is related to the ammonia oxidation rate. However, a simulation in a modelling environment shows that alkalinity consumption caused by nitrification activity and the proton concentration do not exhibit a fixed proportional relation over the relevant pH range (cf. Appendix B.1 Fig. B.1). While the alkalinity consumption is almost linearly dependent on the pH in the reactor, the bulk proton concentration exhibits per definition a logarithmic relation to the pH. Consequently, significant changes in the pH will change the relation of ammonia oxidation rate and pH slope.

The OUR derived from DO signal is the total OUR of the system. The main factors contributing to the OUR are: (i) the actual oxygen uptake for the oxidation of ammonia and nitrite, which is the oxygen uptake of interest, (ii) the oxidation of organics by heterotrophic bacteria (HET), and (iii) the endogenous respiration of all the biomass.

Consequently, the OUR and PPR signal would only contain the exact information about AOB and NOB activity if the following assumptions hold. (i) the PPR has a globally valid proportionality to the ammonia oxidation rate, (ii) the HET OUR is either stable, has a stable ratio to the total or at least the AOB OUR and (iii) the endogenous respiration is proportional to the total OUR. The information quality of OUR, PPR, and in turn the PPR2OUR signal will decrease the more a system's behaviour deviates from these assumptions.

To assess to what extent the PPR is influenced by buffer systems and the OUR by heterotrophic activity, a scenario in which the expected stoichiometric OUR fractions and stoichiometric proton production is derived and discussed in the result section. Based on the assumption that the inhibition constants for NOB are lower than the ones for AOB (e.g., Zhou et al., 2011), the following three states are expected (cf. Table 2.1). They differ in their nitrite concentration levels.

Table 2.1: States for three different levels of nitrite concentration

	State 1	State 2	State 3
Nitrite concentration	limiting NOB	inhibiting NOB	inhibiting NOB & AOB
AOB sensitivity to nitrite	0	0	–
NOB sensitivity to nitrite	+	–	–
OUR sensitivity to nitrite	+	–	–
PPR sensitivity to nitrite	0	0	–
PPR2OUR sensitivity to nitrite	–	+	?

In state 1 the nitrite concentration range goes from 0 to a rather small concentration (reportedly 5-15 mg N/L in urine nitrification). Hence, the OUR dynamics are expected to be strongest when the nitrite starts to accumulate and the system changes from state 1 to state 2. In this case the NOB are initially less limited by their substrate and the OUR increases relatively to the PPR. Once nitrite starts to inhibit the NOB (i.e., State 2) the OUR decreases again. Eventually, nitrite inhibits not only the NOB but also the AOB (i.e., State 3). In state 3 the quantitative response of the PPR and OUR to nitrite dynamics are unclear. Hence, the sensitivity of PPR2OUR to nitrite remains unclear. However, it is very unlikely that the function describing the relation of PPR2OUR to nitrite is monotonic over the three states.

Two differently designed experiments to induce nitrite dynamics in a lab-scale urine nitrification reactor are executed. OUR and PPR are calculated and visually compared with nitrite reference values and an online UV-Vis based nitrite signal. Visual inspection will reveal if and in what quality information about a mismatch of AOB and NOB activity and consequently nitrite concentration levels can be derived from the PPR and OUR signal.

These are the four main hypotheses of this study:

- (i) PPR2OUR is informative about nitrite concentrations.
- (ii) Dynamics in the PPR2OUR due to nitrite should be mainly driven by the NOB and in turn the OUR.
- (iii) Absolute pH and temperature as measured disturbances do affect the sensitivity of the PPR2OUR to nitrite.
- (iv) Heterotrophic oxygen consumption, endogenous respiration and buffer systems as unmeasured disturbances do affect the sensitivity of the PPR2OUR to nitrite.

2.2 Material and methods

It has to be noted that all the data (i.e., sensor signals, laboratory data etc.) used in this chapter were generated within the very same experiments described in Chapter 1. Therefore, additional and more detailed information about reactor setup and experimental design can be found in Section 1.2.

2.2.1 Reactor setup and operation

The experiments are conducted in a continuous stirred tank reactor nitrifying urine under alkalinity-limited conditions. The source-separated male urine fed to the reactor is collected in the same system as described in Fumasoli et al. (2016), who present a comprehensive composition list of the urine. The COD/N ratio is 0.9-1.

Oxygen is controlled with an on-off controller between 5 mg O₂/L and 6 mg O₂/L. The high oxygen concentration range is not necessary from a process perspective but minimises the risk of denitrification. The feed pump activation is pH controlled. The pH setpoint is either 5.9 for the *spiked nitrite degradation* experiments or 6.1 and 6.6 for the *AOB driven nitrite dynamics* experiment. The feed pump deactivation is time controlled (i.e., 6 s runtime). All sensor and actuator data have a 10 s measurement resolution. The actuator data is based on a cumulative timer, which runs when the actuator is active.

It is important to note that the pH controlled feeding controls the loading according to the AOB activity. Consequently also the COD load to the reactor is depending on the AOB activity.

2.2.2 Experimental design

Two experimental designs are executed to record data with dynamic nitrite concentrations. They differ in terms of how the nitrite concentration is excited.

2.2.2.1 Spiked nitrite degradation experiments

In this experiment nitrite is spiked into the reactor. The pH setpoint is kept constant at 5.9. In turn, all the subsequently observed phenomena are assumed to be caused by the spiked nitrite. The experiment consist of three series. In each series, NaNO_2 stock solution was spiked to reach the following five nitrite concentrations in the reactor, 15, 30, 45, 60, and 75 mg N/L. After each addition, nitrite is degraded below 0.6 mg N/L before the next spiking. In each series the five concentrations had a different sequential order. In the first series (Series 1) the temperature in the reactor is not controlled. Consequently, the temperature in the reactor exhibits the diurnal cycle in temperature of the ambient air (24 – 28°C). In series 2 and series 3, the temperature is controlled at 25°C. More details can be found in Section 1.2.3.3.

2.2.2.2 AOB driven nitrite dynamics experiment

This experiment is conducted in the same reactor as the nitrite spiking experiments. By increasing and decreasing the pH setpoints the AOB activity is increased and decreased in such a way that the nitrite production is either higher or lower than the current maximal nitrite oxidation rate the NOB could exhibit. Consequently, nitrite is either accumulated or degraded. This design leads to a positive correlation of nitrite and the pH. However, we selected two datasets at which the time point of pH change is separated as far as possible from the timepoint of significant nitrite changes. More details can be found in Section 1.2.3.1.

2.2.3 Theoretical steady state calculations

These calculations give a quantitative idea how OUR and PPR are impacted by other factors than the AOB and NOB activity. To assess the expected dynamics in the OUR when the NOB activity changes, two steady state situations are investigated. One with HET activity and one without. For both scenarios, NOB inhibition varies from 0 to 100% in 10% steps. AOB or HET nitrite inhibition is neglected. In both scenarios, the ammonia oxidation rate is fixed at 200 mg N/L/d and a 50% conversion of ammonium is assumed. Consequently, the ammonia loading rate is 400 mg N/L/d. In the feed a COD/N ratio of 1 is assumed. Consequently, 400 mg O_2 /L/d COD is fed to the system. The degradation for COD is assumed to be 80% (Udert et al., 2003). The OUR is calculated based on following numbers: AOB need 3.43 mg O_2 /mg N, NOB need 1.14 mg O_2 /mg N and HET need 1 mg O_2 /mg COD.

Furthermore, the impact of the buffer on the difference between stoichiometric AOB, PPR, and the measured net PPR is compared. These calculations are based on the same scenario as for the OUR calculations. The measured net PPR was determined at a phase in which the ammonia loading rate was at around 400 mg N/L/d.

2.2.4 From pH to proton concentration

Prior to the PPR calculation the pH signal is converted to H^+ concentration (C_{H^+}) (cf. Eq. 2.4). This approximates the definition of the pH, which is the negative of the base 10 logarithm of the *activity* (a_{H^+})

of the hydrogen ion. Since nitrified urine has a stable ionic strength, we do not expect any changes in the proportionality of activity and concentration and thus equate the H^+ concentration with the measured H^+ activity.

$$C_{H^+} a_{H^+} = 10^{-pH} \quad (2.4)$$

2.2.5 Rate calculations

Both OUR and PPR are calculated based on raw DO and pH sensor data, respectively. With the cumulative runtime data for the air valve and the inflow pump the relevant pieces within the DO and pH time series to calculate the rates are identified. Each period from a deactivation of the inflow pump till the subsequent activation is called a *pump cycle*. Similarly, each period from a deactivation of the air valve till the subsequent activation is called a *air valve cycle*. For each pump cycle one PPR and one OUR is calculated.

The PPR is obtained based on the second half of the pH data in a pump cycle. Discarding the first half minimises two potential disturbances: (i) the CO_2 stripping effect due to the oxidation of ready biodegradable COD right after the feeding and (ii) the insufficient mixing of the new feed into the reactor. However, visual inspection of the pH signal reveals that the pH signal is influenced by the aeration thus most likely by CO_2 stripping.

For the OUR calculation only the last air valve cycle that lies fully within the pump cycle is considered. Taking the last cycle minimises the influence of the ready biodegradable COD oxidation at the beginning of the pump cycle. The rate calculation proceeds analogously to the PPR calculations. Only the second half of the DO data of the last air valve cycle is considered.

Both rates are calculated with a linear regression Eq. 2.5. Y is the H^+ concentration or DO concentration data respectively and t is the time. β_1 is then taken as the corresponding rate.

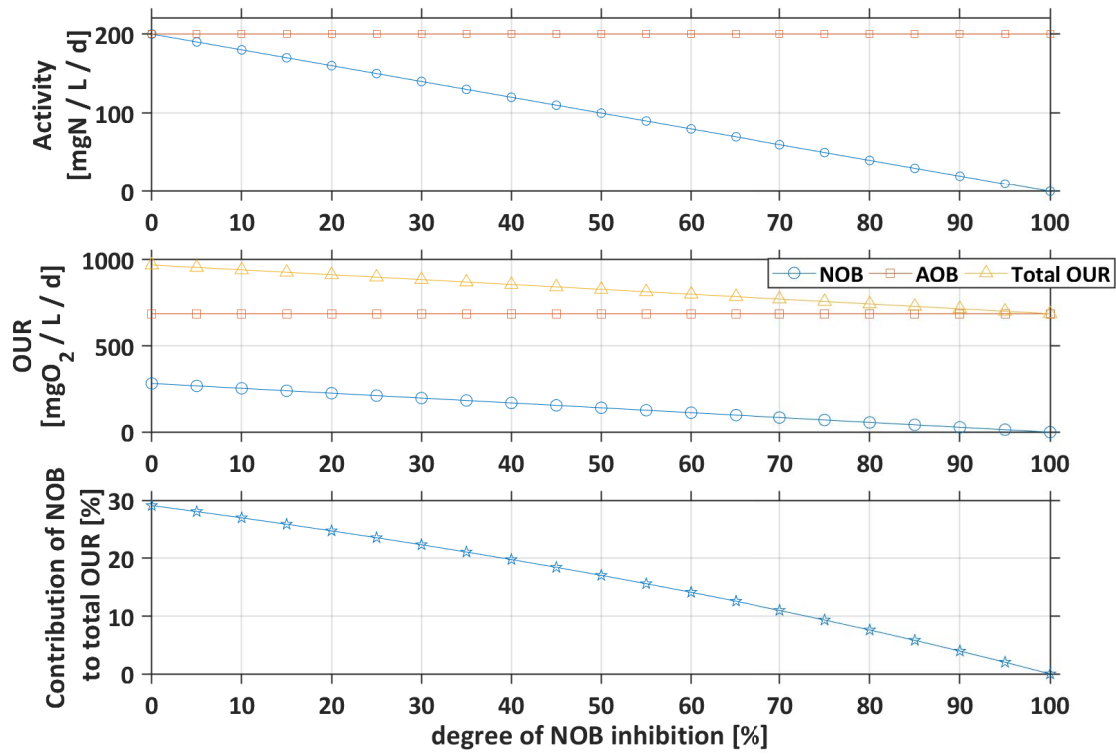
$$Y = \beta_0 + \beta_1 t \quad (2.5)$$

2.3 Results

2.3.1 Relation between OURs of AOB, NOB, and HET

Fig. 2.1a and Fig. 2.1b show two theoretical steady state situations that assess the potential impact of NOB inhibition by nitrite on the OUR: Fig. 2.1a shows calculations in a pure nitrification system (i.e., AOB and NOB) without heterotrophic activity (HET). Fig. 2.1b shows a system with AOB, NOB, and HET activity. The figures show OUR data in dependence of the degree of NOB inhibition. For a nitrification system without HET activity, the stoichiometry reveals that AOB consume a large fraction of the oxygen needed to oxidise ammonia to nitrate. The AOB consume 3.43 mg O_2 per mg N oxidised while the NOB only consume 1.14 mg O_2 /mg N. Consequently, even if the NOB start to get inhibited and the AOB OUR remains constant the total OUR is not dramatically affected. With a 20% inhibition of the NOB activity, the total OUR drops by only 5.9%. Compared to the system without HET activity, the total OUR raises by 33-45%. In this case, a 20% inhibition of the NOB will reduce the total OUR by 3.9%. Consequently, the OUR determination should have less than 1% measurement variability in order to detect NOB inhibition in its early phase.

(a) Nitrification without heterotrophs



(b) Nitrification with heterotrophs

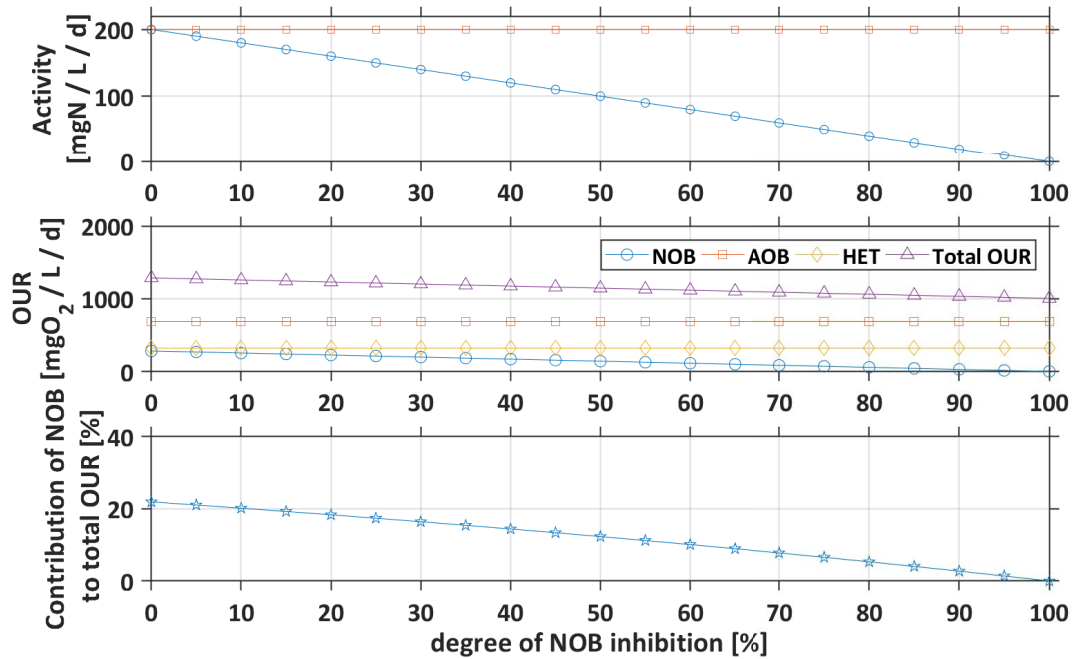


Figure 2.1: Theoretical bacterial activity at different levels of NOB inhibition for a 400 mg N/L/d ammonia loading with 50% degradation assumed. 1st panel: AOB and NOB activity. 2nd panel: Total, AOB, NOB (and HET) oxygen uptake rate. 3rd panel: NOB OUR fraction of total OUR.

2.3.2 Relation of theoretical AOB PPR and measured PPR

Table 2.2 shows the theoretical PPR (i.e., alkalinity consumption) derived from the theoretical steady state scenario above. The AOB activity of 200 mg $\text{NH}_4\text{-N/L/d}$ results in an OUR of 686 mg $\text{O}_2\text{/L/d}$ (i.e., 3.43 g $\text{O}_2\text{/g NH}_4\text{-N}$) or 2.1E-02 mol $\text{O}_2\text{/L/d}$ (i.e., 32 g/mol O_2) respectively. For 3 mol O_2 consumed, 2 mol H^+ are produced. This results in an AOB proton production rate of 1.4E-02 mol $\text{H}^+\text{/L/d}$. Compared with the typical measured PPR in the bulk at an AOB activity level at the same order of magnitude reveals that the measured PPR is more than 1000 times smaller than the expected PPR from the AOB activity. It is assumed that buffer systems contribute largely to this discrepancy (Appendix B.1).

Table 2.2: Derivation of calculated PPR based on AOB activity and comparison with measured PPR at approximately same activity level.

Scenario AOB proton production rate				Measured PPR
AOB activity	AOB OUR	AOB OUR	AOB PPR	Measured PPR
$[\text{mg N/L/d}]$	$[\text{mg O}_2\text{/L/d}]$	$[\text{mol O}_2\text{/L/d}]$	$[\text{mol H}^+\text{/L/d}]$	$[\text{mol H}^+\text{/L/d}]$
200	686	2.1E-02	1.4E-02	4.3E-06

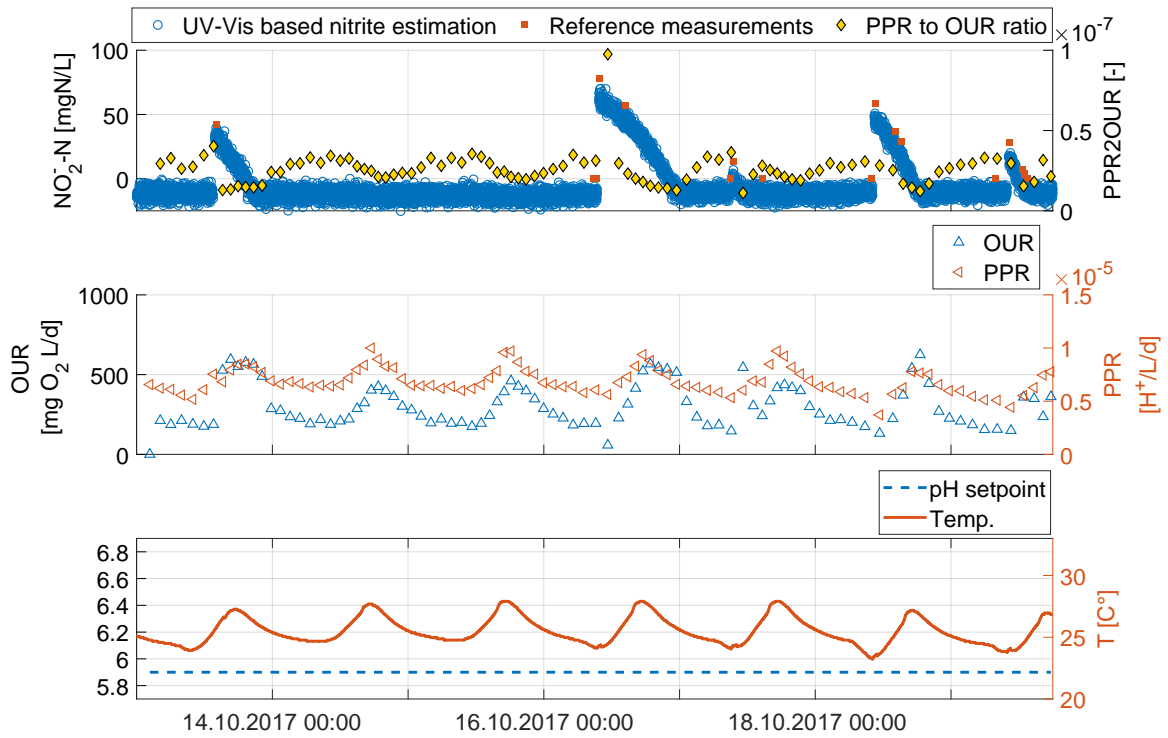
2.3.3 Experimental Data

The obtained data should reveal if based on visual inspection nitrite dynamics could be linked with PPR2OUR dynamics. The figures provide further information that facilitate the discussion of measured disturbances (i.e., pH and temperature) on the PPR and OUR signals that constitute the PPR2OUR signal.

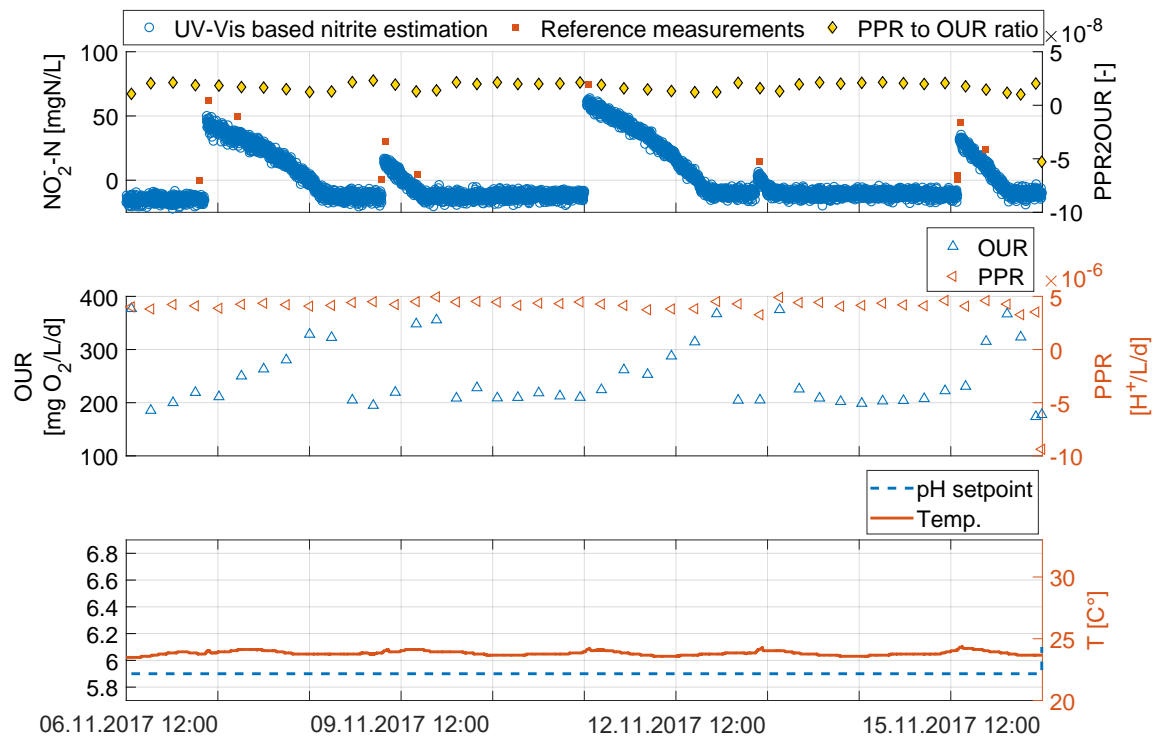
2.3.3.1 Spiked nitrite degradation

The nitrite spiking experiment results are illustrated in Fig. 2.2a (series 1), Fig. 2.2b (series 2) and Fig. 2.2c (series 3). In each figure the 1st panel shows on the left y-axis the nitrite concentration measured offline (red squares) and the UV-Vis nitrite estimation (blue circles). On the right axis the PPR2OUR signal (yellow diamonds) is plotted. In the 2nd panel the OUR signal is illustrated on the left axis (blue up-pointing triangle) and the PPR signal on the right axis (red left-pointing triangle). In the 3rd panel the left axis shows the pH setpoint (blue dashed line) and the right axis the temperature signal (orange line). Fig. 2.2a reveals that the PPR signal and the OUR signals exhibit dynamics matching the dynamics of the temperature signal. This is expected since the activity of the bacteria increases with temperature. However, the temperature peaks and the peaks of the PPR signal and OUR signal do not appear simultaneously but are slightly delayed. Additionally, the dynamics of OUR and PPR do not compensate each other in the PPR2OUR. Consequently, also the PPR2OUR signal exhibits a similar dynamic as the temperature. The nitrite influence on the PPR2OUR signal is not as obvious as the temperature influence. Nitrite spiking events such as the one on the 16.10.2017 alter the trend of the PPR2OUR compared with days at which no nitrite is spiked (e.g., 15.10.2017). The PPR2OUR is increasing as soon as all the nitrite is degraded and the net nitrite production is zero (e.g., 17.10.2017 00:00). However, the limited number of observations and the additional temperature effect does not allow drawing significant conclusions just based on this series.

(a) Series 1 nitrite spiking experiment



(b) Series 2 nitrite spiking experiment



(c) Series 3 nitrite spiking experiment

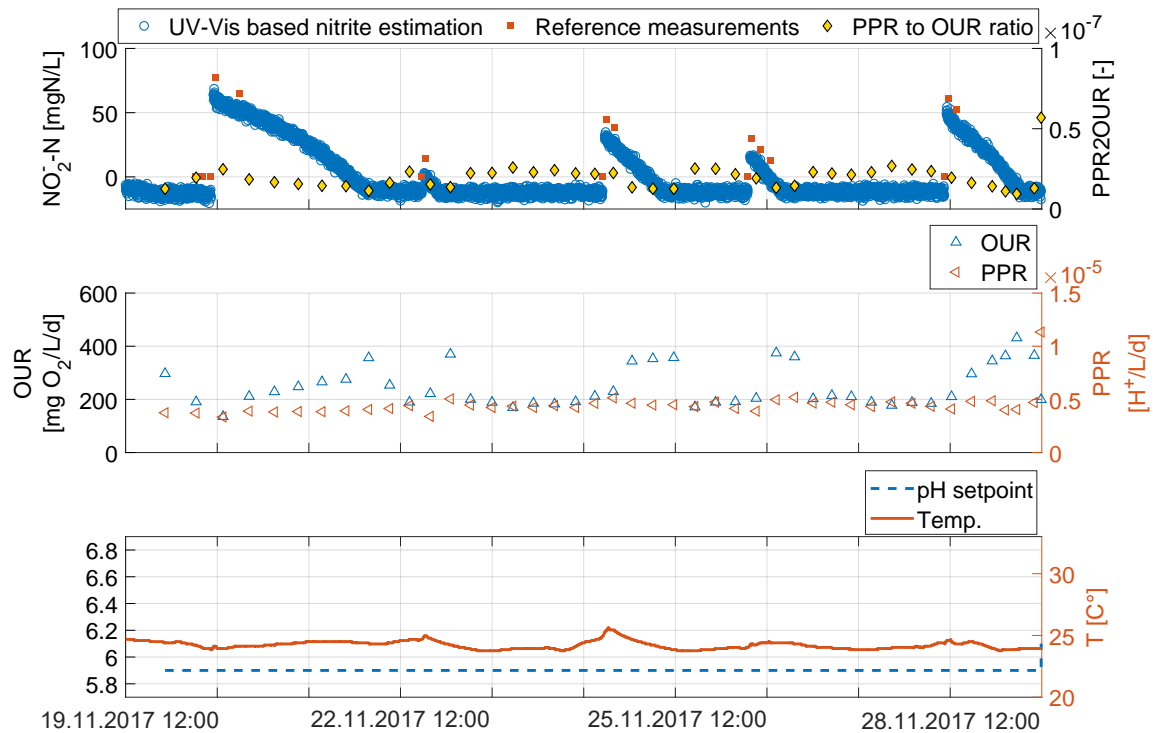


Figure 2.2: Nitrite spiking experiments: 1st panel, left y-axis: nitrite concentration offline (red squares), the UV-Vis nitrite estimation (blue circles), right y-axis: PPR2OUR (asterisk). 2nd panel, left y-axis: OUR (blue up-pointing triangle), right y-axis: PPR (left-pointing orange triangle). 3rd panel left y-axis: pH (blue asterisk), right y-axis: temperature (orange line).

In series 2 Fig. 2.2b and series 3 Fig. 2.2c the temperature dynamics are minimised. The minimised diurnal variations in the PPR signal and OUR signal support the assumption that both are dependent on temperature. Furthermore, both series 2 and 3 confirm the proposition made based on series 1 with respect to the relation of PPR2OUR and nitrite. The PPR2OUR signal is decreasing with decreasing nitrite concentrations but then starts to increase after nitrite is completely degraded.

These PPR2OUR dynamics are mainly driven by dynamics in the OUR. Each time nitrite is spiked the OUR starts to increase or even jumps up substantially. Once all the nitrite is degraded the OUR starts to decrease. It seems that high initial nitrite concentrations (e.g., Fig. 2.2b spiking on 06.11.2017 and 08.11.2017) have a less drastic effect on the OUR dynamics than the lower concentrations (e.g., Fig. 2.2b spiking of 07.11.2017, 09.11.2017 and 10.11.2017).

2.3.4 AOB driven nitrite dynamics

In this section, the two data sets in which nitrite is accumulated Fig. 2.3 and degraded Fig. 2.4 respectively by means of pH setpoint adaptation are presented. The figures are structured in the same way as the previous Fig. 2.2a - Fig. 2.2c.

2.3.4.1 Degradation of nitrite

In this experiment, nitrite is accumulated to NOB inhibiting levels at high pH. The pH setpoint is then reduced and the previously accumulated nitrite is degraded. The data confirm the findings of the *spiked nitrite degradation* experiment. Once the nitrite almost reaches 0 mg N/L the PPR2OUR increases sharply (Fig. 2.3 morning of the 27.05.2017). Thus, the end of a net nitrite degradation phase is observable in the PPR2OUR signal independent of the way the nitrite appeared in the reactor.

Even though the temperature is dynamic in this experiment, the effect of nitrite on the PPR2OUR is clearly visible. Furthermore, the experiment confirms the hypothesis that the pH has a big impact on the PPR and in turn PPR2OUR. The drop in pH at the 20.05.2017 causes a jump in the PPR2OUR, which is not related with nitrite. This jump is caused by a jump in the PPR signal. The kinetics of the AOB suggest that a drop in pH should reduce the AOB activity and in turn the PPR should drop. Thus, the observed relation of pH and PPR is counter-intuitive.

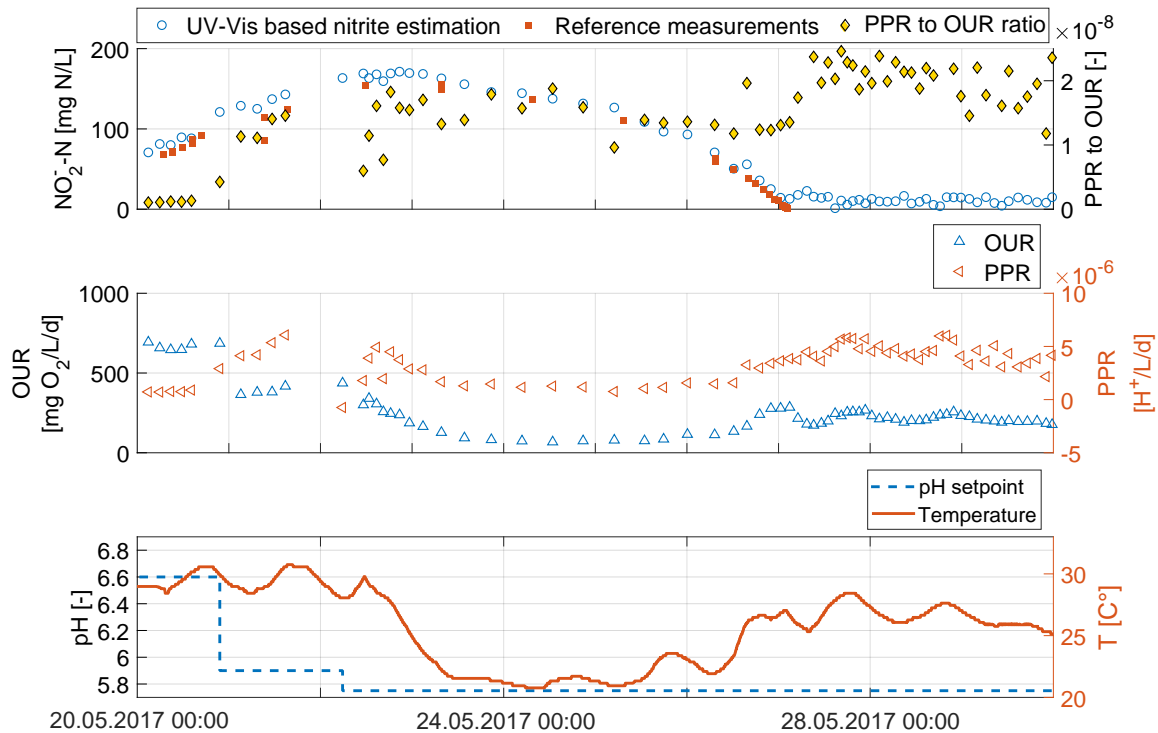


Figure 2.3: Low pH setpoint and net nitrite degradation: 1st panel, left y-axis: nitrite concentration offline (red squares) and the UV-Vis nitrite estimation (blue circles), right y-axis: PPR2OUR (yellow diamond). 2nd panel, left y-axis: OUR (blue up-pointing triangle), right y-axis: PPR (left-pointing orange triangle). 3rd panel left y-axis: pH (blue asterisk), right y-axis: temperature (orange line).

2.3.4.2 Accumulation of nitrite

Fig. 2.4 illustrates the results from a slow accumulation of nitrite at constant high pH values. Normally, such delays in nitrite accumulation were only observed after long periods of operation at low pH setpoints. However, the exact reason why the accumulation is delayed is not known. The results show that a slow

accumulation of nitrite is not detectable by means of the PPR2OUR. Despite increasing nitrite, there are almost no dynamics in the PPR2OUR, once the pH was increased (11.05.2017). The drop in OUR and PPR from the 15.05.2017 on is most likely caused by an overall performance decrease.

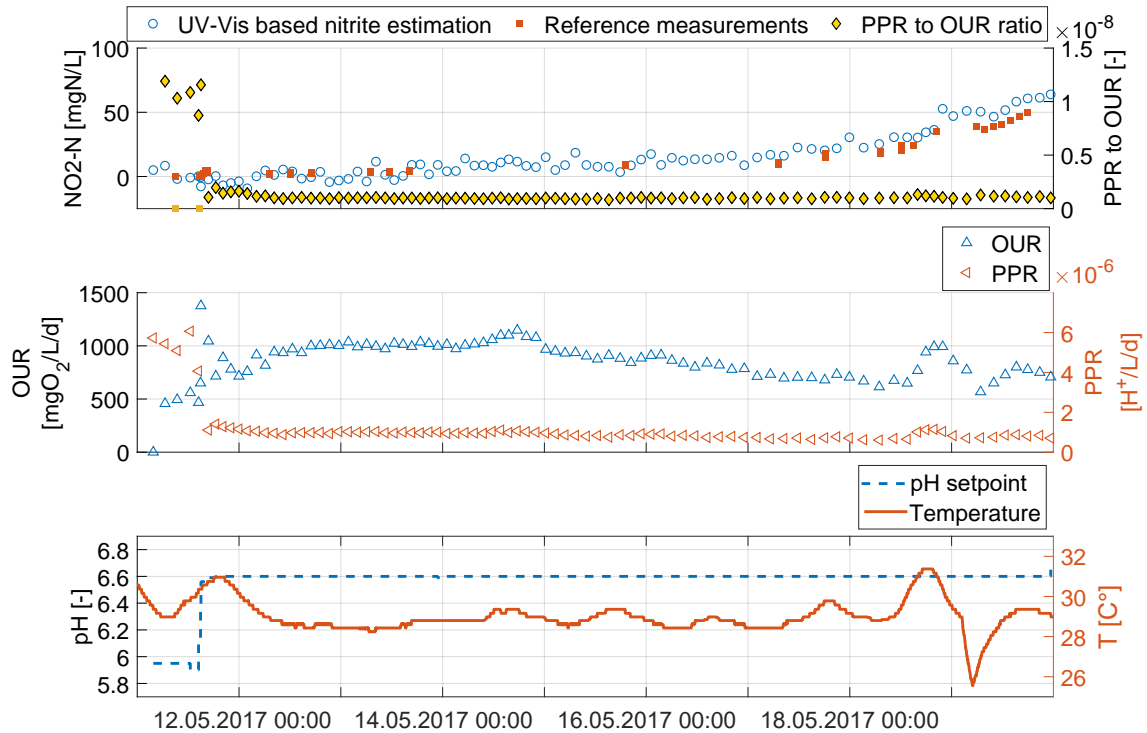


Figure 2.4: High pH setpoint and net nitrite accumulation: 1st panel, left y-axis: nitrite concentration offline (red squares) and the UV-Vis nitrite estimation (blue circles), right y-axis: PPR2OUR (asterisk). 2nd panel, left y-axis: OUR (blue up-pointing triangle), right y-axis: PPR (left-pointing orange triangle). 3rd panel left y-axis: pH (blue asterisk), right y-axis: temperature (orange line).

2.4 Discussion

2.4.1 Theoretical OUR fractions

The theoretical results show that the contribution of the NOB to the OUR is rather low. Thus, identifying changes in the OUR based on NOB dynamics is difficult. However, the high sensitivity of the NOB to nitrite in the low concentration range also indicates that a steady state perspective on the expected impact has its limitations. It only considers dynamics once the NOB reached their maximum growth rate and start to get inhibited. This ignores the dynamics in the OUR caused by an initial increase of nitrite when the NOB are still substrate limited. As long as nitrite is limiting the NOB, their contribution to the OUR will increase sharply with increasing nitrite concentrations just to drop once the NOB start to be substrate inhibited. Consequently, the OUR dynamics can be expected to be more pronounced than what the steady state analysis shows. The data from the experiments support this expectation. The difference between the OUR of the NOB and the total OUR becomes more distinct if the COD/N ratio is even lower

due carbon removal prior to the nitrification stage. The theoretical PPR calculations are discussed below in 2.4.3.

2.4.2 Empirical relation of PPR2OUR with nitrite

Both experiments showed that the end of a net nitrite degradation period could be detected in the PPR2OUR. The high sensitivity of the NOB activity to nitrite at low concentrations induces pronounced OUR dynamics. Unfortunately, this relation cannot be seen when nitrite accumulates. This scenario would be the most relevant for practice. The PPR2OUR showed no relevant dynamics correlated with the increasing nitrite concentrations. It remains unclear why the degradation of nitrite affects the PPR2OUR differently than an initial accumulation. One factor could be biomass growth and decay dynamics. The AOB driven nitrite accumulation experiment shows that the accumulation was not directly related with the sudden pH increase (i.e., the AOB activity increase) but developed slowly. Thus, it is likely that the nitrite accumulation was a consequence of the adaption of AOB and NOB to the new steady state. Consequently, the dynamics in the PPR2OUR signal due to the adaption to a new steady state were most likely masking the rather subtle dynamics the slowly increasing nitrite concentration induced on the PPR2OUR signal.

The nitrite decreasing experiment design suffered from the same challenge. Also in this experiment, the system is far away from steady state. However, in the given experiment the nitrite degradation is uncoupled from the convergence of the microbial community to the new steady state. Since pH is a very important parameter to optimise the process performance, more comprehensive experiment in terms of separating pH and nitrite effects should be executed.

2.4.3 PPR2OUR dependency on temperature and pH

A further limitation of the presented method is the dependency of the PPR to the pH setpoint. The theoretical calculations also show that only around 1‰ of the stoichiometrically calculated H^+ actually contribute to the proton production rate and the rest is buffered. Thus, it is not surprising that with small changes in the buffer systems due to changing pH, the correlation of PPR to the AOB activity changes. This is also confirmed in a brief simulation experiment (Appendix B.1). Consequently, for each used pH setpoint the PPR2OUR to nitrite relation needs to be characterised again.

In addition, temperature dynamics seem to hamper the analysis of the PPR2OUR. This was not observed in all experiments. Nevertheless, the assumption of a stable ratio between OUR and PPR over the temperature range seems not to hold. It is most likely caused by different sensitivities of PPR and total OUR to temperature. Thus, both pH and temperature dynamics have to be limited or explicitly modelled to use this soft-sensor.

2.4.4 Further analysis

This study only dealt with an exploratory data analysis based on visual comparison of the most relevant signals: nitrite, pH, DO, temperature, OUR, and PPR. Moreover, the analysis is purely based on stoichiometry. However, there is also additional expert knowledge about AOB and NOB kinetics that could be included in the analysis. Mašić and Villez (2014) used a model with a state observer (e.g., Kalman filter). Using such a multivariate model would also allow incorporating explicitly the pH and temperature dependency of OUR and PPR. Another way to incorporate more expert knowledge into

the soft-sensor would be to deploy a fuzzy logic framework using the PPR and OUR as input. This was successfully done by Boiocchi et al. (2015) for partial nitrification/anammox.

The controller presented in Chapter 3 relies on the correct identification of the end of a deliberately accumulated and degraded nitrite peak. So far, the controller input signal is a UV-Vis based nitrite estimation signal. The deliberate accumulation and degradation matches the experimental design of the *AOB driven nitrite dynamics* experiment. Consequently, future research should test if the PPR2OUR signal dynamics at the end of the nitrite peak are of sufficient robustness and quality to replace the UV-Vis sensor as the input for the controller.

2.5 Conclusion

In this chapter the information content in the ratio of the proton production rate, measured by means of pH and the oxygen uptake rate, measured in the DO signal (PPR2OUR) about the activity ratio of AOB to NOB were investigated. Such a soft-sensor can indicate nitrite accumulation. Based on the four hypotheses stated in the introduction the following is concluded:

- (i) PPR2OUR is only informative about nitrite concentrations in selected situations. One such situation is the detection of nitrite depletion subsequent to a nitrite accumulation. These are nitrite concentration levels at which NOB show a much higher sensitivity to nitrite than AOB and HET. The onset of nitrite accumulation events could not be detected on the basis of the PPR2OUR signal.
- (ii) When pH and temperature as measurable disturbances are kept constant, the PPR2OUR signal dynamics related to nitrite can be retraced to dynamics in the OUR signal.
- (iii) Temperature and pH are measured disturbances that influence the PPR2OUR dynamics unrelated to nitrite. Thus, they should be accounted for in future investigations.
- (iv) Unmeasured disturbances with a large theoretical impact on OUR and/or PPR are heterotrophic activity and buffer systems. No conclusion regarding endogenous respiration can be drawn on the basis of the available data.

Acknowledgement

The authors want to thank Kito Ohmura for his assistance with the experiments, Karin Rottermann, and Sylvia Richter for their assistance with the laboratory analysis.

3 Stabilising control of a urine nitrification process in the presence of sensor drift

This chapter is based on the following manuscript, submitted for publication:

Thürlimann, C. M. ^{a,b,c,d,e,f}, Udert, K. M. ^{a,f}, Morgenroth E. ^{a,f}, Villez, K. ^{a,b,d,f} Stabilizing control of a urine nitrification process in the presence of sensor drift.

^aStudy concept and design, ^bSoftware development, ^cAcquisition and analysis of data, ^dInterpretation of data, ^eDrafting of chapter, ^fCritical revision.

3.1 Introduction

Control loops relying on absolute sensor values are often suffering from sensor faults. This study presents a novel control concept to stabilise a high strength nitrification reactor in the presence of sensor drift. To this end, the controller is designed to exploit information from the signal derivatives in a deliberately excited process. In wastewater, biological, chemical, and physical factors lead to particularly intense wear and tear of sensors. Hence, even mature sensor hardware such as pH sensors still exhibit drift when exposed to this harsh medium. This drift occurs at time scales that are much longer than typical process dynamics, challenging a comparison with the sensor data history (temporal redundancy) (Ohmura et al., 2018). Furthermore, drift tends to occur in all sensors exposed to the same medium challenging its detection based on redundant placement of sensors (spatial redundancy). Lack of spatial and temporal redundancy impedes the application of tools such as active fault tolerant control that correct drift automatically based on redundant information (Blanke et al., 2016).

The root causes of sensor drift are generally assumed to be known well – e.g., biofilm formation, salt deposition, electrode oxidation etc. – but are typically hard to quantify. There are a few attempts to investigate drift of sensors quantitatively by controlled offline experiments (Ohmura et al., 2018) or by online experiments (Samuelsson et al., 2018). However, drift is typically identified by means of on-site manual reference measurements in practice. This makes drift expensive to detect and correct, particularly when remote or decentralised systems are considered.

The very limited understanding of sensor drift in wastewater processes on the one hand and the need to control these processes on the other hand, led to the development of methods that disregard absolute sensor values and extract information that is represented in the derivatives of the sensor signal. The most discussed (soft-)sensor signals that reveal relevant information without relying on a classical notions of accuracy are pH, oxidation-reduction potential (ORP) (Al-Ghusain and Hao, 1995), and oxygen uptake rate (Baeza et al., 2002). Al-Ghusain and Hao (1995) used the derivatives of pH and ORP to operate an aerobic/anoxic sludge digestion reactor. Owing to the sequenced operation (i.e., anoxic and aerobic) the system dynamics were intense enough to extract valuable information from the derivatives of the signals. Even in continuously operated processes, derivative signals can be useful for process monitoring and control. Thürlimann et al. (2018a) used the diurnal dynamics of the inflow in continuously operated municipal wastewater treatment plants (WWTP) to detect and control elevated ammonium concentrations based on the derivative of a pH difference signal. In this case, the information in the derivative signal is caused by a naturally occurring periodicity of the (unmeasured) process input disturbances (i.e., influent flow rate and composition). The application of such control concepts is expected to be more challenging in systems without any significant and regular oscillations. The alkalinity limited nitrification of source-separated urine, as studied in this work, is an example of such a system. This process occurs in a continuous-flow stirred tank reactor and is not exposed to process disturbances with a regularly occurring oscillatory pattern.

The most frequently cited process disruption of the urine nitrification process is caused by the accumulation of nitrite (Fumasoli et al., 2016; Sun et al., 2012), which often leads to a complete failure of the process (cf. 2.1). Thus, controlling the ammonia oxidizing bacteria such that they do not produce more nitrite than the nitrite oxidizing bacteria (NOB) can oxidise is crucial to ensure economic feasibility.

An economically viable method to measure nitrite online is UV-Vis absorbance spectrophotometry. However, this measurement principle has a lack of specificity and therefore needs a model to extract the nitrite concentrations from the absorbance measurement. Despite the availability of robust hardware, the subsequent use of a model makes drift of the nitrite signal a very likely phenomenon (Thürlimann et al.,

2018b).

The lack of natural or operational dynamics, the presence of signal drift, and the open-loop unstable process of urine nitrification requires developing a new control concept to operate the process in a stable manner. For this reason, we hypothesize in this study that key information about the stability of the nitrification can be extracted by combining (i) the deliberate induction of process dynamics (i.e., excitation) and (ii) trend analysis of a drifting sensor signal. This, in turn, enables the construction of single-in-single-out (SISO) controller, which stabilises the open-loop unstable urine nitrification reactor.

3.2 Material and Methods

3.2.1 Conceptual model of the control problem

In this paragraph, a conceptual model of the urine nitrification process is presented. The concept illustrates the different process states (Gujer, 2008), growth rate of the ammonia oxidizing bacteria (μ_{AOB}) and growth rate of the nitrite oxidizing bacteria (μ_{NOB}) and connections indicating the direction in which the subsequent process state or rate develops when the preceding one is changed. In the control literature, this is referred to as sign of gains (Åström and Murray, 2008). It is important to note that this conceptual model only includes the effects considered relevant to understand and tackle the identified process stabilization challenge. Only dynamic effects with a lower time constant than the controller are considered (e.g., biomass concentration stays approximately constant within this time constant). The sign of gains only apply if all other states and rates remain constant and under constraints given in Fig. 3.1.

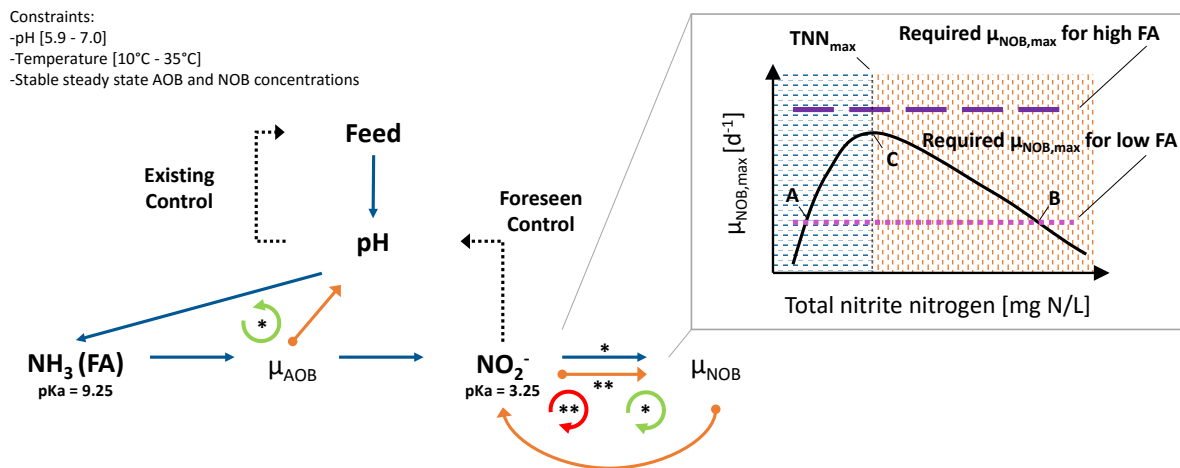


Figure 3.1: Conceptual model of urine nitrification. Left: Process states, growth rates and gains. Blue arrows: positive gains, orange/dot-arrows: negative gains. Right: Nitrite oxidizing bacteria growth rate (μ_{NOB}) as a schematic function of total nitrite nitrogen concentration. Blue horizontally dashed: NOB substrate limited, orange vertically dashed: NOB substrate inhibited. Two horizontal lines indicate the required μ_{NOB} to oxidise all the nitrite produced by the AOB given a high/low free ammonia (FA) concentration.

The blue arrows indicate a positive gain, the orange dot-arrows indicate a negative gain of the connected elements. For example, an increasing loading rate leads to an increased pH (i.e., positive gain) or an increasing AOB rate (μ_{AOB}) leads to a decreased pH (i.e., negative gain). This network of causal

relationships among process states and growth rates can form loops. Such loops are open loop stable if the product of the gains in the loop is negative (green/* circle arrows) (e.g., pH - NH_3 - μAOB). This means these loops are self-stabilizing. For example, an elevated pH will increase the free ammonia (NH_3 or FA) concentration in the bulk, which in turn raises the μAOB . This in turn lowers the pH again and the loop is stabilised. A loop with a positive product of its gains is a positive feedback loop and can lead, when not controlled properly, to a complete disappearance of elements in the loop (i.e., open loop unstable). E.g., the relation of NO_2^- and μNOB in case of high nitrite concentration (red/** circle arrow). This is explained in more detail in the top right box of Fig. 3.1. It shows the maximum μNOB as a function of the total nitrite concentration (TNN) (full line). The growth rate is composed of both the substrate limiting effect and the inhibition effect nitrite has on the NOB. Most studies, but not all, list nitrite as the substrate and free nitrous acid (FNA) as the inhibiting substance for NOB (Park and Bae, 2009). This means that the growth rate is pH dependent. For simplicity, we neglect any effect of the pH and assume that TNN is both the substrate and the inhibitory substance. Later this also applies to the control input signal that only considers TNN.

In any case, if nitrite concentrations are elevated (i.e., vertically orange dashed area) nitrite has a negative gain to μNOB . The reduced nitrite oxidation rate leads to further nitrite accumulation and in turn to an even stronger inhibition of the NOB. NOB are washed out and the process fails. Only if nitrite concentrations stay low (i.e. horizontally dashed blue area) the loop is open loop stable; higher nitrite concentration leads to a higher μNOB and in turn to lower nitrite concentrations. Practically, the process can only be stabilised by reducing the μAOB when the nitrite concentration reaches the substrate inhibiting range. This is possible by making the reactor anoxic, in which case nitrite is reduced by denitrification. Repeated application of this may induce growth of denitrifiers, in turn leading to a loss of nitrogen to the environment. A better approach consists of reducing the nitrite production rate by lowering the pH setpoint. Low pH values equate to low FA concentrations, so that eventually the nitrite oxidation rate is higher than the nitrite production rate (Fig. 3.1 right).

To achieve stabilization of the process the black dashed arrows indicate the existing pH control loop and the newly proposed nitrite control loop. The pH control loop is described below and is designed to protect the AOB from washout (cf. 3.2.2.3). The second dashed arrow indicates the proposed master control of the pH control loop in the reactor based on the nitrite concentration, which should prevent the washout of the NOB.

3.2.2 Basic Reactor set-up and operation

The reactor used for this study is a cylindrical 12 L quasi-continuous flow stirred tank reactor (CSTR) nitrifying source-separated urine. Alkalinity limits the fraction of the total ammonium converted via nitrite to nitrate at about 50%. The reactor was in operation since 19 months prior to the start of this study. The reactor includes two recirculation loops. One brings the reactor medium to the UV-Vis spectrophotometer with a hydraulic retention time (HRT) of 10 s. The other brings medium to a pH sensor pack used in another study (HRT: 20 s). The feed composition is described in 3.2.6.3.

3.2.2.1 Analytics

Samples are taken regularly from the reactor to evaluate if the proposed controller keeps the nitrite concentration low. To measure chemical species the following steps are executed. Per sample at least 2 ml of reactor media are filtered with 0.45 μm GF/PET filter (Art. Nr. 916 02, Macherey-Nagel, Oensingen,

Switzerland) mounted on a sampling syringe. Ammonium, nitrite, and nitrate concentrations are measured in every sample. The influent ammonium and chemical oxygen demand (COD) concentrations are measured each time the influent tank was replaced. The exchange dates and concentrations are listed in Appendix C.1. Ammonium concentrations are determined either through a Metrohm 930 Compact IC Flex (Metrohm, Herisau, Switzerland, method: Metrohm Metrosep C6, 250/4.0), with flow injection analysis (FIA, Lachat QC8500, Hach Company, Loveland, USA) or with colorimetric test kits (LCK303, Hach-Lange, Berlin, as all LCK test kits). Nitrite reference concentrations are determined either colorimetrically with an LCK341 or with strip tests (MQuant, Merck KGaA, Darmstadt, Germany) to confirm low nitrite concentrations. Due to dilution, the detection limit with the LCK341 kit is approximately 2mg N/L. Nitrate is measured in the laboratory through a Metrohm 881 Compact IC Pro (Metrohm, Herisau, Switzerland, chemical suppression Metrosep A Supp 7, 250/4.0) or with LCK340. For the measurement of the COD, LCK314 are used. A standard deviation of the measurement including the dilution procedure is estimated with a single triplicate of measurements prior to this study: FIA ammonium: 0.60% at 2340 mg N/L, LCK 341 nitrite: 0.60% at 45.7 mg N/L, and IC nitrate: 0.55% at 2226 mg N/L.

3.2.2.2 Sensors

A 2 mm path length spectro::lyser V1 (s::can, Vienna, Austria) is used to measure the UV-Vis absorbance spectrum of the reactor content in-situ. The sensor measures the absorbance from 200 to 750 nm at a resolution of 2.5 nm. The *Ex-situ wBM* model from Thürlimann et al. (2018b) is used to estimate the nitrite concentrations. Each minute a new absorbance measurement and in turn a new estimation of the nitrite concentration is obtained. Furthermore, two pH and two dissolved oxygen (DO) sensors are installed, one of each is used for control (DO: COS61D and pH: CPS11D, Endress&Hauser, Reinach, Switzerland)

3.2.2.3 Low-level control

The DO concentration is controlled between 5 and 6 mg O₂/L by turning the airflow to a fine-bubble diffuser on and off. The relatively high concentrations were chosen to minimise the risk of denitrification. The feed pump is pH controlled (cf. 3.2.3). The reactor is equipped with a water based heating/cooling system (FN-25, Julabo, Seelbach GmbH, Germany). The temperature of the reactor was controlled at 25°C with an accuracy of ±0.5°C due to diurnal variations unless stated otherwise.

3.2.3 Stabilizing Nitrite Control

The ultimate goal of our controller is to ensure that both AOB and NOB are retained and remain active in the studied reactor in the presence of typical disturbances. The envisioned control system has to ensure that the net nitrite production rate is zero, meaning that the ammonia oxidation is the rate-limiting step and that no ammonia is accumulating in the system. To this end, the master controller manages the nitrite oxidation (i.e., NOB) and the slave controller manages the ammonia oxidation (i.e., AOB). At the top of Fig. 3.2, the proposed cascaded control loops are illustrated. The slave control loop, using pH to control the inflow was described by Udert et al. (2003). It controls the AOB by manipulating the inflow rate based on the pH setpoint given by the master control. The master control takes the nitrite concentration estimation as an indicator to decide if the ammonia oxidation rate is higher or lower than the theoretical maximum nitrite oxidation rate and sets the pH set point accordingly. The slave controller

turns on the inflow pump when the pH drops below the pH setpoint. Instead of a second pH setpoint the pump is turned off again based on a timer (6 s). In each pump event 20 ± 5 mL of urine is fed to the reactor. The master controller sets the pH setpoint to the high setpoint (6.8) when the nitrite concentration is such that the NOB are dominated by substrate limitation (i.e., open loop stable, Fig. 3.1 right, horizontally blue dashed area). This is referred to as controller state 1. If nitrite is so high that the NOB are dominated by substrate inhibition (i.e., open loop unstable, Fig. 3.1 right, vertically orange dashed area) the controller sets the pH to the low setpoint (6.1). This is further referred to as controller state 0. The two pH setpoints were chosen based on the previous operational experience such that the intended net nitrite production (6.8) and degradation (6.1) respectively were very likely to happen.

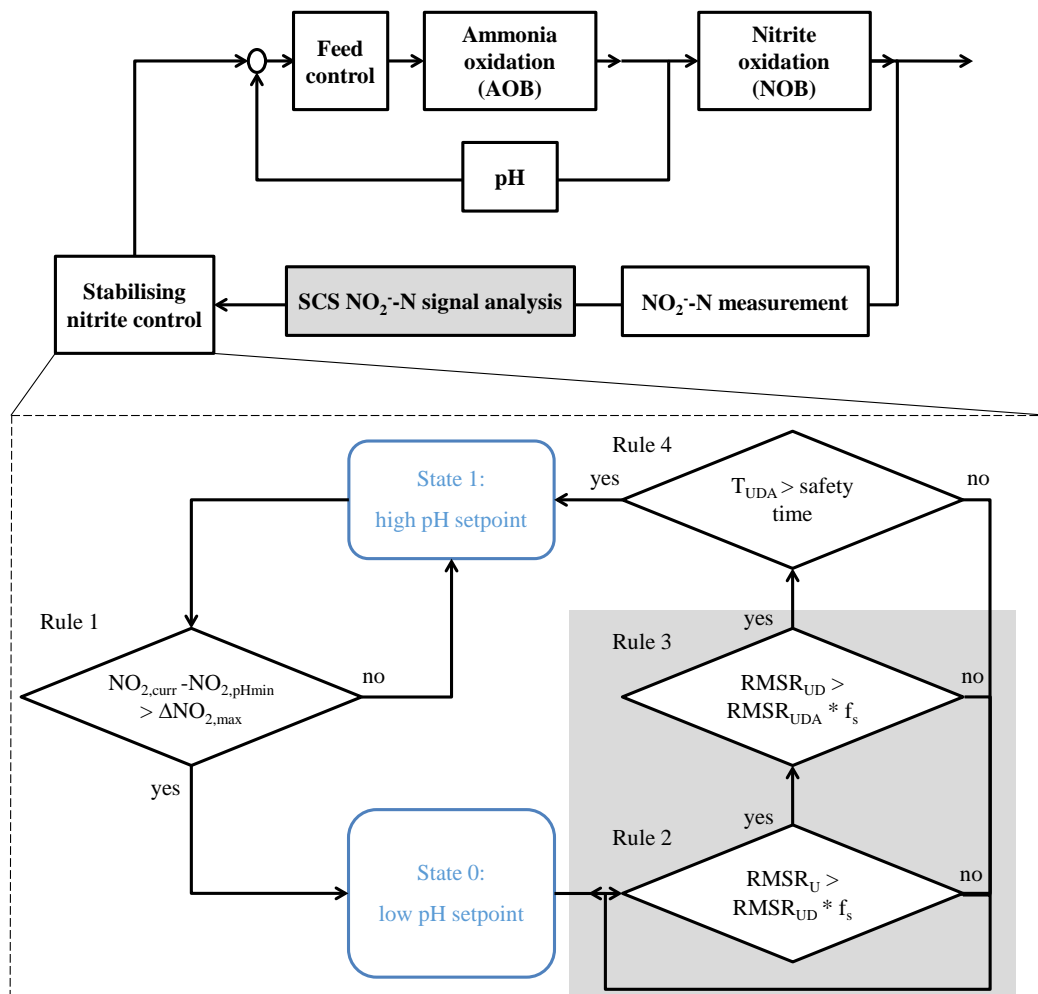


Figure 3.2: Control loops. Top: Cascade control of AOB and NOB. Bottom: rule based decision process to change master controller states. Grey box rules that evaluate results from the shape constrained splines method.

The drift in the controller input signal forces to design the controller such that it relies on the information contained in the first and second derivative of the signal to distinguish between NOB inhibitory and NOB limiting nitrite concentration levels. The information that is actually used in the controller is the identified presence of the inflection point in the downward trend (i.e., negative first derivative, second derivative

sign switches from negative to positive). It is assumed, that in the period during which the inflection point appears μAOB is constant: First, at this time, the pH has already reached its low setpoint value and the influent composition is assumed constant, thus there are no changes in the FA concentration. Second, the temperature is assumed constant. Furthermore, it is assumed that AOB activity is almost insensitive to changes in the nitrite concentration at the nitrite concentration level where the μNOB starts to be dominated by substrate limitation (Fig. 3.1, TNN_{max}) (Wang et al., 2014). Consequently, when the inflection point appears, the nitrite dynamics are only driven by the NOB.

When NOB are dominated by substrate inhibition and a low pH results in low FA availability for AOB (Fig. 3.1, right, pink dotted line), the NOB activity increases as nitrite concentrations are decreasing (Fig. 3.1, moving from Point B to Point C). At the landmark value (Kuipers, 1986) TNN_{max} , the μNOB and in turn the net nitrite degradation rate reach their maxima and then start to decrease (Fig. 3.1, moving from Point C to Point A). Thus, under normal circumstances, the appearance of the inflection point in the decreasing signal is linked with the NOB achieving their maximum growth rate (point C) and the start of substrate limitation dominating the NOB. Note that the precise value of TNN_{max} is considered unknown.

Identifying an inflection point in the downward trend requires first and foremost that the nitrite concentration has been high enough to induce observable inhibition of the NOB. Thus, the controller has to be designed in such a way that NOB-inhibiting conditions are reached in a way that allows reducing the nitrite concentration as soon as inhibiting conditions are detected.

Accordingly, the master controller increases the pH setpoint such that the increased FA concentration leads to an ammonia oxidation rate (i.e., nitrite production rate) higher than the maximal nitrite consumption rate (Fig. 3.1, right, purple dashed line). The nitrite increase is controlled by monitoring the absolute increase of the signal value. In our case, the last nitrite value prior to the pH increase is taken as a reference for a relative increase of 15 mg N/L. Once this threshold is reached the controller switches from state 1 to state 0. In control state 0, the controller re-stabilises the process by lowering the pH (Fig. 3.1, right, pink dotted line). As long as the nitrite concentration in the previous increase never exceeds point B (Fig. 3.1, right), the reduction in the FA concentration to the lower line puts the steady state concentration back to point A and a net nitrite reduction starts. The controller gets the confirmation of reaching a stable nitrification by identifying the inflection point in the downward trend. This ends one control cycle.

3.2.4 Identification of inflection point

To identify the inflection point in the downward nitrite signal, the signal is analyzed by means of a qualitative trend analysis (QTA) method. In general, QTA methods segment data series into *episodes*. Each episode describes a non-empty time interval of the analysed time series. In each episode, the sign of the first derivative and the sign of the second derivative of the signal are constrained to be solely positive, negative, undefined, or zero. Every possible combination is known as a *primitive*. They are defined in Table 3.1. For example, primitive *U* has a positive (+) first derivative sign and an undefined (?) second derivative sign. Assigning this primitive to an episode means that the signal is believed to be increasing during the time span covered by the episode, while the second derivative can take on any feasible value at any time within this time span. Any list of one or more primitives is named a *qualitative sequence* (QS). Each switch from one primitive to another corresponds to a *qualitative feature* (QF), e.g., a maximum, a minimum or an inflection point. In this study, only the primitives *U*, *D* and *A* are used.

Table 3.1: Thirteen primitives defined by the signs of the first and the second derivative of the signal. ND: Not defined.

		First derivative sign			
		+	0	-	?
Second derivative sign	+	B	ND	A	P
	0	G	F	E	O
	-	C	ND	D	N
	?	U	ND	L	Q

3.2.4.1 Shape constrained splines

The applied QTA method is the shape constrained splines (SCS) method (Villez and Rengaswamy, 2013). SCS has been studied for process monitoring (Derlon et al., 2017), fault detection (Villez and Habermacher, 2016) and as a tool for kinetic modelling (Mašić et al., 2017). SCS was originally designed to analyze batch data, meaning that the data processing is only started when all relevant data are available. To the knowledge of the authors, no online application of the SCS method has been reported so far.

SCS fits a cubic spline function, i.e. a function which is a continuous piece-wise cubic polynomial with continuous first and second derivatives. The function is constrained to satisfy the shape defined by means of a QS. The most important tuning parameter is the *knot distance*. The knot distance is chosen to be 50. Thus, only if 50 data points are available the analysis can start. The detailed description of the algorithm can be found in Villez and Rengaswamy (2013). To optimise the (least-squares) fit of the function, the SCS method uses the branch and bound algorithm.

Since for the SCS analysis the QS has to be defined prior to the analysis, expert knowledge about the expected behavior of the signal shape is required yet easy to incorporate. The expected shape for the full control cycle in the studied process is an increasing trend (U (first derivative sign: + / second derivative sign: ?)) followed by a downward concave shape (D (-/-)), followed by a downward convex shape (A (-/+)) (Table 3.1). This is represented by the QS UDA. However, in an online environment the expected shape will first have a U shape later a UD shape and only in its final phase the expected UDA shape. Consequently, this allows using all three models in a model selection approach. By fitting these expected QS over the course of control cycle on to the data, the lack of fit of the different models at one time point allows ruling out certain shapes. For example, we expect the lack-of-fit of the SCS with the U shape to increase dramatically once a maximum becomes apparent and we expect the lack-of-fit of the SCS with the UD shape to increase dramatically once the expected inflection point appears in the recorded signal. In turn, this means the lack-of-fit is only small for the SCS with the UDA shape when the process has returned to NOB substrate-limiting conditions.

3.2.4.2 Data processing for shape constrained splines analysis

The fact that the data set constantly increases in size during online application requires a data structuring prior to the SCS analysis (i.e., feature engineering). To this end, the continuous nitrite time series is split into so-called single *events*. In this study, each event begins when the controller state is set to 0 and ends when the controller state is set to 1. The start and the end of an event are thus defined by the actions of the controller. This means the SCS models are fit with the data collected during the ongoing control event only. At the end of the event, all data collected are discarded and a new data set is built up once a new event starts.

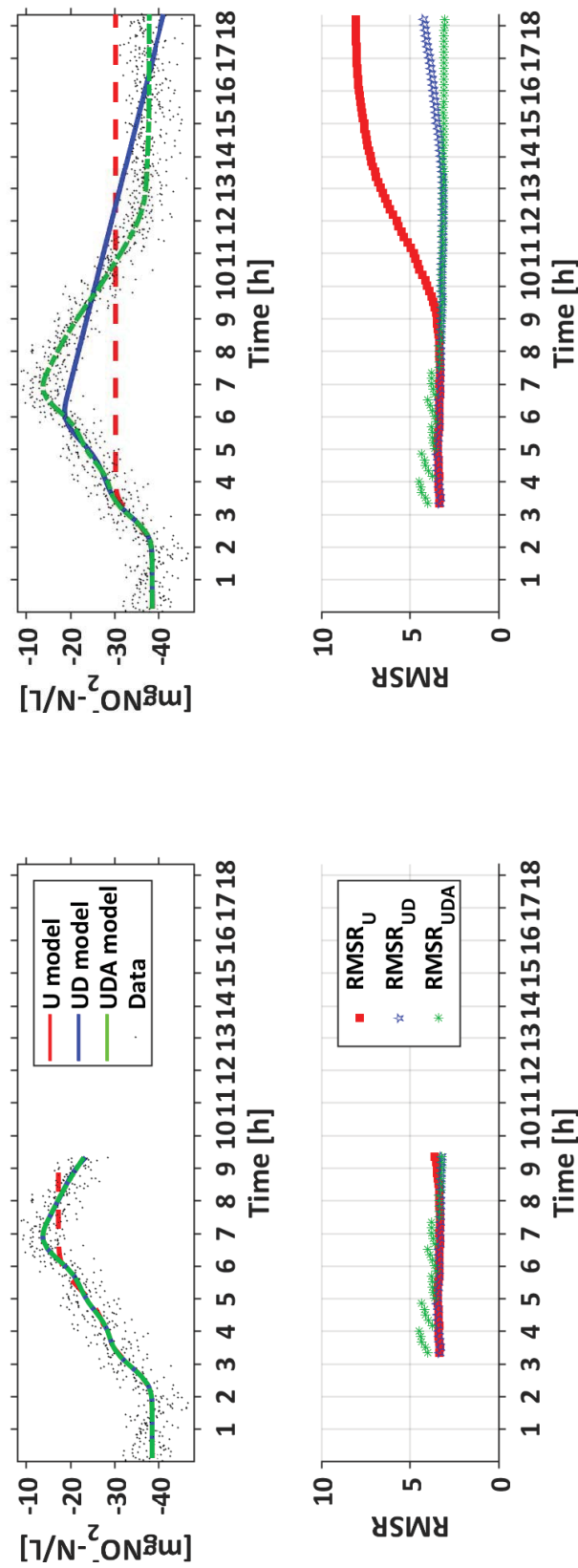


Figure 3.3: Shape constrained spline model fitting. Top panels: Raw data with three different qualitative sequence models fitted to the currently available data in the *event*. Bottom panels: Root means squared residuals of models given the data at this time. Left: Analysis within event. Right: Analysis at the end of the event.

In Fig. 3.3 two different time points in the analysis of the same event is illustrated. The top graphs show the data (black dotted) and the three QS fitted to the data. The bottom plots show the corresponding root mean squared error of the three models evaluated with all the data available until this time. In the left plot, the data already exhibited a maximum and the U model, constrained to be continuously increasing, starts to fit worse than the two others do. This can be seen in the almost flat shape the U function (red, wide-dashed) has from hour 6 on and thus results in an increasing root mean squared error (RMSR) of the U model ($RMSR_U$). Both UD and UDA model approximate the time series well as their shape constraints are flexible enough. The right panel shows the time point at which the full data set of the event is available. Visual inspection reveals that the data exhibited a maximum and an inflection point in the downward trend - as expected. As desired, the $RMSR_{UD}$ increases once the curve exhibits a convex form (hour 14). After hour 9 one can thus infer online that a maximum has appeared. The same applies to the downward inflection point after hour 14.

3.2.5 Controller design

The nitrite controller is implemented as illustrated in Fig. 3.2 (bottom graph). There are three rules in control state 0 and one rule in control state 1 that need to be evaluated as true to change the control state again. *Rule 1* in control state 1 evaluates if nitrite increased above the defined threshold. *Rule 2* and *Rule 3* in control state 0 are based on the results from the SCS analysis (Fig. 3.2 grey box). *Rule 2* evaluates if a maximum has appeared in the data. The maximum is of interest since it indicates if the nitrite concentration rise actually halts and starts to decrease, which is key to keep the process stable. It evaluates the RMSR of the two SCS models, one with U as the QS and one with UD as the QS. When the RMSR of the U model ($RMSR_U$) is significantly larger than the RMSR of the D model ($RMSR_{UD}$), i.e., $RMSR_U > f_s \cdot RMSR_{UD}$ (e.g., $f_s = 1.2$), *Rule 2* is evaluated true and *Rule 3* is evaluated. *Rule 3* identifies the inflection point in the downward trend analog to *Rule 2*. By comparing the two $RMSR_{UD}$ with $RMSR_{UDA}$ i.e., $RMSR_{UD} > f_s \cdot RMSR_{UDA}$ (e.g., $f_s = 1.2$). With decreasing substrate inhibition of the NOB, the nitrite signal gets increasingly steeper. Once the NOB reach their maximum growth rate and become substrate limited, the data exhibits an inflection point which makes the model errors of UD and UDA deviate. *Rule 4* is a timer based rule that is only needed during the development of the controller. It allows taking a sample from the reactor to monitor the nitrite concentration after the identification of the inflection point (i.e., *Rule 3*). Fig. 3.4 illustrates a schematic time-line of a whole cycle.

T1: The example starts when the nitrite oxidation is stable and the controller is in state 1. To destabilise the NOB, the controller increases the pH setpoint from 6.1 to 6.8 (green line). Nitrite starts to accumulate and the signal starts to increase (Fig. 3.4, dashed blue curve). The controller compares it to the signal value at the time of the pH setpoint increase ($NO_2^-_{pHlow}$) (Fig. 3.2, *Rule 1*). Once the difference between the $NO_2^-_{curr}$ and $NO_2^-_{pHlow}$ is larger than a given threshold difference $\Delta NO_2^-_{max}$ (15 mg N/L) the controller switches to state 0. *Rule 1* assumes that the drift of the signal within T1 is negligible compared to the chosen $\Delta NO_2^-_{max}$.

T2: In state 0 the controller switches the pH setpoint back to 6.1. The AOB growth rate decreases due to reduced pH levels (Fig. 3.1). Thus, the nitrite production by the AOB is gradually reduced such that the NOB - despite of their inhibition - start to oxidise more nitrite than the AOB produce. This results in a peak in the nitrite concentration and in turn the nitrite signal. The appearance of the peak is monitored with *Rule 2* and only used to react if nitrite would against the expectation keep increasing. In the current controller this is not automated and was only used as a safeguard in the test phase.

T3: Once the nitrite signal starts to decrease the difference in lack of fit between the U function and the

UD function increases. Thus, after T3 the controller is informed that the nitrite signal decreases (*Rule 2*) and it can start comparing the RMSR of the UD and the UDA function to identify the appearance of the inflection point (*Rule 3*).

T4: The lower the nitrite concentration gets the less inhibited the NOB are. The signal exhibits a downward concave shape (i.e., decreasing inhibition effect). Eventually, the inhibition effect is negligible but the NOB become substrate limited. Therefore, the net nitrite degradation slows down and the nitrite signal starts to become convex (increasing limitation effect) and the inflection point appears in the data. At the end of T4 the controller has identified the appearance of the inflection point.

T5: This period has the sole purpose to allow sampling for nitrite analysis to assess the success of the control decision but is irrelevant for the actual control. It equates with the 2 h timer that is implemented in the form of *Rule 4*. Once this rule is true, the controller switches back to state 1 and a new control cycle starts. We further refer to the nitrite concentrations measured in this period as *end of cycle concentrations* (ECC).

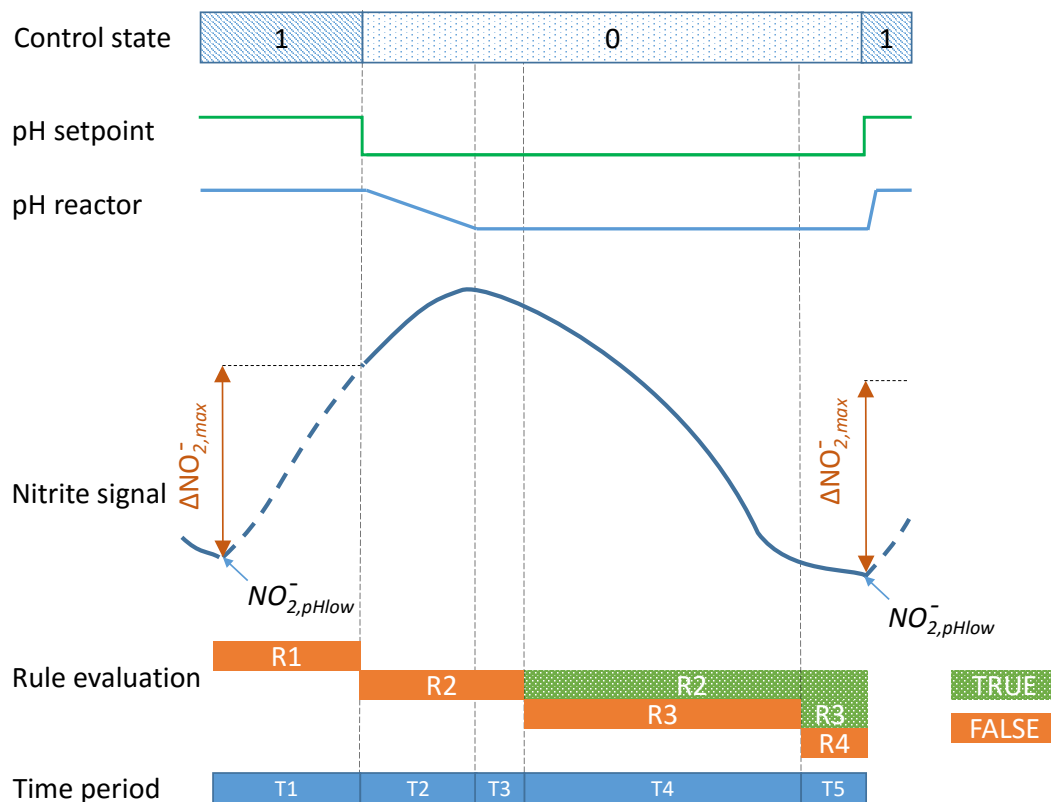


Figure 3.4: Schematic timeline of control states, pH setpoint, measured pH, nitrite signal, rule evaluation and characteristic periods T1-T5.

3.2.6 Unmeasured process disturbances

Three unmeasured disturbances are tested or monitored to evaluate the robustness of the controller. First, the signal drift itself, which is expected to occur under any given practical operational condition. Thus, part of the drift is not actively induced but allowed to occur in a passive manner. Second, the robustness of the controller is tested against temperature dynamics and thirdly against influent composition dynamics.

3.2.6.1 Determination of drift rate

To monitor if the sensor actually drifts the nitrite reference measurements are compared with the estimation of the UV-Vis nitrite signal. The rate at which the difference of these two values change is the drift rate. Periods of drift are selected visually and then described by a piece-wise linear trend line. Drift is monitored in the whole experimental period (19.03.2018 – 30.05.2018, 72 days) including the periods in which the temperature and switch of influent source experiments (see below) take place.

3.2.6.2 Temperature experiments

In the ambient temperature range (10 – 35°C) the μ AOB increases faster with temperature than the μ NOB. To evaluate whether such disturbances pose a challenge to our control system the reactor is cooled or heated by means of the water based cooling and heating jacket. A *temperature low* experiment was executed twice. Each time the reactor was cooled down from 25°C to 22°C within 10-12 h and then heated back to 25°C within 10-12 h (16./17.04.2018 and 19./20.04.2018). A *temperature high* experiment was executed in two versions. In a long version (23.04.2018-25.04.2018), the temperature was increased within 8 h from 25 to 28°C, kept there for 36 h and then cooled down back to 25°C within 10 h. For the two short version experiments (26.04.2018 and 27.04.2018), the temperature was raised from 22.5 to 28°C within 10 h and then immediately cooled back to 25°C within 10 h.

3.2.6.3 Switch of influent source

Another likely unmeasured disturbance can be a feed composition change. To test whether the induced change by such a feed composition change can challenge the controller; the reactor feed is changed. Since the start of the reactor until the 30.04.2018 09:13 the reactor has been fed with source separated urine collected from the male toilets and urinals. After this point in time, source-separated urine from the female toilets has been used. Both female and male urine collection system are located in the Forum Chriesbach Building, Eawag, Switzerland. The urine from female toilets lower concentration in ammonia (-31%) and COD (-37%) due to dilution with flushing water in the NoMix toilets. A more comprehensive overview can be found in Fumasoli et al. (2016). More details can be found in the Appendix C.1.

3.3 Results

3.3.1 Control behaviour

The following paragraph describes one control cycle during which the complete control system was in autonomous use (Fig. 3.5). The data reveals that the controller works as designed (Fig. 3.4). At around 12:00, the controller state is 1 and the pH controller setpoint is 6.8 (“high pH setpoint”, 3rd panel). This induces an increase in nitrite, as expected (top panel). After reaching the threshold for a maximal difference to the previously defined baseline (i.e., *Rule 1*) the controller state is set to 0. The pH setpoint is reduced to 6.1 (“low pH setpoint”, 2nd panel). From this time on, the nitrite signal is recorded for analysis by the SCS models. After collecting the minimal number of nitrite measurements in this time series, the SCS models are fit for the first time. In the 4th panel one can see the incremental changes of the RMSR of the three different models U, UD, and UDA as new nitrite measurements are added to the analyzed data series. One can see that RMSR_U is much larger than RMSR_{UD} and RMSR_{UDA} .

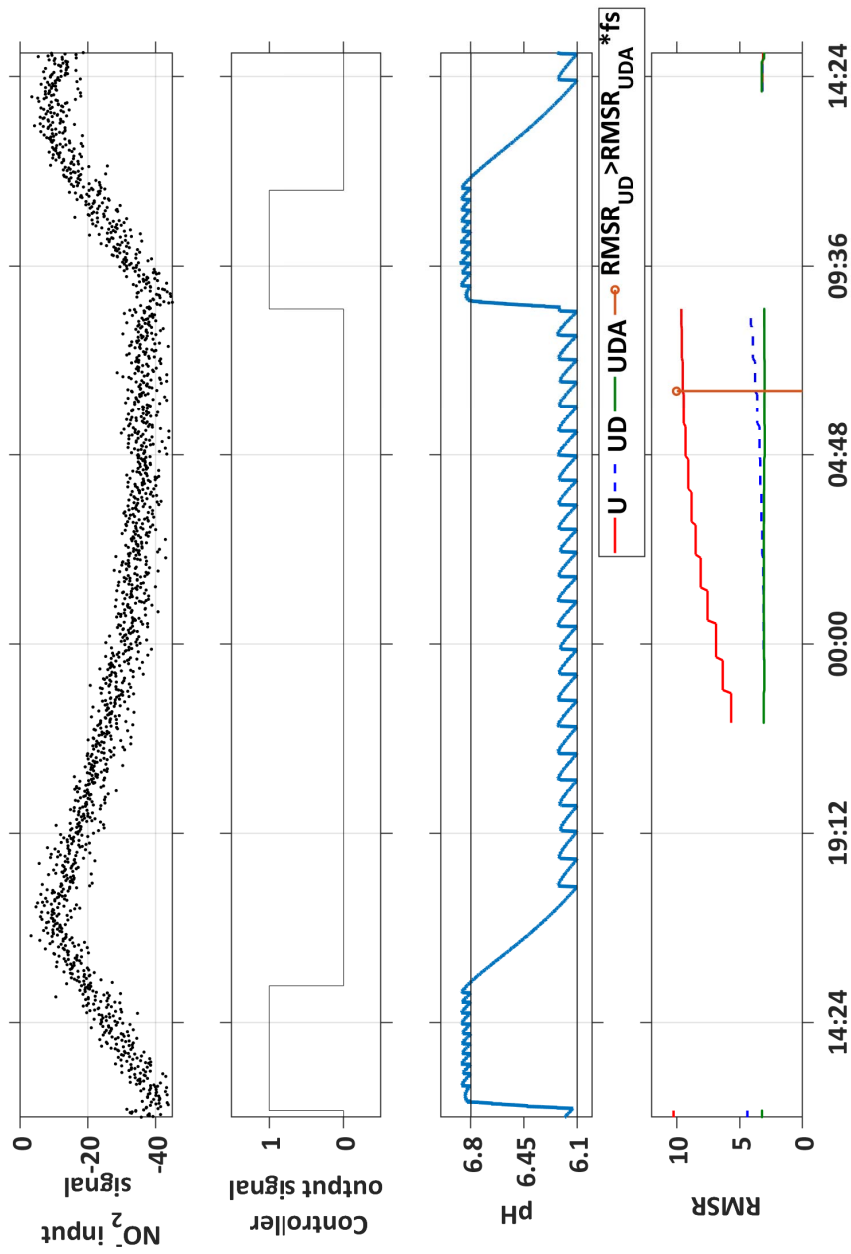


Figure 3.5: Operational data from one control cycle. 1st panel: Nitrite controller input signal. 2nd panel: Controller state. 3rd panel: pH sensor signal with two setpoints. 4th panel: RMSR of the three fitted SCS functions.

The interpretation is that the control algorithm recognises that the peak nitrite concentration has already occurred before this first time of comparative analysis. At 02:30 the RMSR_{UD} starts to deviate visually from the RMSR_{UDA} . The vertical line in the bottom panel indicates when *Rule 3* was evaluated as true shortly before 07:00, meaning that the controller now considers the presence of an inflection point in the nitrite signal as a sure thing. Shortly before 09:00 the 2 h timer *Rule 4* is also evaluated true and the controller switches back to state 1 (“high pH setpoint”). Consequently, the controller memorises the last nitrite value to reference the next nitrite increase and increases the pH setpoint to 6.8. This completes one autonomous cycle of the proposed controller.

3.3.2 Controller performance

Fig. 3.6 illustrates nitrite end of cycle concentrations (ECC) measured after the detection of the inflection point but before the pH is increased again (Fig. 3.4 T5). The ECC is for the complete experimental period at a concentration level that is substrate limiting to the NOB. The ECC progressively decreased during the period of autonomous control. The solid retention time (i.e., equals the hydraulic retention time) never exceeds 13 days (Fig. 3.7 bottom panel) meaning that the experimental period covers more than 5.5 SRTs. Thus, the controller cannot only keep nitrite low in the short term, but also successfully prevents washout of the NOB population within a significant test period.

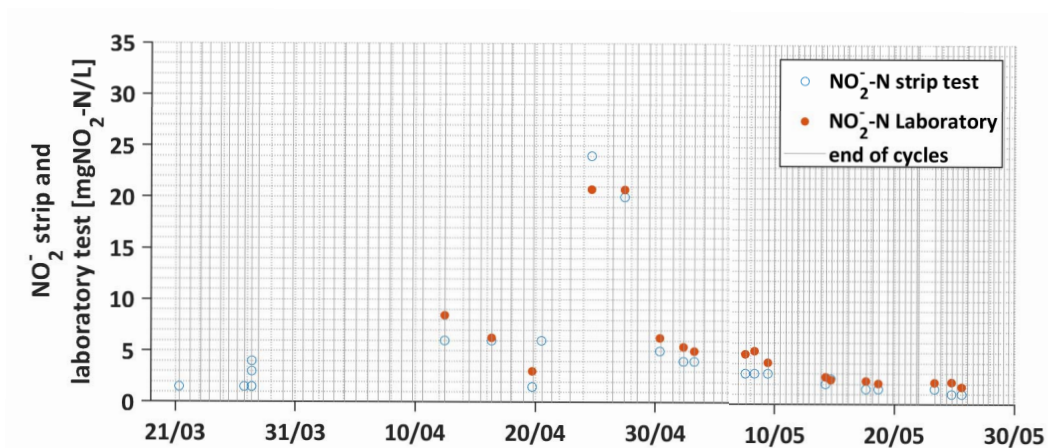


Figure 3.6: Nitrite end of cycle concentrations after identification of inflection point but before start of next cycle (Fig. 3.4 T5). Vertical lines indicate the end of a cycle.

Despite the very noisy input signal, the visual inspection of the results reveals that the model selection by means of comparing the RMSRs of the three models has never resulted in a false negative or false positive identification of the maximum or the inflection point. It has to be noted that most likely there is a certain delay in the identification due to the chosen f_s value. To quantify the delay, in every cycle the ground truth about TNN_{max} (Fig. 3.1) would need to be determined.

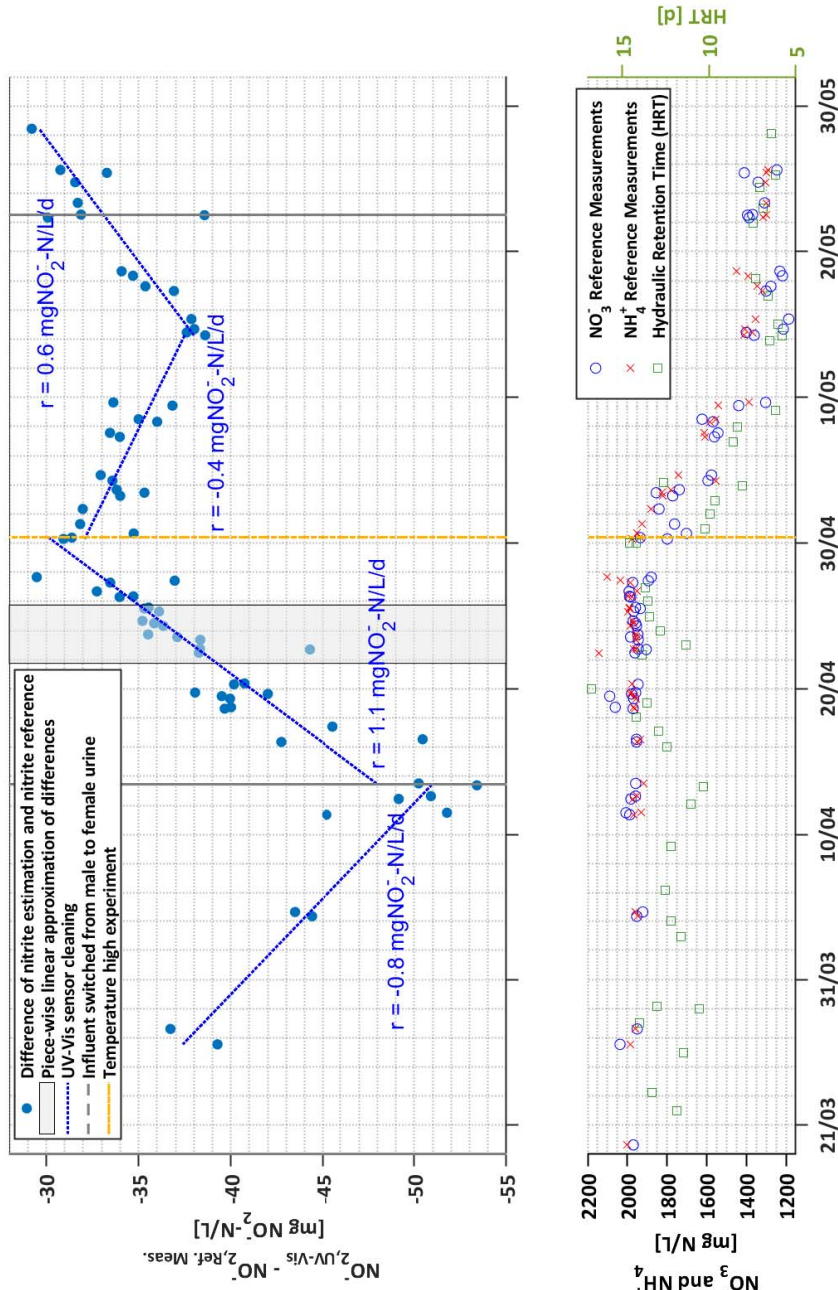


Figure 3.7: Drift rate, nitrogen species concentrations in bulk media and hydraulic residence time. Top panel: difference of estimated and measured nitrite concentrations, drift estimations as piece wise linear approximations of the estimation-measurement differences, sensor cleaning and switch of influent source to female urine, temperature high experiment period. Bottom panel: Ammonia and nitrate concentrations in bulk and hydraulic retention time.

3.3.3 Unmeasured process disturbances

3.3.3.1 Drift

The controller input signal drift is illustrated in the top panel of Fig. 3.7. Drift occurred during the entire experimental period. The estimated drift rates, obtained with the fitted piece-wise linear trend line, range from -0.8 to 1.1 mg NO₂⁻-N/L/d. Thus, one can conclude that the observed signal drift poses a meaningful challenge for process control, which has been mitigated successfully by the proposed control system. It is noted that the changes in the drift rates can only be explained partially. The vertical grey dashed lines indicate sensor cleaning. Sign changes of the drift rate are unexpected for this kind of intervention (i.e., a signal jump is expected when biofilm and solids are removed from the sensor.) Note that the initial difference between the UV-Vis based nitrite value and the nitrite reference measurements has been caused by drift in the 9 months in between the calibration period and the start of this study.

3.3.3.2 Switch of influent source

The change in influent composition (Fig. 3.7, 30.04.2018, yellow dashed line) induces a change in the sign of the drift rate from 1.1 to -0.4 mg N/L/d. In the first 15 days after the influent switch the ammonia and nitrate concentration in the reactor decrease from 2000 to 1300 mg N/L (Fig. 3.7, 2nd panel). The controller reacted to the new lower concentrated influent and increased the hydraulic loading, which is indicated by the decreased hydraulic residence time (HRT) from around 13 to 7 days (Fig. 3.7, 3rd panel). Furthermore, also the control cycle length decreased from around 1 to 0.5 d (Fig. 3.6). Thus, the controller was able to reject this disturbance and keep nitrite levels low. The slave controller was still acting as intended and compensated the decreased specific ammonia load with increased hydraulic loading.

3.3.3.3 Temperature experiment

Fig. 3.8 shows the results of the temperature high experiment. The first cycle on the 21st /22nd is illustrated to have a visual reference to the normal operation. At the start of the experiment, the controller sets the pH setpoint to 6.8 (Fig. 3.8, 2nd panel). The nitrite concentration rises for some time (Fig. 3.8, 1st panel) and consequently the controller decreases the pH setpoint again on the 23rd. However, the nitrite signal remains at a higher level around (-15 mg N/L) compared to the previous cycle (-30 mg N/L) (cf. 22nd). Nitrite reference measurements confirm that elevated nitrite concentrations are the cause for this difference in the signal, which remain around 20 mg N/L instead of around 5 mg N/L as in the previous cycle. This very small drop in nitrite compared to the peak concentration, also lead to a delay in the identification of the inflection point (Fig. 3.8, 4th panel) compared to the visual impression obtained by looking at the figure. Only in the afternoon of the 24th the controller identified an inflection point. An increase in pH at this time point would lead to an even higher accumulation of nitrite. To ensure successful testing of the controller against other disturbances, the controller is deactivated temporarily (cf. grey area 2nd panel) and the temperature setpoint is again lowered to 25°C. The cooling of the bulk media leads to a decrease in the nitrite starting at midnight on the 25th. At noon of the same day, the nitrite signal and reference measurements drop to the levels reach in the first cycle (Fig. 3.8, 22nd) and the controller is restarted shortly after. Thus, the temperature high experiment indicated that fast temperature increases pose a threat to the proposed control system. The temperature low experiment did not reveal any relevant finding with respect to the control performance. The only notable change compared to the 25°C operation is the reduction in the peak nitrite concentration by about 5 mg N/L.

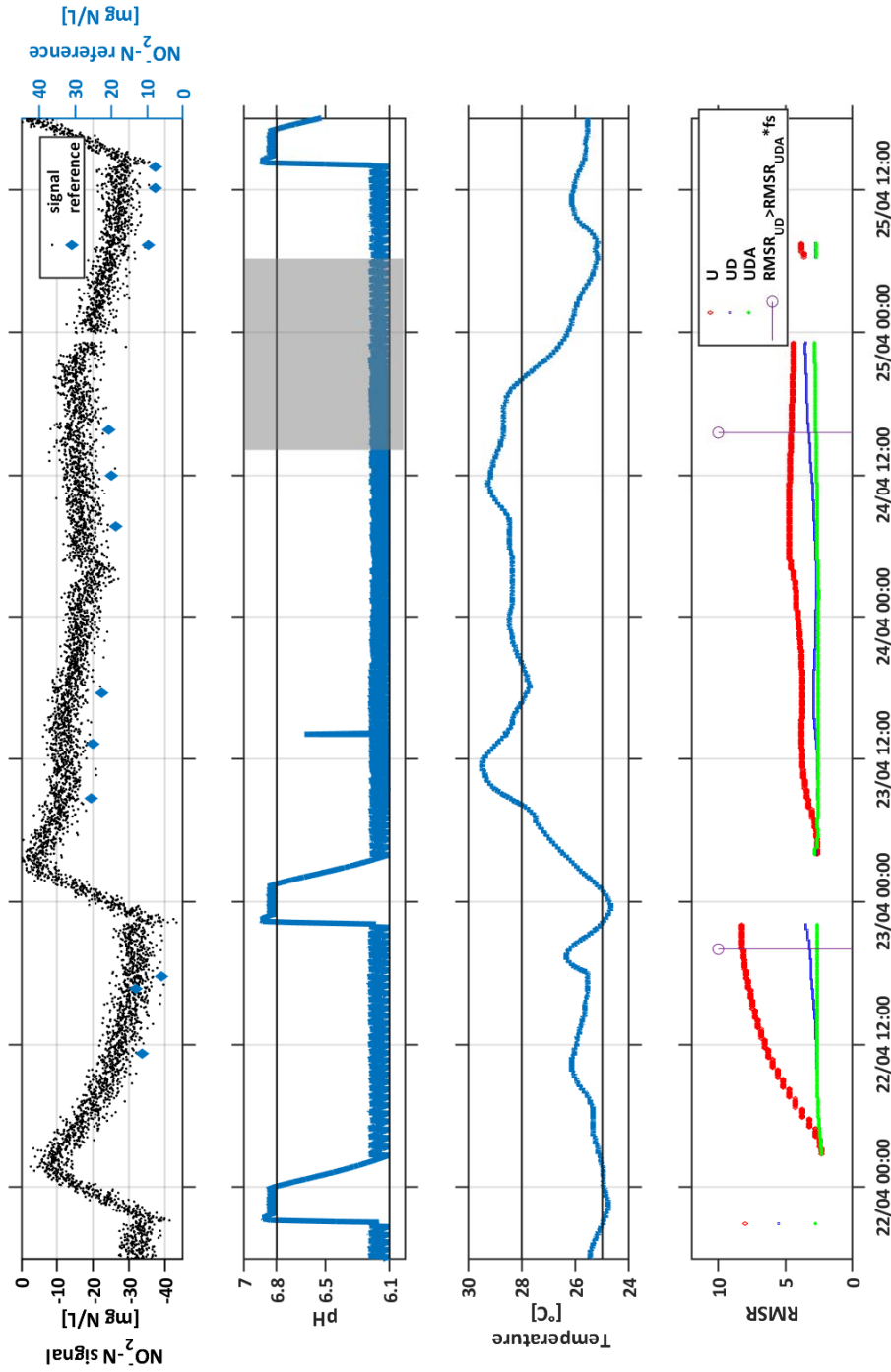


Figure 3.8: Temperature high experiment. 1st panel: Nitrite signal and nitrite reference measurements. 2nd panel: pH measurement. The grey area indicates deactivated controller. 3rd panel: Temperature measurement. 4th panel: RMSR of the three models U, UD, UDA including the time points at which the inflection point was identified.

3.4 Discussion

This study proposes a new concept for a stabilizing control in the presence of signal drift and demonstrates its utility by means of an intensive measurement campaign in a laboratory-scale reactor for urine nitrification. The proposed control system avoids the effects of signal drift by using information in the first and second derivative to distinguish between stabilizing and destabilizing process conditions. However, our study shows that fast introduction of unmeasured disturbances can threaten the suitability of this control concept in practice.

3.4.1 General controller performance

The results reveal that the controller successfully stabilised the nitrification process despite a continuously drifting nitrite estimation signal. The decrease in the end of cycle concentrations may indicate an adaption of the NOB to the elevated nitrite levels or could also be caused by the influent switch. Since steady state was never reached, the data does not allow determining if the lower concentrations were caused by a net decay of the AOB or a net growth of the NOB. Since the average pH in the reactor is higher than in the conventional operation with a constantly safe but low pH, this controller should theoretically also achieve higher nitrification rates (Udert and Wächter, 2012). However, pH is only one among many factors influencing the nitrification rates. Bürgmann et al. (2011) showed that long-term exposure to nitrite could jeopardise the process, while Van Hulle et al. (2007) hypothesised that bacteria became more tolerant when exposed long enough to elevated nitrite concentrations. Consequently, future research should compare comprehensively the presented controller with the traditional operational concept (Fumasoli et al., 2016) in terms of long-term reactor performance and maintenance need.

3.4.2 Unmeasured Disturbances

The proposed control concept is based on one important assumption. Namely, that the appearance of an inflection point in the downward nitrite signal can only be explained by a change of the dominating effect on the μ NOB from substrate inhibition to substrate limitation. To challenge this assumption and the whole controller two very likely confounding factors in the process were induced deliberately (temperature and influent composition) and one was recorded passively (drift).

The drift rates observed during the course of the experiments were as high as 1.1 mg N/L/d but did not lead to a failure of the proposed controller. Assuming that nitrite concentrations should stay below 30 mg N/L it would take less than 28 days for an autonomous controller to fail. However, the drift rate changed its signs multiple times within the experimental period. Importantly, compensation of this drift is only believed possible by means of reference measurements, as is typical.

It has to be noted that the pH sensors used for the feed control also drift. In this chapter we assume that the pH sensor is maintained such that the controller itself is hardly affected by the drift. A more comprehensive overview of the drift behaviour of pH sensors in nitrified urine can be found in Ohmura et al. (2018).

The temperature increase experiment indicates that unmeasured disturbances can make the proposed control system fail. This is explained as an effect on the μ AOB to μ NOB ratio, which increases with temperature. Indeed, the fast temperature increase of the bulk media introduced the appearance of an inflection point. However, the assumption that the inflection point is solely caused by NOB dynamics does

not hold any longer and explains the wrongful control action. Even if the elevated nitrite concentration after one cycle does not lead to destabilisation, it becomes problematic when the controller induces the next nitrite increase. That increase starts at a much higher nitrite level that presumably destabilises the NOB.

The temperature high experiment did reveal another important condition for correct functioning of the controller. The low amplitude of the signal (Fig. 3.8, 24th afternoon) delays the identification of the inflection point. This shows the need for sufficient excitement of the process and the signal to reach a large enough signal-to-noise ratio. However, the larger the amplitude the higher the risk of making the process fail (i.e., Fig. 3.1, exceed point B)

The influent switch experiment did not influence the observed signal profiles in a meaningful way. As a result, the controller was able to execute the right control actions in a timely manner throughout the course of this test. There are two explanations for this: First, the model to derive the nitrite concentrations from the UV-Vis absorbance measurement is apparently quite robust against changes in the reactor media composition, particularly large changes of the nitrate concentration (Fig. 3.7). Second, the dynamics caused by the influent switch are driven by the HRT and decreased from 13 to 7 d. Thus, the disturbance is much smoother than the temperature experiments with a time window of 0.5 d.

3.4.3 Extension of controller

So far, the controller makes the nitrite concentration oscillate around the optimal concentration for maximal μ NOB. The upper pH setpoint has to ensure that nitrite is always accumulating to keep the signal informative. The lower pH setpoint has to ensure net nitrite degradation to stabilise the process. Choosing the setpoints can be challenging and some disturbances may influence the system such that the pH setpoints cannot push the process into the intended operational region. Enabling the controller to decide how the two pH setpoints itself should be set would also facilitate process optimization. One way to have the correct AOB to NOB rate ratio for both pH setpoints was revealed in the high temperature experiment. The increased temperature leads to a relatively high AOB rate at low pH. This in turn resulted in slow net nitrite degradation and thus a flat decreasing trend in the signal compared to the previous increase. Thus, the pH setpoints and in turn, the overall process performance were generally rather high for the given NOB capacity. Thus, the ratio of the increasing and the decreasing slope in one cycle allows optimizing the pH setpoints and in turn the process performance. Furthermore, using this kind of information would also help to reject additional disturbances without the need for additional instrumentation (cf. high temperature experiment).

The adaptations made to enable SCS analysis in an online environment worked without any complications. The adaptations embedded the SCS as a model selection tool in a moving horizon estimation framework with a fixed start point. SCS proved to be reliable for online analysis of data and the 13 primitives (Table 3.1) facilitate its use for more complex sequences. Despite concerns about the computational costs by Villez and Rengaswamy (2013) the three SCS models could be fitted to the data within less than 3 seconds on an Intel® core i7 4970k 4 GHz processor. Thus, conventionally available computational resources are expected to be sufficient for most biochemical process monitoring applications. Faster computations when dealing with high-frequency data collection systems, can be facilitated by increasing the knot distance of the spline functions. If computational cost is no concern at all, then the knot distance can be reduced to improve the fit of the applied SCS models.

3.4.4 Linking to control theory

The proposed controller is based largely on a conceptual model of substrate affinity and inhibition in nitrifying bacteria. Assuming that the NOB activity rate has a unimodal shape with respect to the nitrite concentration, one can expect to observe an inflection point whenever the process shifts from conditions dominated by nitrite inhibition to conditions dominated by nitrite limitation. This information is key to avoid the need for any explicit correction of the signal drift since it is contained in the derivatives. Importantly, the actions taken by the controller can also be interpreted as the execution of an online experiment to determine the NOB kinetics. Microbial populations adapt over time and thus it is highly likely that the inhibition and affinity constants of these population change. Consequently, a sensor signal without relevant drift as input would allow tracking the optimal concentration of nitrite for a maximal μ NOB.

This is also important with view on the many nitrification controllers equating nitrification with ammonia removal while nitrite oxidation is assumed to be completed simultaneously. Consequently, single indicators such as ammonia concentration, pH valley, or OUR drop have been assumed informative enough to control the process (Åmand et al., 2013; Jaramillo et al., 2018; Thürlimann et al., 2018a). This is justifiable in some situations (e.g., municipal WWTP). However, in certain situations analysis of both ammonia oxidation and nitrite oxidation is key for process stability and optimization. Partial nitrification/anammox (Lotti et al., 2012) or on-site WWTP, which can be limited by alkalinity due to the undiluted inflow. Thus, this concept can be translated to any given bacteria population when derivatives are informative about the concentration trend of a relevant substance.

The benefits of controllers executing online experiments to determine process states in continuously operated reactors are rarely studied in wastewater treatment. Steyer et al. (1999) also deliberately induced process disturbances to gain information about the performance of an anaerobic reactor. In contrast to the presented controller, they compared the information against a simple model to determine the performance. The intentional excitement or perturbation of a system to obtain information which is then used to control the system has its basis in the dual control theory (Feldbaum, 1960). The controller also has similarities with extremum seeking control (ESC) (Liu and Krstic, 2012). Both, ESC and the presented controller are model-free, feedback controllers that purposely excite the system to gain information. ESC generally requires an excitement frequency that is much lower than the dominant process frequency. This is not the case here as the biomass growth dynamics ($HRT = 13$ d) and the excitement frequency (1 d⁻¹) appear in the same time scale. Trollberg et al. (2014) found that the combination of a slow process and low excitement frequency as found in wastewater treatment make current forms of ESC impractical. However, they further stated that knowledge about the system behaviour close to the optimum is crucial to facilitate the use of ESC. We believe that in this controller knowledge about the NOB sensitivity to nitrite, in the range around TNN_{max} (Fig. 3.1), is implicitly incorporated. Using ESC would also facilitate to include the ideas presented in 3.4.3 thus, not only stabilization but also optimization could be achieved. Therefore, ESC should be further investigated.

3.5 Conclusion

In this study, a controller for stabilizing nitrification in high strength wastewater was tested. The controller prevented the accumulation of nitrite in an alkalinity limited urine nitrification reactor for the entire test period of 72 days. These are the conclusions:

- Information contained in the derivatives of a drifting signal combined with qualitative knowledge about kinetics allowed for the control of an open-loop unstable system without the need for drift rate estimation or correction.
- Systems without any dynamics due to input or operation can be excited deliberately in such a way that the signal derivatives contain the information of interest about the process states. In this study, the controller was designed to destabilise the nitrification such that the signal derivatives contain the necessary information about the process state, in turn enabling stabilizing feedback control. Somewhat counter-intuitively, deliberate short-term destabilization facilitates the assurance of long-term process stability.
- The controller is based on a conceptual model of the process. This model currently excludes the effect of unmeasured disturbances other than the signal drift. This constitutes the most sensitive component of our proposed controller. Whereas slow unmeasured disturbances were successfully rejected, information in the controller input signal informing about fast, unmeasured disturbances were identified and considered for inclusion into the control logic.

Acknowledgement

The authors want to thank Benjamin Stucki and Kito Ohmura their assistance with the experiments, Karin Rottermann and Sylvia Richter for their assistance with the laboratory analysis. Dominique Bonvin and Juan Pablo Carbajal for their inputs regarding the control theory. This research was made possible by the Swiss National Foundation (Project: 157097).

4 Soft-sensing with qualitative trend analysis for control in full-scale wastewater treatment plants

This chapter is based on the following journal publication:

Thürlimann, C. M.^{a,b,c,d,e,f}, Dürrenmatt, D. J.^{a,b,d,f}, Villez, K.^{a,b,d,f} (2018) Soft-sensing with qualitative trend analysis for wastewater treatment plant control, *Control Engineering Practice*, 70, 121-133.

^aStudy concept and design, ^bSoftware development, ^cAcquisition and analysis of data, ^dInterpretation of data, ^eDrafting of chapter, ^fCritical revision.

4.1 Introduction

Ammonia removal from municipal wastewater is conventionally achieved with biological nitrification. This process requires aerobic conditions for the bacteria to oxidise the ammonia to nitrite and further to nitrate. Fine bubble aeration is an efficient way to supply the required oxygen into an activated sludge reactor (Rosso et al., 2008). Ingildsen (2002) reported that on average aeration accounts for up to 60% of the total energy consumption of a wastewater treatment plant (WWTP). Since municipal WWTPs exhibit nutrient and flow dynamics, the control of the plants aeration intensity is essential for operational efficiency.

Initial attempts to make the oxygen supply more efficient by automation were pursued in the 1970s (Olsson, 2012). These first automation attempts were aimed at controlling the aeration rate to maintain the dissolved oxygen (DO) concentration in the aeration basins close to a fixed oxygen concentration setpoint. This prevents an under- and, especially, over-supply of oxygen to the bacterial community (e.g. Andersson, 1980). Today this is a standard control strategy for WWTPs. Further aeration efficiency gains can be realised by controlling the ammonia concentration (e.g. Åmand et al., 2013). Practically this is achieved by means of cascade control: The master control sets the DO set points in the slave aeration controller according to the ammonia concentration. The slave controller, in turn, adjusts the aeration intensity to reach the given DO setpoint. Reducing the DO concentration in low load situations results in two main aeration efficiency gains: (i) it decreases the volume-specific nitrification capacity, which in turn shifts part of the load downstream, thereby involving otherwise unused downstream aerobic reactor volumes in the nitrification process and (ii) the larger oxygen concentration gradient between the gas and liquid phase improves oxygen transfer efficiency. In addition, ammonia based aeration control can enhance the nitrogen and phosphorus removal efficiency and can decrease the need for external carbon dosage (Rieger et al., 2014). Today such advanced aeration control is available for many large WWTPs. Commercially available ammonia control systems rely on in-situ ion selective electrodes or ex-situ analysers for the measurement of the ammonia concentration. However, these instruments are costly to operate as they require frequent maintenance by skilled staff (Kaelin et al., 2008). This is why installation and maintenance costs may not be covered by the energy cost savings on small or remotely controlled WWTPs. To overcome this obstacle soft-sensors offer an interesting alternative to using high-end yet error-prone instruments. Soft-sensors are based on the identification of stable relationships between the variable of interest and the signals of one or multiple cheaper and/or more robust sensors (Haimi et al., 2013). If these relationships are based on empirical black-box modelling instead of first principles, such soft-sensors are often challenged in practice due to their lack of transparency, lack of general validity and/or their (re-)calibration and fine-tuning needs (Dürrenmatt and Gujer, 2012). The use of mechanistic concepts for soft-sensor development - if available - is therefore considered the preferred approach. For biological wastewater treatment in sequencing batch reactors (SBR), soft-sensors based on a mechanistic understanding such as conductivity for ammonia (e.g. Joss et al., 2009) or pH/ORP for control of biological denitrification (e.g. Peng et al., 2002) are described in the literature. Zanetti et al. (2012) derived a comprehensive list of soft-sensors used for the control of wastewater treatment.

For continuously operated WWTPs, Ruano et al. (2009) introduced a mechanistic ammonia soft-sensor. They demonstrated that the pH difference over the aerobic zone contains information about the ammonia concentration present in the tanks. Indeed, the pH signal reflects the balance between nitrification and CO₂-stripping. An increasing ammonia load boosts the nitrification and the proton production. Unless an increased aeration rate equalises the proton production by CO₂-stripping, the reactor will experience a net proton production and its pH will drop. The opposite happens if the ammonia load drops: the lower proton production of the reduced nitrification does not outweigh the CO₂-stripping, and the pH rises

unless the aeration intensity is decreased.

Ruano et al. (2012) kept the pH difference over the first and last tank of an aerobic tank series at a fixed setpoint by manipulating the airflow in these activated sludge tanks. By maintaining this pH difference close to a given setpoint value, they were able to adequately react to changes in the ammonia load. A given pH difference setpoint corresponds to a certain ammonia effluent concentration in a steady state system (Ruano et al., 2012).

As pH sensors are prone to drift, the controlled pH difference value will tend to deviate from the intended pH difference value. Consequently, the effective ammonia concentration at the WWTP outlet is expected to deviate from the intended setpoint as time progresses. Despite the difference in their time constant, actual process dynamics and sensor drift are hard to distinguish. Thus, a frequent and strict sensor management remains necessary in spite of using state-of-the-art pH sensors.

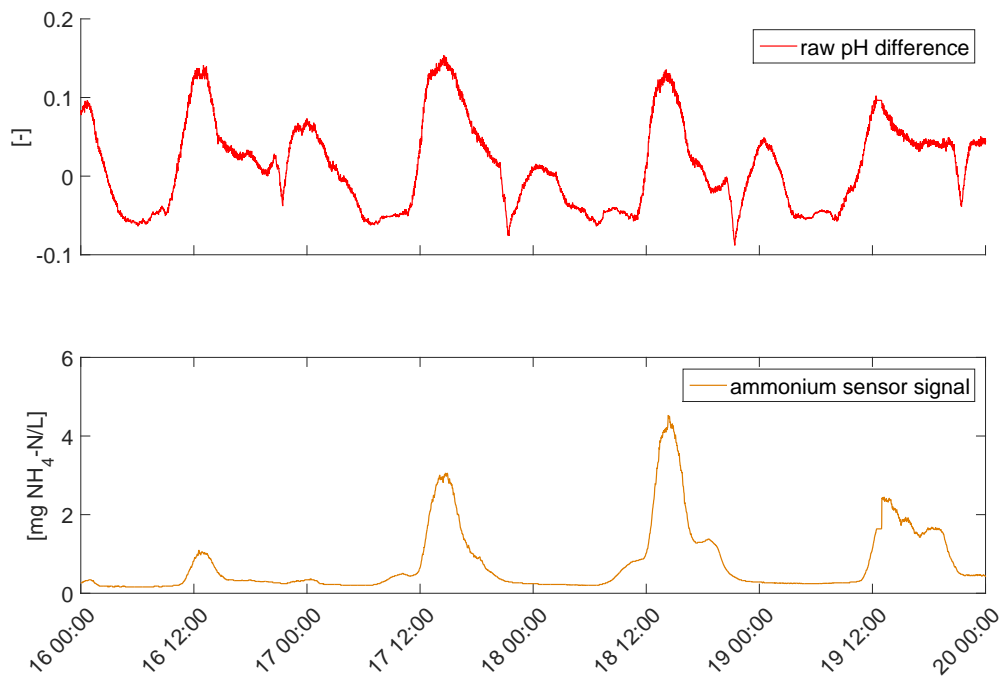


Figure 4.1: pH difference between first and last tank in a series of three aerated activated sludge tanks (top) and $\text{NH}_4\text{-N}$ concentration (bottom) measured in the middle tank. Each of the $\text{NH}_4\text{-N}$ peaks is matched with a peak in the pH difference.

Despite the expected drift of pH sensors, information about the ammonia load can be extracted from the pH difference signal. The pH and ammonium time series in Fig. 4.1, recorded at the Hard WWTP (details follow), show the synchronous appearance of their extrema. The maxima in particular appear well-synchronised. The pH difference signal (top Fig. 4.1) exhibits two peaks per day. The one with the higher amplitude exhibits a shape which is similar to the shape of the ammonia concentration peak (bottom Fig. 4.1). The sharp drop and increase in the pH difference every evening is caused by an air flushing which is used to clean the ceramic diffuser domes. In this study the identified minima and maxima of the pH difference signal (further referred to as qualitative features) are used in a semi-quantitative rule-based control to distinguish between high and low ammonia load situations. Based on this information the controller will determine the DO setpoint in the slave aeration controller.

Qualitative trends and the corresponding features of the signal can be detected by means of qualitative trend analysis (QTA) methods. QTA algorithms split time series into time periods called *episodes* within which the signs of one or more of the signal's derivatives are constant. Cheung and Stephanopoulos (1990) introduced seven primitives which can qualitatively describe most of the trends occurring in a time series. Based on this study, methods were developed to identify these primitives in online signals. A piece-wise fitting method was presented by Konstantinov and Yoshida (1992). Bakshi and Stephanopoulos (1994) used wavelet analysis to extract trends. Another approach was taken by Rengaswamy and Venkatasubramanian (1995), who identified the primitives by means of a neural network. So far, QTA has been used for process monitoring (e.g. Charbonnier and Gentil, 2007), fault diagnosis (e.g. Scali and Ghelardoni, 2008; Maurya et al., 2007) and fault detection (e.g. Villez and Habermacher, 2016). More recently, QTA-like models have also been used for image analysis (Derlon et al., 2017) and for kinetic modelling (Thürlimann et al., 2017). First ideas to use QTA also in process control were mentioned by Villez et al. (2008). However, QTA has not been applied for any autonomous control purpose yet. The use of this qualitative information in a control system requires an algorithm that detects the qualitative features in a timely and robust manner. In contrast to the mentioned methods, shape constrained splines (SCS) methods are robust to noise yet computationally expensive (Villez and Rengaswamy, 2013; Villez and Habermacher, 2016; Derlon et al., 2017). A recently developed method called Qualitative Path Estimation (QPE) approximates the performance of the SCS in a computationally efficient manner (Villez, 2015). QPE fits a given sequence of shapes, defined by the first and second derivative, to a given signal and optimises the identified change of the shapes within the sequence (i.e., maxima, minima, and inflection point). This means that the sequence of shapes needs to be known beforehand. This is why QPE as well as the SCS methods are, despite their accuracy, simplicity, and speed, not suited well for online applications. Therefore, a new algorithm tailored for online application, called Qualitative State Estimation (QSE) based on the QPE algorithm, is proposed in this study.

Tests on six different municipal WWTPs, which differ in size and treatment technologies, demonstrate the long-term validity and ease of deployment of the QSE method in combination with the rule-based controller for ammonia based aeration control. The paper focuses mainly on the results from the WWTP Hard where the QSE technique was developed initially and the longest experimental phase: 15 months of virtual testing (i.e., post-processing of recorded data without closed loop control) and live testing (i.e., with closed loop control) took place. Experiences gained on other plants are listed and discussed with a focus on the opportunities and limitations of the method. The paper is structured as follows: In the Material and Methods section the theory of the newly developed QSE algorithm is described in detail. Furthermore, a new control strategy for pH based ammonia aeration control is presented. This includes the hardware-setup as well as the rule-based control. Finally, information about the performance evaluation procedure and the characteristics of the WWTPs where the controller was tested are provided. The Results section is used to demonstrate the QSE algorithm and the rule-based controller, and to evaluate the controller performance with regard to various full-scale plants. The implications of the results are discussed at the end of this study.

4.2 Material and Methods

4.2.1 Work flow summary

Fig. 4.2 gives an overview of the data processing steps from the initial pH sensor measurements to the final adaptation of the nitrification process. The first four steps are described in detail in the Material and Method section. First, the signal is processed by the two-step QSE algorithm, then the rule-based control evaluates the QSE result. In parallel to this procedure, the raw signal and some of the plant's process states are analysed to check for anomalous data or events and override the rule-based control decision when necessary. After this final check, the DO setpoints are passed to the DO controller which will adapt the airflow in the biological reactors and subsequently the nitrification rate and the pH in the bulk phase. An implementation of the QSE algorithm in Matlab[®] is available in the supplementary information of the journal publication. Additionally a Matlab[®]/Octave toolbox enables to reproduce our results.

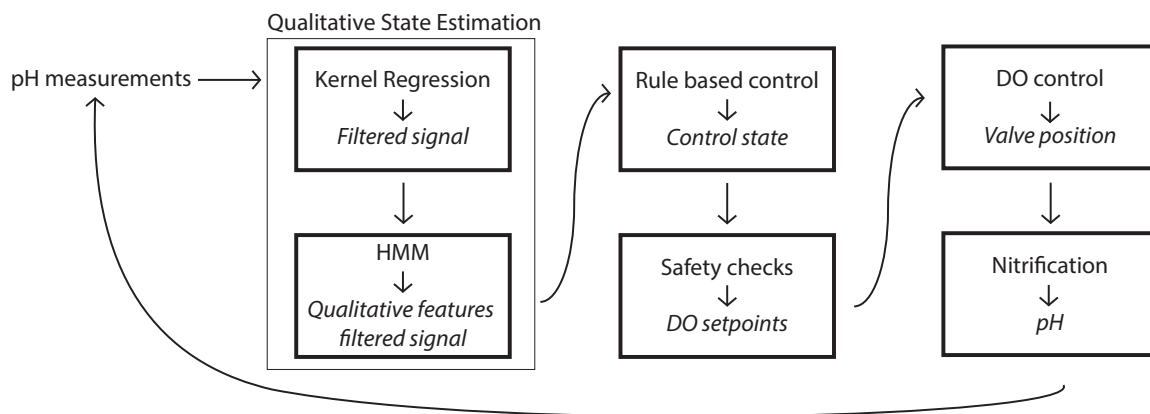


Figure 4.2: Preprocessing of raw signal with QSE and subsequent control cascade steps leading to an adaptation of the nitrification performance. The normal text names the step, the italic text names the outcome of the step which is passed on to the next step.

4.2.2 Qualitative State Estimation algorithm

The Qualitative State Estimation (QSE) is an algorithm for the segmentation of time series into *episodes*. Each episode has a distinct set of signs for the signal's derivatives. Each such unique set is referred to as a *primitive* and is reported as an unique alphabetic character. Table 4.1 shows the thirteen primitives based on the sign of first and/or the second derivative. A character is attributed to each primitive. Some are meant as abbreviations of their form while others are assigned arbitrarily. Depending on the use case, episodes can either be defined by the first and second derivative (i.e., A (antitonic acceleration), B (boost), C (concave deceleration), D (deceleration), E, F (flat), G) or only by one derivative (i.e., L (lower), N (negative), P (positive), and U (upper)) or by none (i.e., Q (undefined signs)). The end point of one episode is the start point of the next and represents either a maximum, a minimum, or an inflection point. In the application studied in this work, only the primitives defined on the basis of the first derivative sign are used. Moreover, only positive and negative signs are considered while zero-valued or undefined derivative signs are excluded. Therefore, only the primitives U and L are of practical use in this work. The QSE algorithm is however general and allows - in principle - for all primitives in Table 4.1 to be considered.

Table 4.1: Thirteen primitives defined by first and second derivative sign of the signal. ? stands for undefined sign. Adapted from (Villez and Rengaswamy, 2013). (*) primitives shared with Cheung and Stephanopoulos (1990). (+) primitives are listed for completeness but are deliberately ignored in this paper.

Derivatives	First				
	Signs	+	0	-	?
	+	B*	/	A*	P
	0	G*+	F*+	E*+	O+
Second	-	C*	/	D*	N
	?	U	/	L	Q

The proposed algorithm is based on Qualitative Path Estimation (QPE) by Villez (2015), which allows fast batch process diagnosis. Both QPE and QSE can be separated into two steps. The first step of both QPE and QSE provides a forward flow of information based on locally weighted least-squares regression. In this step, time-local probabilities for the sign of the derivatives are computed. It is noted that the first filtering step of the QSE algorithm is designed to estimate probabilities for the derivatives' signs to facilitate the further processing.

The second step of QPE is based on the Viterbi algorithm (Viterbi, 1967) for optimal path estimation and is used to convert the continuous probabilities into discrete values for the derivative signs. The Viterbi algorithm includes a forward and a backward pass which renders QPE especially useful for off-line and end-of-batch applications. As the current application is focused on control in continuous-flow processes, we replace this step with a maximum likelihood estimation of the discrete state at every measurement sample. As a result, QSE only requires a forward pass which makes the method especially suitable for on-line application.

Both steps in the QPE and QSE algorithms induce a denoising effect. Importantly however, the second step also allows enforcing a certain order of appearance of the identified inflection points, minima, and maxima. This means that both QPE and QSE allow incorporation of prior knowledge about the shape of the expected signal, similarly to the SCS method and in contrast to conventional QTA methods. The following paragraphs describe the QSE algorithm. The method is first presented in a general form (*General treatment*) and then applied to the pH difference example (*Application*).

Step 1 – Kernel regression to estimate qualitative trend probabilities

General Treatment First, kernel regression is used to smoothen the raw signal with a moving window approach. i is the data point at the window centre. The point $i + w$ represents the most recent data point in the window. An equidistant spacing of the data points is assumed. For each window $[i - w, i + w]$ around the window centre, a polynomial function with a degree d is estimated by minimising a weighted least square function. The chosen weighting is known as the tri-cube kernel (Hastie et al., 2009). This kernel is parametrised by τ , which is the critical distance from the reference data point i after which all data points have zero weight. The complete vector of measurements included in the window

centred around i is given as \mathbf{y}_i . The number of data points considered in the kernel regression increases with τ given that $w = \lfloor \tau \rfloor$. This generates two effects which one has to trade off against each other: (i) with increasing value for τ the filtered signal is smoother and QSE therefore identifies fewer qualitative features and (ii) the delay of the filtered signal increases. Kernel regression enables the computation of the expected distribution for the derivatives of the signal f_i^a as:

$$f_i^a \sim N\left(\hat{f}_i^a, \sigma_{f^a, i}\right) \quad (4.1)$$

with $\sigma_{f^a, i}$ as the variance of the signal a th derivative. For details we refer to Villez (2015).

The probability for a positive sign of the a th derivative at the sampling point i ($\Lambda_i^{(a)}$) is computed by integrating the normal probability density function from infinity to zero:

$$\Lambda_i^{(a)}(+ | \mathbf{y}_i) = \Lambda\left(f_i^{(a)} > 0 | \mathbf{y}_i\right) = \int_{u=0}^{+\infty} \frac{1}{\sqrt{\sigma_{f^a, i} \Pi}} \exp\left(-\frac{(u - \hat{f}_i^a)^2}{\sigma_{f^a, i}}\right) du \quad (4.2)$$

The difference of 1 to the positive sign probability corresponds to the probability for a negative sign:

$$\Lambda_i^{(a)}(- | \mathbf{y}_i) = 1 - \Lambda_i^{(a)}(+ | \mathbf{y}_i) \quad (4.3)$$

Note that zero-valued derivatives are deliberately ignored. With Eq. 4.2 and Eq. 4.3 one can derive the probability for the primitives L, N, P, Q, and U (Table 4.1). For the primitives defined by the first and second derivatives one multiplies the probabilities for the sign of the first and the second derivatives to obtain the probability for the primitive. In words, the probability for the primitive (κ_i) to be A is equal to the probability that the first derivative is positive times the probability that the second derivative is negative.

$$\Lambda_i(\kappa_i = A | \mathbf{y}_i) = \Lambda_i^{(1)}(+ | \mathbf{y}_i) \cdot \Lambda_i^{(2)}(- | \mathbf{y}_i) \quad (4.4)$$

This product ignores the presence of correlation between the estimates for the first and second derivative. However, as pointed out in Villez (2015), no significant loss in accuracy has been demonstrated so far. For each primitive, the products are derived analogously according to Table 4.1. This concludes the first step.

Application For the pH difference example, the procedure is limited to Eq. 4.1-Eq. 4.3 as only the sign of the first derivative is of interest. Thus, the second derivative is neglected and only the primitives U (positive first derivative) and L (negative first derivative) (cf. Table 4.1) are used.

Step 2 – Probability estimation by hidden Markov model

General Treatment To identify the change of the primitive (derivatives signs), a hidden Markov model (HMM) is used. Every state s in the HMM is associated with a primitive $\mathbf{q}(s)$. \mathbf{q} is the vector containing all the possible primitives. This HMM model predicts the likelihood of a certain process state t at point i , depending on the likelihoods of all possible states at point $i - 1$ as follows:

$$\Lambda\left(\mathbf{s}(i) = t | i - 1\right) = \sum_{p=1}^q \mathbf{T}(t, p) \cdot \Lambda\left(\mathbf{s}(i - 1) = p | i - 1\right) \quad (4.5)$$

At any given time instant, i , the likelihood that the state equals t is a sum of products, where each product consists of the likelihood that the state equalled p at time $i - 1$ times the associated transition likelihood,

i.e., the likelihood that at point i the process is at state t , conditional to the process state being p at time point $i - 1$. The complete set of transition likelihoods is given as a matrix \mathbf{T} with $\mathbf{T}(t, p)$ the transition likelihood for states p and t . Thus, the prediction of the process states in i are only dependent on the likelihoods at $i - 1$ (first-order Markov property).

$$\mathbf{T}(t, p) = \begin{cases} 1, & p = t \\ \lambda_i(t, p) = \lambda, & \text{otherwise} \end{cases} \quad (4.6)$$

All diagonal elements are equal to one. Each off-diagonal element $\lambda_i(t, p)$ of the transition probability matrix $\mathbf{T}(t, p)$ may take any value between 0 and 1. The lower the value of these off-diagonal elements, the more effective is the filtering by the HMM (i.e., less likely switch from state p to t). Any $\lambda_i(t, p)$ equal to zero prohibits the identification of a state change from p to t within a single time step.

The predictive model is now completed with a sensor model. According to Villez (2015) the HMM sensor model and the underlying assumptions can be written as follows:

$$\Lambda(\mathbf{y}_i \mid \mathbf{s}(i) = t) = \Lambda(\boldsymbol{\kappa}(i) = \mathbf{q}(t) \mid \mathbf{y}_i) \quad (4.7)$$

In words, the likelihood of the observed data (\mathbf{y}_i) conditional to a given state (t) is assumed equal to the probability of the primitive associated with the considered state ($\mathbf{q}(t)$) conditional to the observed data (\mathbf{y}_i). The latter probability, i.e., the right side of Eq. 4.7, is calculated in the first step of the QSE (cf. Eq. 4.4).

Based on Eq. 4.5 and Eq. 4.7, the maximum likelihood state estimate \hat{s} at time i is now given as:

$$\hat{s}_i = \max_t \Lambda(\mathbf{s}(i) = t \mid i) \quad (4.8)$$

with

$$\Lambda(\mathbf{s}(i) = t \mid i) = \Lambda(\boldsymbol{\kappa}(i) = \mathbf{q}(t) \mid \mathbf{y}_i) \cdot \sum_p \mathbf{T}(p, t) \cdot \Lambda(\mathbf{s}(i-1) = p \mid i-1) \quad (4.9)$$

Each change in the maximum likelihood state corresponds to the identification of a change in primitive and therefore implies the presence of a qualitative feature such as a maximum, a minimum, or an inflection point.

Application For the pH difference signal the HMM identifies the change in the first derivative's sign (zero-crossing) in the signal resulting in one of the two model states (i.e., upward and downward trend). The vector \mathbf{q} has the following form:

$$\mathbf{q} = \begin{pmatrix} L \\ U \end{pmatrix} \quad (4.10)$$

In contrast to the work in Villez (2015) the transition matrix \mathbf{T} is symmetric in this study as both maximum likelihood transitions (i.e., L to U and U to L) have the same λ values. This implies that both state changes are a priori equally likely (cf. section 4.4.2).

$$\mathbf{T} = \begin{pmatrix} 1 & \lambda \\ \lambda & 1 \end{pmatrix} \quad (4.11)$$

The time instants where the state estimate \hat{s}_i changes correspond to maxima and minima are used in the proposed rule-based controller.

4.2.3 Hardware and Control strategy

The next paragraph describes the hardware setup as well as the rule-based controller.

4.2.3.1 General experimental design

A pH difference signal is computed as the difference between two pH sensor signals. These sensors are placed in the first and the last aerated tank in the biological treatment line as shown in Fig. 4.3. The difference is calculated as the upstream tank measurement minus downstream tank measurement. It is important to know that this difference is influenced mostly by nitrification and CO_2 -stripping (i.e., no denitrification, no control of the pH by any other means). Both pH signals are recorded simultaneously with a high enough sampling interval (e.g., 1 minute) to capture the relevant process dynamics. For development and validation purposes an ion selective electrode (ISE) is installed to record ammonia concentrations. This ammonia signal is only used for performance evaluation and fine-tuning.

4.2.3.2 Hardware setup, maintenance, and signal processing

Fig. 4.3 shows the chosen hardware setup. The two pH sensors (Orbisint CPS11D, Endress & Hauser, Reinach, Switzerland) are placed in the first and the last aerated tank. Both pH signals are recorded with a sampling interval of one minute. The ion selective electrode (ISE, ISEmax CAS40D, Endress & Hauser AG, Reinach, Switzerland) is placed in the middle tank and is not used for control.

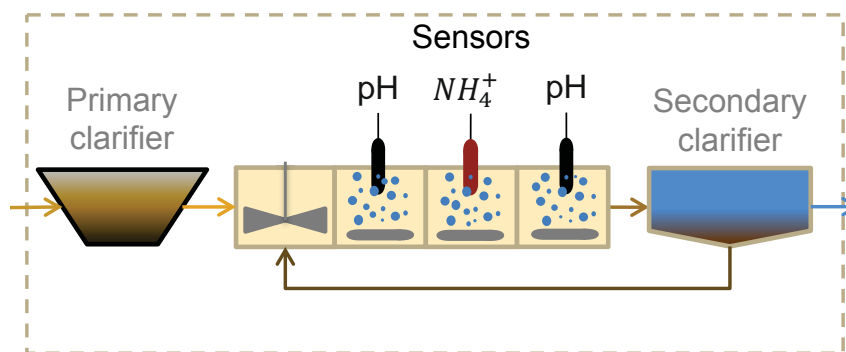


Figure 4.3: Hardware setup for soft-sensor development and validation on the a wastewater treatment plant. pH sensors (black) are placed in front and rear aerated reactor tanks. An ammonia sensor (red) is placed in the middle tank (not used for control).

All sensor signals are converted to 4-20 mA signals (Liquiline CM444, Endress & Hauser AG, Reinach, Switzerland) and fed into the supervisory control and data acquisition system (SCADA, RITOP[®], Rittmeyer Ltd., Baar, Switzerland). The final version of the controller is implemented in and fine-tuned with RITUNE[®] (Rittmeyer Ltd., Baar, Switzerland), a platform for WWTP optimisation. This platform communicates with RITOP[®] to receive process data and send control tasks. Initial tests and algorithm development are executed in Matlab[®]. The maintenance of the hardware is limited to a weekly cleaning

of the sensors. Recalibrations are executed based on a visual inspection of the signal but not more than once a month. This is applied on all WWTPs considered.

4.2.3.3 Rule-based control

The extrema resulting from the QSE require further processing for two reasons: First, the QSE step fed with the noisy and dynamic raw signal (Fig. 4.1 top) results in more detected extrema than one would expect given the rather smooth ammonia concentration time series (Fig. 4.1 bottom). Second, the variable of interest is the ammonia concentration, which is a continuous signal; the QSE output, however, is binary (i.e., downward trend/maximum, upward trend/minimum) and forces one to distinguish between ammonia peaks that can be handled with low DO concentrations and ammonia peaks that require an enhanced nitrification performance (high DO).

Consequently, additional semi-quantitative rules are added to obtain a meaningful control output. These rules are implemented into a rule-based controller which is the master control in the aeration cascade control. It is designed as a gain scheduling controller which switches between two states: An *Eco* controller state which demands a low DO setpoint and a *Normal* controller state which demands a high DO setpoint. These setpoints are passed to the existing DO based airflow controller. These two master control states are further referred to as Eco ($c = 1$) and Normal ($c = 2$). First the general treatment is presented in a formalised way. Then the rule evaluation is explained with an illustrative example. Finally the sought intention for all rules are explained by drawing relationship between the rules, the pH difference signal and the nitrification activity.

4.2.3.4 General treatment

A set of three rules to trigger controller state change and in turn a DO setpoint adjustment are used in each of the two control states c ($c=1,2$). Each of them was developed based on an empirical analysis of typical similarities in the pH difference and ammonia concentration signal for the corresponding control state. The applied rules differ depending on the control state. The rules are further referred to as *EtN1*, *EtN2* and *EtN3* for the switch from Eco ($c = 1$) to Normal ($c = 2$) and as *NtE1*, *NtE2* and *NtE3* for the switch from Normal ($c = 2$) to Eco ($c = 1$). The controller only switches the state c if all three rules are simultaneously true.

The rule based control consists of two while-loops. One of these is active when $c = 1$ while the other one is active when $c = 2$. Both loops are described by pseudo-code in Table 4.2 and Table 4.3. In the pseudo-code the following states are used: c is the control state (i.e., $c = 1$: Eco, $c = 2$: Normal) and, \hat{s} is the HMM state estimate (i.e., $s = 1$ downward trend (primitive L), $s = 2$ upward trend (primitive U)). pHd_{LM} is the value of the lowest minimum in the Eco and is initialised with the current pH difference $pHd(i)$. Furthermore, the following parameters are used: *EtN2* is parametrised by ΔpHd_{MID} . T_{MIN} is a critical wait time to allow a control switch from Eco to Normal (*EtN3*). ΔpHd_{MAD} parametrises the *NtE2* rule.

Table 4.2: While loop of rule based control used while the controller is in the Eco state with pseudo-code and explanations.

Pseudo code	Comments
WHILE $c = 1$	
IF $s(i - 1) = 1 \wedge s(i) = 2$	
EtN1 = TRUE	EtN 1: monitors if at least one minimum was identified, updates pHd _{LM} if minimum is lower than current pHd _{LM}
IF $pHd_{LM} > pHd(i)$	
pHd _{LM} = pHd(i)	
END	
END	
IF $pHd(i) > pHd_{LM} + \Delta pHd_{MID}$	
EtN2 = TRUE	EtN 2: monitors if current pH difference value pHd(i) is larger than lowest minimum pHd _{LM} plus a threshold ΔpHd_{MID}
ELSE	
EtN2 = FALSE	
END	
IF $s(i) = 1$	
EtN3 = TRUE	EtN 3: monitors signal for downward trend
ELSE	
EtN3 = FALSE	
END	
IF $EtN1 = TRUE \wedge EtN2 = TRUE \wedge EtN3 = TRUE$	
EtN1 = FALSE	Checks if all rules are true and if so, resets all rules, resets the Normal timer and switches the controller state
EtN2 = FALSE	
EtN3 = FALSE	
T _{Normal} = 0	
c=2	
END	
END	

Table 4.3: While loop of rule based control used while the controller is in the Normal state with pseudo-code and explanations.

Pseudo code	Comments
WHILE $c = 2$	
IF $s(i - 1) = 1 \wedge s(i) = 2$	
NtE1 = TRUE	NtE 1: monitors if at least one minimum was identified
END	
IF $pHd(i) < pHd_{LM} + \Delta pHd_{MAD}$	
NtE2 = TRUE	NtE 2: monitors if current pH difference pHd(i) value is smaller than lowest minimum pHd _{LM} plus a threshold ΔpHd_{MID}
ELSE	
NtE2 = FALSE	
END	
IF $T_{Normal} > T_{MIN}$	
NtE3 = TRUE	NtE 3: monitors if Normal control state is active for sufficient time period
END	
IF $NtE1 = TRUE \wedge NtE2 = TRUE \wedge NtE3 = TRUE$	
NtE1 = FALSE	Checks if all rules are true and if so, resets all rules, initialise pHd _{LM} , and switches the controller state
NtE2 = FALSE	
NtE3 = FALSE	
pHd _{LM} = pHd(i)	
c=1	
END	
END	

the value of $pHd_{LM} + \Delta pHd_{MAD}$, with pHd_{LM} lastly updated at point(3). This means all NtE rules are evaluated as true and the controller state is changed to the Eco state ($c=1$). All *EtN* rules are reset to false. As soon as the while-loop in Table 4.2 is activated gain, *EtN3* is set to true given that the pH continues to decrease after point (8). The first new minimum in Eco at (9) triggers the same changes as the minimum at point (1). In other words, the controller state has cycled through all possible states.

4.2.3.5 Empirical relation between nitrification activity and rule evaluation

EtN1 ensures that the minimal nitrification activity is identified. *EtN2* is used to distinguish between low ammonia load peaks which only elicit a minor pH difference increase and enhanced ammonia loads. The example shows that relevant peaks (5) lead to a change in the controller state while irrelevant ones (2) do not. The updating of pHd_{LM} from (1) to (3) ensures that *EtN2* and *NtE2* are evaluated based on the lowest nitrification activity recorded and compensates for any drift between the two time points (1) and (3) and for any drift before point (1). *EtN3* delays the switch to the Normal controller state until the ammonia peak load has broken through and reached the last aerated tank.

NtE1 monitors the identification of a first minimum. This minimum can be an indication that the nitrification activity is stabilising at a low level. However, as such minima can also be identified at high nitrification activities, the condition is only sufficient and therefore paired with *NtE2*. *NtE2* ensures that a switch to a lower oxygen level is only pursued when the observed minimum in nitrification activity is close enough to the last known minimum nitrification activity characterised by the parameter pHd_{LM} . The tolerance ΔpHd_{MAD} is a parameter describing the maximally allowed upward drift since the last known minimum in nitrification activity, i.e., the last time pHd_{LM} was updated. *NtE3* safeguards the hardware such as blowers and valves from unnecessary and excessive wear and tear.

4.2.4 Controller performance monitoring

Initial tests On all six tested plants, the hardware (i.e., pH sensors and ammonia ISE) is installed first and the signals are recorded without using them for control. With these initial tests, the QSE and the rule-based control can be tested and tuned off-line first.

Controller tests In three plants extended tests were executed by activating the control which automatically adapted the DO setpoints. In these cases the controller performances were evaluated in terms of energy efficiency gains and nutrient removal performance of the plants. To this end, a comparison is made between period with and without active rule-based control. The turbo blower energy consumption was normalised by the ammonia load converted in the biological treatment line to enable a fair comparison. This load was derived from the effluent flow from the primary clarifier and both volume proportional 24h composite sample concentrations in the outflow of the primary clarifier and the outflow of the secondary clarifier (cf. Appendix D.4 and Fig. 4.10). The WWTP's laboratories determined the nitrogen species concentrations in the 24h composite samples with LCK 303, 304, and 305 test kits for ammonia, LCK 341 and LCK 342 for nitrite, and LCK 340 for nitrate (Hach-Lange, Berlin, Germany).

4.2.5 Wastewater treatment plant characteristics

The use of the QSE-based control at the WWTP Hard (Winterthur, Switzerland), which treats wastewater of about 130'000 population equivalent, is studied in greatest detail. The WWTP Hard treatment line

consist of a mechanical treatment step for removal of solids, a primary clarifier, a secondary treatment by means of a biological activated sludge process including a series of reactor tanks and settling tanks, and a tertiary sand filtration. After the primary clarifier, the water is separated into two parallel treatment lines. The proposed control is only tested in one of the biological treatment lines. In the biological treatment step the wastewater first enters a stirred anoxic tank for denitrification followed by a series of three aerated tanks for the oxidation of organic compounds and ammonia. Each biological treatment line has its own separated turbo blower group, aeration pipe system, automatic samplers, and secondary clarifier tanks. Thus, the evaluation of the controller is not affected by the line without ammonia based aeration control. The existing aeration control is a cascade controller: First, all three aerated tanks are equipped with an oxygen sensor that controls the airflow coming from the main collector. Then, the line's turbo blower group is controlled by a sliding pressure control in the collector. The diffusers are ceramic domes which require a minimal constant airflow to avoid clogging.

The five other treatment plants differ in size and their biological treatment technology (cf. Table 4.4). However, all of them are continuously operated, receive typical municipal wastewater and include a predenitrification step. The WWTP Buchs (BCH, Buchs SG, Switzerland) has an additional denitrification step in-between the aerated tanks.

The two other plants in which the control was activated were WWTP Pfäffikon (PFA, Pfäffikon ZH, Switzerland) and WWTP Pfungen (PFU, Pfungen, Switzerland). They have a slightly different aeration setup than the WWTP Hard: PFU has three aerated compartments in each of the two lines, yet only one airflow valve per line which manipulates the airflow to all three compartments at once. The oxygen is only controlled in the second compartment and reach. In PFA, the biological treatment is separated into two lines with two tanks each. The front tanks are pure activated sludge tanks and the second tanks are designed as hybrid moving bed systems which require a minimum air flow at all time. All tanks have separate DO sensors and airflow valves.

Table 4.4: WWTP characteristics and performance evaluation of the pH difference based ammonia aeration controller of six different municipal wastewater treatment plants.

WWTP	Altenrhein (ALT AS)	Altenrhein (ALT FB)	Buchs (BCH)	Hard (AS)	Pfäffikon (PFA)	Pfungen (PFU)
Wastewater treatment plant characteristics						
Location	Altenrhein, Switzerland	Altenrhein, Switzerland	Buchs SG, Switzerland	Winterthur, Switzerland	Pfäffikon ZH, Switzerland	Pfungen, Switzerland
Design capacity [p.e.]	120'000 ^a	120'000 ^a	45'600	180'000	15'000	15'200
Biological treatment	Activated sludge	Fixed bed	Activated sludge ^b	Activated sludge	Hybrid moving bed	Activated sludge
Controller performance evaluation						
Evaluation type (# days [d])	virtual test (32)	virtual test (18)	virtual test (63)	live test ^c (142)	live test ^c (50)	live test ^c (25)
Active control and reference period (active control / benchmark) [d] ^d	0/0	0/0	0/0	79/23	7/10	7/7
Energy efficiency improvement [%]	N/A	N/A	N/A	-7.2	-13	-8.2 ^e
Legal effluent requirements	N/A	N/A	N/A	fulfilled	fulfilled	fulfilled
Control potentially feasible	Yes	No	Yes	Yes	Yes ^f	Yes

^a Total capacity of WWTP Altenrhein: Activated sludge reactors account for 70% and the fixed bed reactors for 30% of this number.^b This plant has an additional anoxic zone in between the aerated tanks. The pH difference was measured over this second anoxic zone.^c Preceding virtual tests executed^d Numbers do not sum to total days, as benchmarking days are only those at which laboratory nitrogen measurements were available.^e This number is not normalised with the ammonia load.^f pH difference does not exhibit the same dynamics as other plants. For a more efficient control, adaptations in the rules based control are needed.

4.2.6 Oxygen slave controller

On all actively tested plants the presented controller was installed as a master controller which sets the DO setpoints in the existing DO based aeration control. The Normal control state DO setpoints were set to the values in use prior to this study (WWTP Hard, 2.0 mgO₂/L). For the Eco control state DO setpoints at WWTP Hard a variability of combinations were tested. First, the setpoint spread was kept conservatively small for safety reasons (2.0 to 1.5 mgO₂/L) as the effects of the controller on the pH signal dynamics were not known exactly. Later this spread was increased to maximise efficiency (2.0 to 0.8 mgO₂/L). The details regarding the different DO setpoints can be found in Appendix D.2. The combination for the Eco DO setpoints which was used the longest was 1.3 mgO₂/L in the front, 1.1 mgO₂/L in the middle and 1.0 mgO₂/L in the rear tank. The pH difference was amplified with decreasing Eco DO setpoints and urged an adjustment of the parameters in the rule-based control (i.e., *Etn2*, *NtE2*). With an increasing setpoint spread the aeration system's time lag increases and the safety margins decrease. In PFU the DO was controlled at 1.8 mgO₂/L for Normal and 1.3 mgO₂/L for Eco. In PFA the airflow is governed by the hybrid moving bed tank sensor which measures the lower DO concentration of the two lines. This sensor DO setpoint was set to 3 mgO₂/L for Eco and 4.5 mgO₂/L for Normal. The front tank DO setpoints were kept at 1.5 mgO₂/L independent of the controller state.

4.3 Results

In the next paragraphs the QSE algorithm and the subsequent control strategy are first demonstrated on the basis of a 4-day dataset recorded on the WWTP Hard. After these demonstrations the performance evaluation is presented.

4.3.1 Demonstration of Qualitative State Estimation algorithm

First, the results from the kernel regression step leading to the trend probabilities are shown. In the kernel regression the moving window filter computes a new filtered signal from the raw signal (Appendix D.5 Fig. A.1). The chosen window length τ is 19 minutes. This corresponds to 39 considered measurements within the moving window and causes a delay of 19 minutes (cf. section 4.2.2). For this study τ has been selected by trial and error. A good first estimate can be derived from the sensor, process, or actuator time constants. Methods such as generalised cross validation Hastie et al. (2009) also allow tuning of τ . This, requires a cost-function which can be computed with limited uncertainty. For this reason, this is not explored further in this study.

The first derivative and its standard deviation is computed to characterise the distribution of the second derivative of the pH difference signal (Eq. 4.1). Fig. 4.5 illustrates the distribution's mean and a $\pm 3\sigma$ band around it for the pH difference first derivative over time. The probabilities for a positive first derivative sign are derived by integrating the positive mass of the distribution shown in Fig. 4.5 (Eq. 4.2). The corresponding probability for a negative sign is computed with Eq. 4.3. Fig. 4.6 shows the resulting positive (upward trend) probability of the pH difference signal. This concludes the kernel regression step of the QSE.

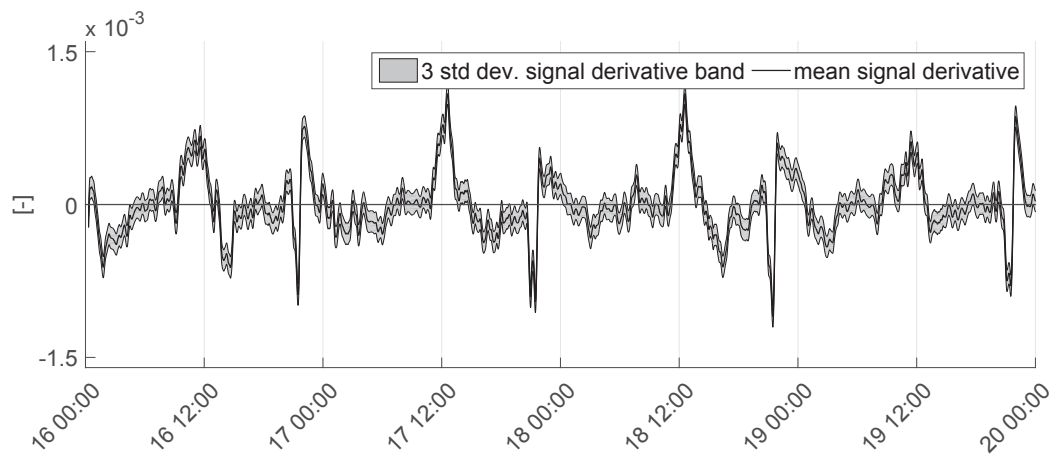


Figure 4.5: Mean and expected $\pm 3\sigma$ band around the mean characterising the calculated signal first derivative's distribution.

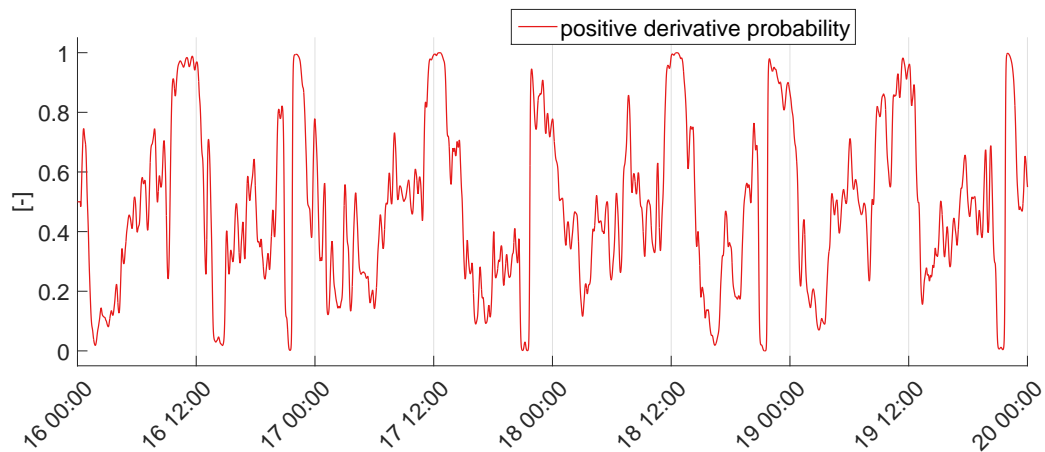


Figure 4.6: Positive derivative sign (upward trend) probability of the signal. This probability is derived from the point-wise distribution of the signal's first derivative.

In the QSE's second step, the probabilities computed above are used to compute the maximum likelihood HMM state (Eq. 4.8). Fig. 4.7 shows the resulting maximum likelihood states based on the pH difference signal. Several values for λ were tested by trial and error. Good results were obtained with $\lambda=0.4$. This however means, that the filtering effect by means HMM state estimation is marginal. In our case, the HMM therefore primarily functions as a way to transform the continuous probabilities into discrete states. Results obtained with more aggressive filtering $\lambda = 0.05$ are plotted in the Appendix D.5 Fig. A.2 and Appendix D.5 Fig. A.3 (cf. 4.4.2). The identified trends and extrema are now further processed by the proposed rule-based control.

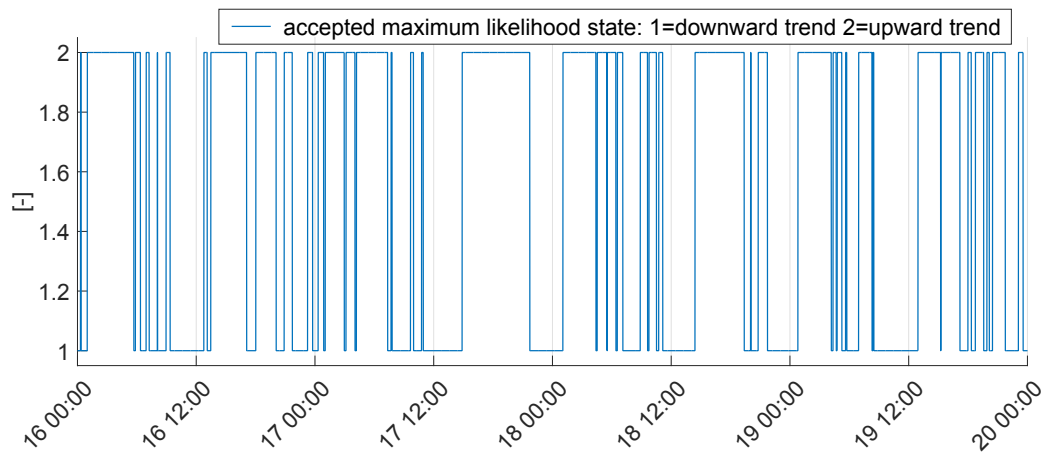


Figure 4.7: Accepted maximum likelihood state of the signal. 1 = downward trend, 2= upward trend. Changes in the maximum likelihood state indicate the identified maxima and minima.

4.3.2 Demonstration of the control strategy

Rule-based control The rule-based control uses the qualitative features identified by the QSE algorithm. It evaluates rules which analyse the filtered pH signal and the appearance of the qualitative features on the signal. Fig. 4.8 shows the evaluation of these rules in the two different control states based on the example signal from above. Most typically, the $EtN3$ is the last rule to become activated before a switch from Eco to Normal. The most influential rule with respect to the aggressiveness of the controller is $EtN2$ which defines the length of the Eco to a great extent. For changes from the Normal and Eco state, the $NtE1$ and $NtE2$ rule tend to be the last to become evaluated as true. Therefore, we have primarily focused on tuning the controller by manipulating the parameters for the rules $EtN2$, $EtN3$, $NtE1$, and $NtE2$.

The example shows that the four rules $EtN2$, $EtN3$, $NtE1$, and $NtE2$ are critical when it comes to controller state switches. In the Eco state (Fig. 4.8 top) as well as in the Normal state (Fig. 4.8 bottom) one can see that the rules $EtN2$ and $NtE2$ typically stay for the longest on false. An exception is found for the third time the controller is in the Normal control state. In this particular case $NtE1$ was the last rule to be evaluated as true. This indicates that it is an essential rule for a safe operation. $EtN3$ determines the exit from the Eco state. The example further reveals that, as expected, $NtE3$ and $EtN1$ had no direct influence on the control output since they were always set to true long before the control state switched. Fig. 4.9 shows the raw pH difference, the ammonia signal and the final control decision when the pH difference is processed with the QSE algorithm and the rule-based control. The example shows that the algorithm can detect high and low ammonia load situations accurately. Ammonia was measured in the middle tank of the tank series, which explains the slight time shift of the control state switch compared to the ammonia signal, especially given the fact that the controller is designed to delay the increase of the oxygen setpoint until ammonia is present in the last tank. A comparison between the output of the QSE (Fig. 4.7) and the controller output (Fig. 4.9) shows the importance of the additional filtering effect induced by the rule-based controller.

Internal and external safety checks For additional operational safety, safety checks were introduced. These safety checks can overrule the rule-based control decision and will override the oxygen

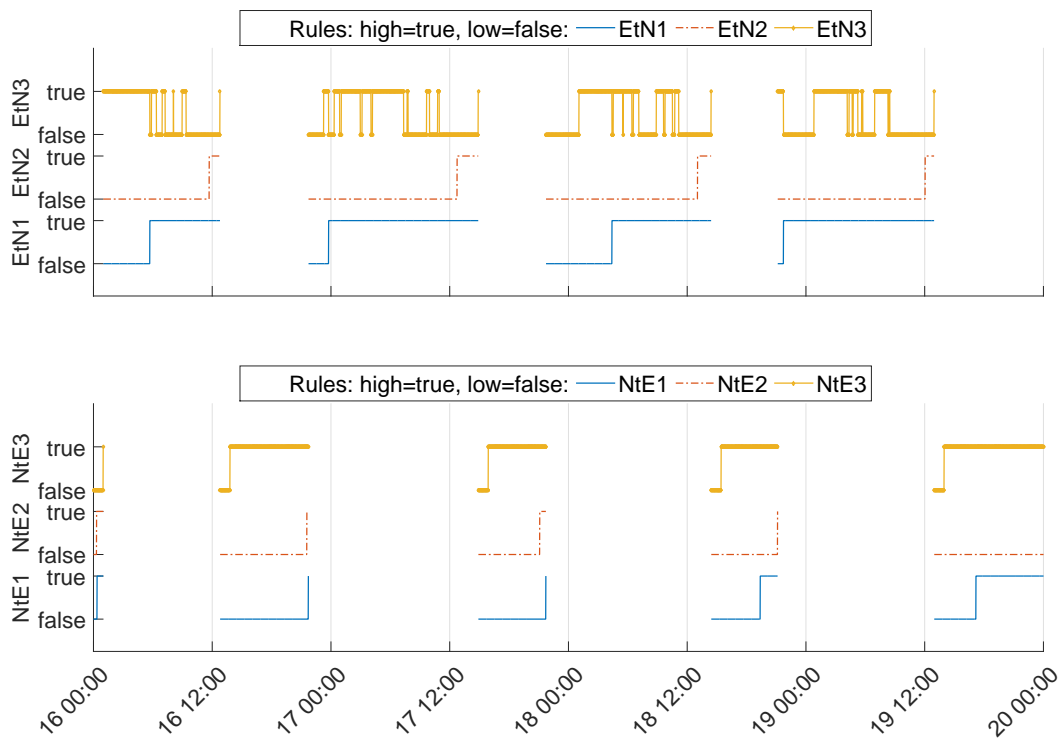


Figure 4.8: Rule evaluation and pH difference; Top: Eco to Normal (EtN) rules; Bottom: Normal to Eco (NtE) rules.

setpoints with the Normal DO setpoints in case one or more of the safety checks are violated. Two internal safety checks were defined for the whole cascade control: First, a lower and higher threshold was defined for both pH sensors. Outside of these thresholds, the signals are considered abnormal. Second, RITUNE[®] assigned an expiration time on the Eco DO setpoints which ensures that the SCADA falls back to Normal DO setpoints in case the communication between RITUNE[®] and the SCADA fails. Additionally, external safety checks were provided to ensure adequate nitrification capacity at all times. Very common situations in which high loads occur are wet weather events. They increase the load to the plant due to the higher inflow rates and with the first flush a lot of deposits from the sewer system reach the plant, additionally increasing the nutrient load (Larsen et al., 1998). Monitoring the inflow for high flows prepares the biological system for an increased load before it actually attains that state. The pH at the inlet of the plant was also monitored to safeguard against abnormal pH levels. Indeed, unusual pH conditions in the inflow might lead to a faulty control decision. High and low pH values can be linked to toxic wastewater compositions and the abnormal pH values themselves can push the microbiological community to its thermodynamic limits (Park et al., 2007), at which point the control should not impair the bacterial growth conditions further by also lowering DO concentration.

Upon successful evaluation of the safety checks, the desired DO setpoints are sent to the slave aeration control programmed in the basic SCADA system. Quite logically, the external safety checks are not specific to the proposed trend-based controller but can also be applied for any type of cost-reducing ammonia aeration control.

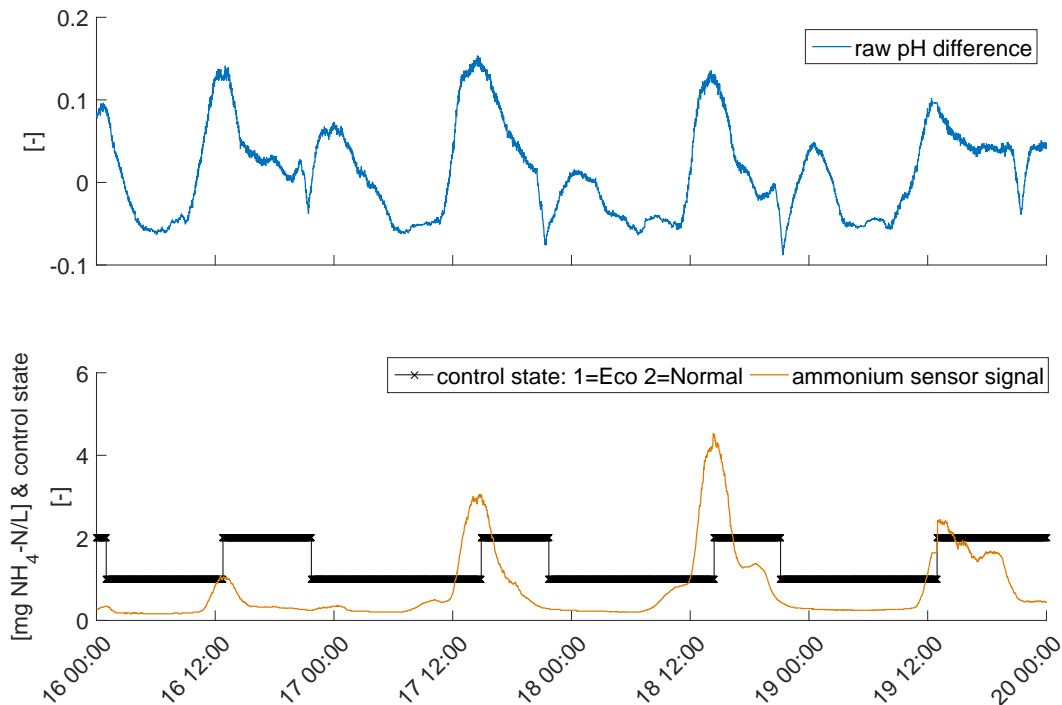


Figure 4.9: Final resulting control decision with ammonia signal as a reference. Top: Raw pH difference underlying the control decision. Bottom: Reference ammonia signal for validation of the controller and the final control decision 1= Eco control state (low DO setpoints), 2 = Normal control state (high DO setpoints). The control decisions made on the basis of the usage of the pH difference signals match well with the peaks in the ammonia concentration in the central aeration tank.

4.3.3 Performance evaluation

The extensive long-term test in the WWTP Hard is discussed first. The measurement campaign took place from 25th July 2013 until 30th September 2014. The control was tested and benchmarked from 12th March 2014 until 30th September 2014. A list of the set parameters during the test period can be found in Appendix D.3. The control decision and the corresponding adaptation of the dissolved oxygen setpoints have an impact on the slave oxygen controller as well as the plant performance in general. First, the detailed results from the longest test on the WWTP Hard, Winterthur are presented. The two other fully tested plants are briefly summarised. Table 4.4 summarises the results of all tested WWTPs.

Energy Based on the assumptions stated in the method section, a decrease of 6.6% in the specific energy demand per kilogram of ammonia degraded ($\text{kWh}/\text{kgNH}_4^+ - N_{\text{deg}}$) was computed. This efficiency gain was even slightly higher if only dry weather flow days are considered (7.2%). This is partly caused by the decreased efficiency in the ammonia removal due to dilution and partly by the higher proportion of high DO setpoints due to the high inflow safety check during wet weather. Moreover, the two other fully tested plants PFA (13%) and PFU (8.2%) exhibited substantial energy savings (cf. Table 4.4).

Removal efficiency The control system reduces the process' safety margins. Therefore, the primary aim of the WWTP - to degrade and remove compounds in the wastewater which have a negative impact on

the environment - is more likely to be jeopardised. Hence, the legal effluent limits and removal efficiencies were monitored closely (Fig. 4.10). Neither the ammonia or nitrite effluent concentrations violated the legal limits Appendix D.1. More information regarding the received and discharged nutrient loads can be found in Appendix D.4. No negative impacts on the operation of the plant were noticed (e.g., foaming due to low DO concentrations (Martins et al., 2003)). The two other plants PFA and PFU were not additionally monitored but the analysis of the regular sampling days did not unveil any legal threshold violations.

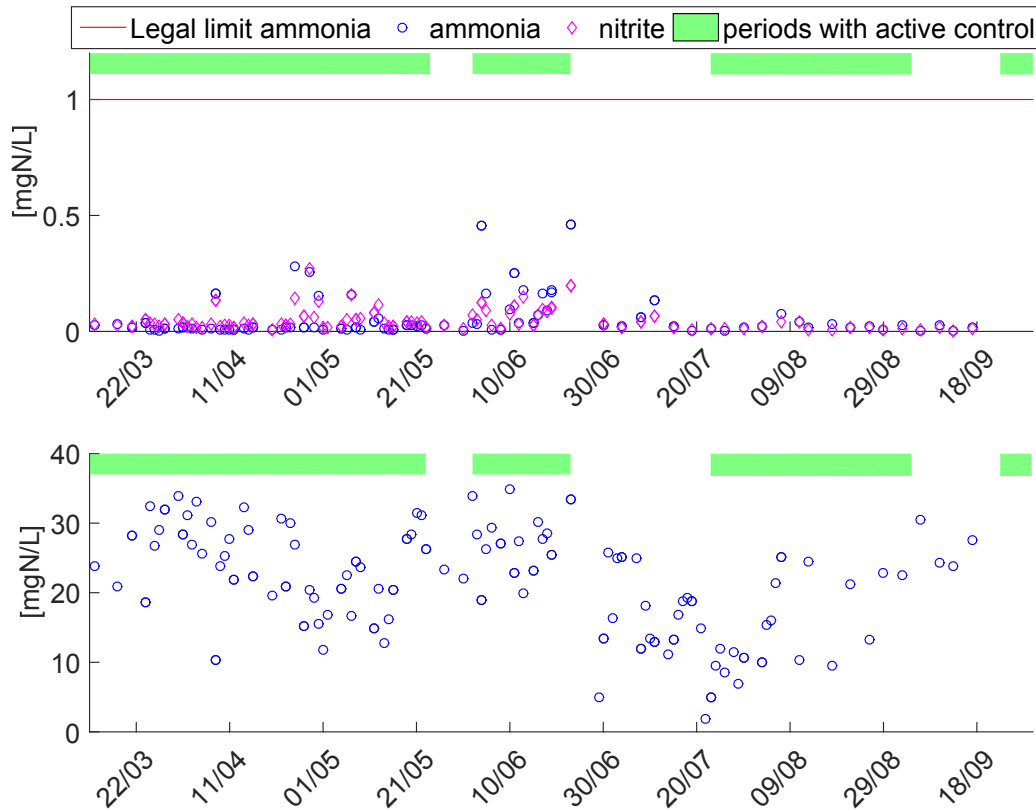


Figure 4.10: Ammonia and nitrite concentration measured in 24h composite samples at the WWTP Hard, Winterthur. Top: Secondary clarifier effluent. Bottom: Primary clarifier effluent. The legal threshold for ammonia in the effluent is 1 mgN/L. For nitrite there is only a non-binding guideline value of 0.3 mgN/L.

4.4 Discussion

The proposed controller based on the QSE algorithm showed robust behaviour during the tests. Not only were significant energy savings achieved, but all effluent limits were respected as well (cf Fig. 4.10 and Appendix D.4). The first tests on multiple full-scale plants produced evidence that the control method can be applied successfully on many plants and indicates a general applicability of the control setup. A number of strengths and limitations of the control setup could already be identified.

4.4.1 Data sources

The kernel regression assumes equidistant spacing between all the data points. This facilitates the implementation of this step as an efficient convolution. If the data are irregularly spaced or when data points are missing, kernel regression is still feasible yet requires an adaptive solution in which the data point weights are continuously re-evaluated. The QSE method is currently limited to the analysis of univariate signals. However, we have not yet observed an immediate need for multivariate QTA in the context of wastewater treatment automation.

4.4.2 Kernel regression and hidden Markov model

The two filtering steps in the QSE have different purposes: The kernel regression is the first filter which obtains the qualitative information and smooths the signal symmetrically. This filtering results in probabilities for a set of derivative signs of interest. Note that alternative filtering techniques may be used as well to compute such probabilities. Second, the HMM allows penalising (using small λ values) or even restricting (using zero-valued λ values) certain state sequences according to the prior expert knowledge about the expected signal shape characteristics (e.g., (un)likely sequences of primitives, smoothness condition). During the development and tuning phase of the pH difference based ammonia aeration control we observed that the HMM filtering has limited effects in the studied system. Two reasons are responsible for this effect. Firstly, all λ values are identical. Secondly, all λ values are non-zero (cf. Eq. 4.11). Under these two conditions, the amount of filtering in the kernel regression step can be traded off against filtering by means of the HMM step. Indeed, decreasing τ and therefore decreasing the smoothing in the kernel regression can be compensated by decreasing λ . In the present study, this meant that the effect of HMM filtering was marginal. The main reason to keep the HMM step within the proposed QSE method is to ensure that incorporation of prior knowledge is feasible with the method, should this be valuable to the tentative user.

4.4.3 Qualitative information

One of the main advantages of the proposed method is the reduced sensor maintenance (see below). In our experience, the pH sensors that are used for control are far more robust and less prone to malfunctioning compared to ion selective ammonia sensors. Additionally, the use of qualitative information allows for a certain drift in the pH difference signal which reduces the recalibration effort compared to a controller which relies on a drift-free measurement (i.e., absolute values). Sensor drifts are compensated each time the minimal minimum of the pH difference signal is identified (see Fig. 4.4 point (1) and (3)). As long as the drift of the pH difference within the evaluation period of the parameter is smaller than the set value for the parameter (i.e., ΔpHd_{MID} , ΔpHd_{MAD}), the drift can be compensated. For the downward drift the problem is less severe as only the drift within the time period between the registration of the lowest minimum (pHd_{LM}) and the activation of *EtN2* (ΔpHd_{MID}) has to be compensated. The parameters for the rules *NtE2* and *EtN2*, ΔpHd_{MAD} , and ΔpHd_{MID} , define the accepted upward and downward drift rate of the signal. Their successful use relies on the frequent referencing with pHd_{LM} . Nevertheless, the benefit obtained by using the qualitative information is, theoretically, also one of the largest limitations of this type of control. As the controller is based on the detection of specific features such as minima and maxima, it is important that such dynamic features regularly appear in the analyzed signal. More specifically, the relevant features should appear in shorter time-scales than the drift in the analyzed signal.

This caps the theoretical efficiency gains given that theoretically optimal ammonia control would eliminate all dynamics of the pH difference signal and thereby render the controller useless. Further work is aimed at quantifying to which extent the the efficiency gains are actually limited by the need for a dynamic and information-rich pH difference signal.

4.4.4 Implementation and fine-tuning

Experience with the applied implementation approach At each plant the pH difference and the ammonia signal were first recorded without any active ammonia based aeration control. This dataset allowed us to evaluate the applicability of the controller at the specific plant (i.e., virtual testing). Additionally a first set of parameters fitting the controller’s sensitivity to the pH difference signal was estimated with which the controller was eventually activated on the plant. The comparison of these first parameter sets showed that they are very similar across the studied plants, despite differences in treatment technology and substantial size differences (cf. Appendix D.3).

Alternative approaches The experience explained above indicates that one could implement such a control without a reference ammonia signal. This would facilitate the roll-out. A potential strategy could be the activation of the controller with a pre-existing conservative parameter set followed by a fine-tuning of the parameters with grab and composite samples. In this way, the use of the maintenance intensive and drifting online ammonia sensor for the implementation could be avoided.

Fine-tuning Tuning can be delicate. Firstly, multiple tunable parameters exist within the QSE (i.e., τ and λ) and the rule-based controller (i.e., ΔpHd_{MAD} , DO setpoints, T_{MIN}). Secondly, the tuning parameters have a non-linear effect on the control decision. Hence, it is recommended to tune all parameters with care and with small and incremental changes only. Limiting the fine-tuning to either the QSE or the rule-based control can simplify the tuning. Note that the aeration system’s and biological system’s dead times (e.g., sliding pressure control in the aeration system) should be considered when choosing the parameters.

4.4.5 Energy savings and maintenance effort

The energy savings achieved are substantial, even though this study was aimed at proving a concept rather than fine-tuning the controller. The ammonia removal efficiency remains excellent. Consequently, there is potential for increased energy efficiency through even more aggressive parameter tuning.

An average weekly effort of about 10 minutes is expected to maintain a pair of pH sensors, including replacement, cleaning, and calibration. In comparison the average maintenance effort for our ISE ammonia used to validate the method presented took up to 60 minutes per week. These numbers depend on the location of the sensors, the wastewater characteristics, and the possibility of incorporating the maintenance into other regular maintenance cycles of the plant (e.g., DO sensor cleaning). For the control algorithm, an average of 10 minutes effort per week is needed to check the control output. Repetitive manual checks can be automated and linked to the alarm system, which should reduce the effort. For one controlled system this results in a total effort of 18 hours per year. Given a salary of 70 Swiss Francs (CHF)/h the operation costs sum up to roughly 1’350 Swiss Francs CHF (1’215 EUR). At the Hard WWTP (130’000

p.e.) with two separate lanes the maintenance cost is doubled to monitor both lanes (2'700 CHF/y). On the consumption side the total aeration energy saving of 140'000 kWh/y (7% of 2'000'000 kWh/y result in monetary savings of roughly 17'500 CHF/y (0.125 CHF/kWh). For smaller plants (15'000 p.e.) with 25 kWh/p.e./y as the specific aeration energy consumption this leads to savings (7%) of 3'150 CHF/y. This means that depreciation for hardware and software can be maximally 1'800 CHF/y for a smaller plant and 14'800 CHF/y for a larger plant. The current conservative estimation of 7% energy savings, the ignored indirect effects (i.e., improved nutrient removal, less external carbon dosage) and the potential to improve the controller tuning make this controller a promising alternative to the conventional measured ammonia aeration control in particular for smaller WWTPs with limited staff capacity.

4.4.6 Treatment technologies

The control was initially tested on three different types of biological treatment, of which two exhibited the required qualitative relation between the pH difference and the ammonia concentration. The technology in which the control did not work was a fixed bed reactor in the WWTP Altenrhein (ALT FB, Altenrhein, Switzerland). Based on all tests we assume that the following two factors can impede the controller performance. First, a too short hydraulic residence time between the two pH sensors delivers a signal with a low signal-to-noise ratio, which in turn makes the controller more prone to noise. This was observed on the PFA plant, the ALT FB plant as well as on the conventional activated sludge plants when the hydraulic residence time between the pH sensors was reduced by measuring the difference only over one two instead of three tanks. A second factor is a time-varying relationship between airflow, DO concentration and nitrification activity: This might have caused the failure in the fixed bed system and the weaker pH difference dynamics in the hybrid moving bed system. Both systems work with a biofilm system which is less controllable in terms of nitrification performance given a bulk oxygen concentration and therefore might prevent a clear identification of ammonia peaks by means of the pH difference. Due to the higher volume specific nitrification rate in biofilm systems the hydraulic residence time is also shorter in this case. Consequentially, it is not clear at this time which of these factors is most important. Overall, the controller showed general applicability for conventional activated sludge systems. Modifications of the control concept are considered to address the observed limitations.

4.4.7 Future work

The findings of this study are promising. Further research regarding the use of QSE in control loops should be directed towards handling multivariate data sets. Despite the limited applicability in the wastewater field such a development would allow the use of QSE in fields with a higher prevalence of multivariate control loops (i.e., Multi-Input-Multi-Output or Multi-Input-Single-Output). In its current form the QSE algorithm can also be applied in any other field (e.g., biotechnology, chemical engineering) where sensors are prone to drift and the signal represents information in its derivatives. In the wastewater field redox potential sensors are common and exhibit the described sensor characteristics. The presented controller could be improved by the identification of intermediate ammonia load levels - either with quantitative rules or by taking both extrema and inflection points into account.

Another modification of the tested state estimation and control approach is to modify the output of the HMM-based state estimation so that a continuous probability for the state is computed instead of a discrete maximum likelihood estimate. This would allow using continuous controllers (e.g., PID controller, Linear-quadratic regulator) instead of discrete ones (e.g., rule-based). However, the continuous

controller output bears two challenges: *(i)* there needs to be a sufficiently high confidence in the continuous information, which is not the case in our study. In the presented case only the confidence in the sign of the first derivative - not its value - is sufficiently high. *(ii)* continuous feedback control may dampen the dynamics of the monitored signal, which is critical for application of QTA (cf. section 4.4.3).

For a more comprehensive assessment of the rule-based controller some open questions remain: First, a direct comparison with a conventional ammonia sensor-based control would allow the life-cycle costs and benefits of both options to be assessed. Second, the controller was tested only on plants where the nitrification capacity was reduced by decreasing the volume-specific nitrification rate. However, adaptation of the aerobic volume could be considered as well. The constant DO setpoint in such systems and the reduced residence time between the pH sensors presumably require dramatic changes in the control structure. Eventually, a robust method to introduce and auto-tune the controller without the need for an ammonia ISE sensor would make this controller even more attractive.

4.5 Conclusion

A new algorithm for qualitative trend analysis (QTA) has been proposed and evaluated. In the example presented, a pH difference measured with two pH sensors over an aerobic activated sludge tank series was considered as the raw signal. These are the conclusions:

- The QSE algorithm is a fast and robust QTA method to extract qualitative information from a continuous signal.
- Using QSE for control is especially interesting in cases where sensor signals exhibit well-recognised dynamics but lack accuracy due to drift and other incipient faults. With QSE, aeration control based on an ammonia soft-sensor using only measurement of two pH levels is shown to be feasible. The qualitative analysis is especially valuable as it enables automatic compensation of drift in the pH sensors.
- The automatic drift compensation and the more robust nature of the control concept reduces the sensors' maintenance needs and makes it more attractive for smaller and remote plants to introduce ammonia aeration control.
- The soft-sensor exhibits general applicability mainly because of its mechanistic nature. This makes the controller transparent and allows operators to retrace and inspect the control decision so to critically evaluate the performance of the proposed controller.
- The controller is applicable in continuous activated sludge and continuous hybrid moving bed reactors with sufficient short-term variations in the ammonia influent concentration. So far this kind of control does not appear viable for fix bed reactors. This limitation originate from the need for sufficiently dynamic and thereby information-rich signals. Too short hydraulic residence time and/or weak correlation of airflow, DO concentration and nitrification rate hamper the application of the controller.

Acknowledgement

This work was supported by the Commission for Technology and Innovation (CTI) of the Swiss Federal Department of Economic Affairs Education and Research (EAER). (CTI project no. 14351.1 PFIW-IW). The authors thank Prof. Dr. Eberhard Morgenroth (Eawag, Switzerland) and Prof. Dr. Hansruedi Siegrist (Eawag, Switzerland) for their helpful discussions leading to this article and the staff of the participating WWTPs for their support in the field campaigns.

Part III

Conclusions and Outlook

Conclusions and Outlook

Conclusions

The overall goal of this thesis is to investigate soft-sensors and automation for nitrification processes to treat wastewater. The results reveal that a combination of robust hardware sensors, advanced data analytics, and incorporation of qualitative expert knowledge can reduce the need for human interventions to maintain the intended operation of sensors and control loops. Consequently, nitrification processes can be operated more autonomously and in turn more cost-efficient.

Soft-sensors A first objective of this thesis was to develop soft-sensors as a replacement for costly instrumentation to monitor nitrification. The hardware to obtain the input signals of the presented soft-sensors in Chapter 1, 2, and 4 is more robust than the hardware that the soft-sensors are going to replace. Each soft-sensor is based on a distinct physical principle underlying the monitored process (i.e., grey-box soft-sensor). However, the three developed soft-sensors show substantial differences in their calibration and modelling complexity. Two of the three presented soft-sensors do not aim at replacing absolute sensor values but serve only as an indicator for elevated concentration of the targeted species. For UV-Vis sensors, (Chapter 1) the calibration is necessary due to vast amount of species to which this sensor is sensitive. The dynamics that all non-target species exhibit can mask the dynamics of the target species in the absorbance spectrum. Thus, a comprehensive model is required. The results suggest that the amount of effort put into the realisation of the calibration experiments does not serve as an indicator for the final model performance. However, it is the careful selection of the relevant dynamics in the design of the calibration experiment by an expert that reduces the calibration effort effectively.

The DO-pH based nitrite soft-sensor (Chapter 2) faces similar challenges. Many processes irrelevant for the nitrite concentration do influence the soft-sensor signal. The results suggest that with some more explicit incorporation of expert knowledge in form of models at least a qualitative nitrite detection should become feasible.

A very different situation was found for the pH based ammonia detection (Chapter 4). It highlights that if almost exclusively relevant dynamics are obtained by the raw signal, the calibration effort can be negligible small. Consequently, no model is required and plant-to-plant transfer of the soft-sensor is simple.

In conclusion,

- *Considering expert knowledge simplifies the design of soft-sensors. Depending on the actually monitored phenomena in the process, expert knowledge is either directly incorporated in the calibration of the soft-sensor itself or then used for the design of the calibration experiments. In both cases, the effort to constitute and maintain a soft-sensor can be reduced.*
- *Soft-sensor only serving as an indicator for the relevant presence of the targeted species need less design effort. There are situations in which the benefits of simplification can outweigh the drawbacks.*

Drift tolerant control loops The second aim of this thesis was to develop control loops that tolerate sensor drift. In Chapter 3 and 4 two control loops, which both rely on derivatives of the signal instead of the absolute signal value are presented. While soft-sensors based on robust hardware sensors certainly reduce sensor faults with more abrupt characteristics (e.g., membrane rips, clogged filtration units etc.), gradual errors such as drift remain a relevant challenge. Thus, drift tolerant controllers can lower the requirements for maintenance further.

Using derivatives as a source of information requires process dynamics. Such dynamics are not a big challenge in sequenced processes (e.g., SBR) but are rare by default in continuous processes. We showed that either external dynamics such as diurnal variation can be exploited or that online experiments induced the desired dynamics in the process on purpose.

Interestingly, the underlying mechanistic principles for the two control loops are very different. In Chapter 3 the kinetics of nitrite oxidising bacteria are exploited. For the soft-sensor in Chapter 4 the acidification-alkalization balance that is induced by ammonia oxidation and CO₂-stripping is monitored.

In conclusion,

- *Using derivatives as input for control can significantly reduce the need to maintain a high-quality sensor signal in terms of classical notions of accuracy.*
- *The use of derivatives circumvents the need to correct drift in the absolute sensor values.*
- *Intentional excitation of the process by the controller is a promising way to obtain informative derivative signals, even in continuously operated processes.*

Integrated development of instrumentation and control Pursuing the two main goals of this thesis, (i) soft-sensor development and (ii) drift tolerant control loop development, revealed that an integrated development of instrumentation and control loop entails benefits compared to two independent developments. First, the quality requirements for the soft-sensor can be optimised in the sense that certain sensor errors do not need to be specifically addressed within the soft-sensor but may be tolerable if the control loops is also customised. Furthermore, the customised design of the controller allows implementing features that minimise the effects of the sensor drift or in other words maximise the information contained in the signal.

However, it is important to note that even though the information is maximized, in some cases the soft-sensor signal alone needs the same maintenance effort as a conventional sensor signal to reach a quality standard that is useful for other purposes (e.g. monitoring concentrations).

In conclusion, an integrated development of soft-sensor and controller can reduce the development efforts because the mutual requirements both elements have, can be coordinated. In this thesis, this was explicitly done by choosing binary output for the control loops as well as for the soft-sensor signals.

Qualitative trend analysis The results of this thesis indicate the QTA can serve as a tool to incorporate expert knowledge into control loops in a transparent and simple way. My results are the first demonstrations that QTA can be used for process control. QTA is key to post-process the signals in order to obtain the informations contained in the derivatives. Both QTA methods presented in this thesis showed great robustness towards noise in the input signal and did not produce any false negative identifications.

In conclusion, qualitative trend analysis is a viable tool for process control in particular if qualitative expert knowledge needs to be incorporated.

Urine nitrification The presented soft-sensor and stabilising controller for urine nitrification addresses one of the major problems operators of such systems face. This thesis showed that nitrite accumulations in this system can be controlled with ICA.

In conclusion, nitrite accumulation in urine nitrification systems can be successfully prevented.

Outlook

In this thesis, we relaxed the requirements for the application of ICA in nitrification systems. As a result nitrification processes become more economic. Nevertheless, these results should only be seen as an intermediate step on the path towards an even wider spread application of ICA in wastewater treatment processes in general.

Further soft-sensor development

The presented soft-sensors can be optimised in two directions. Either by using more data (i.e., black-box) or by incorporating more expert knowledge (i.e., white-box).

UV-Vis sensors For UV-Vis sensors, where theoretical knowledge in form of compound specific spectra as well as data are abundant, developments shall go in both directions. The highly multivariate output generated by a single sensor makes UV-Vis very attractive. Therefore, it is worthwhile to invest the resources into further research and development. Allegedly, commercial providers of UV-Vis sensors are calibrating their internal models by collecting numerous different water and wastewater samples to make their models as generic as possible. However, the exact details on their procedures are not publicly available. Given today's possibilities in terms of online and offline data collection worldwide (e.g., internet of things) the bar has never been lower to gather large quantities of absorbance and reference data. This should allow third parties such as the research community to even collect larger data sets that may lead to even more comprehensive models. In terms of theoretical knowledge, I see the potential to exploit the large libraries of compound specific spectra to execute virtual calibration experiments on the computer.

General soft-sensors In the case of the other discussed soft-sensors (Chapter 2 and 4) the expert knowledge approach is recommended. It requires less data and thus can lead to a reduction of the needed efforts for implementation. In my opinion, the main research direction shall thereby aim at designing the online experiments in reactors such that the information can be obtained effectively and efficiently. As shown in this thesis, in a system with no effluent to receiving waters such experiments can be explicitly executed in the reactor. In systems that do not allow disturbing the process to such an extent, online experiments are more difficult to execute. In some situations the educated combination of actuator and sensor data may be a possibility to retrieve relevant information without the need to execute an experiment.

Optimisation of control loops

If the information in the control loop should be gained by means of online experiments then this may result in contradicting control actions (e.g., reducing capacity to gain information). Consequently, there is a trade-off between information availability and process performance. In robotics this is a classical trade-off also known as the dual control theory. The optimisation of this trade-off practically leads to the question how frequent an online experiment is needed to have sufficient information.

Furthermore, I recognise also the necessity to consider the possible expansion of the potential output set which can be exhibited by the presented soft-sensors and control loops. With the presented binary output set, the dynamics in the system is maximised but the control may not be as optimal as it could be. In contrast, an output set with three or more elements would push the focus towards a more optimal control at the cost of the system dynamics. Addressing the optimal number of elements in the output set and the optimal frequency of online experiments is in my opinion favourably done in a modelling environment.

Part IV

Appendices

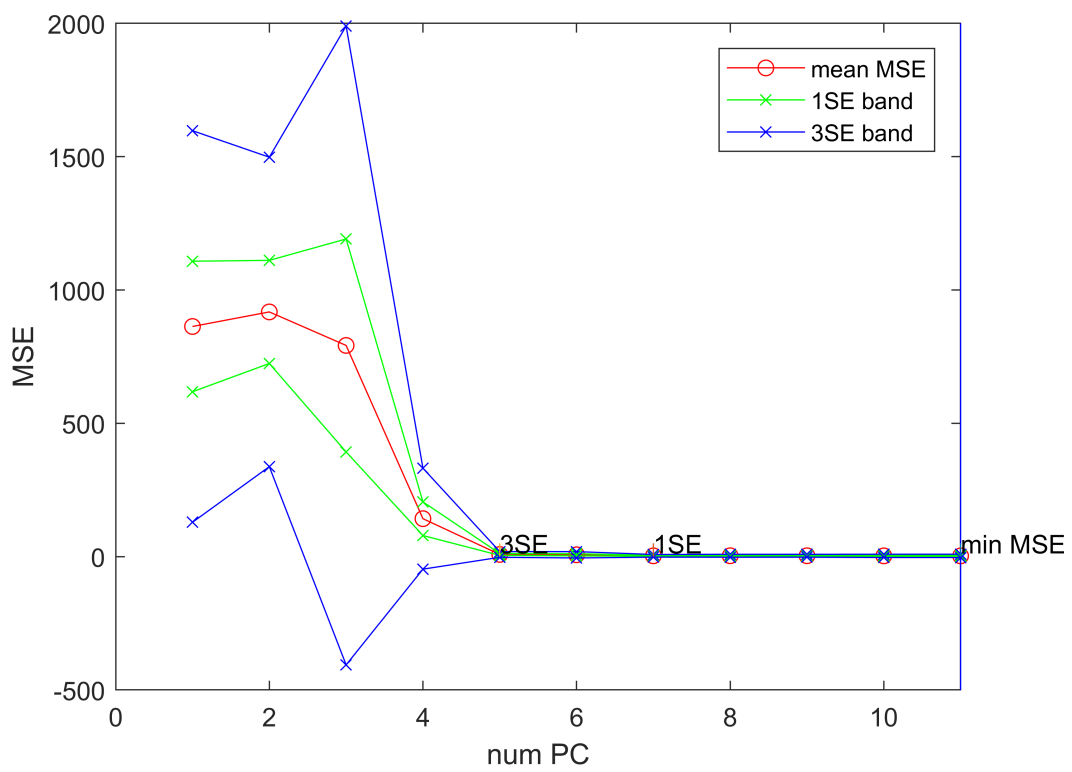
A Appendix Part II Chapter 1: UV-Vis Calibration

This appendix is the printable part of the supplementary information of the following manuscript, submitted for publication:

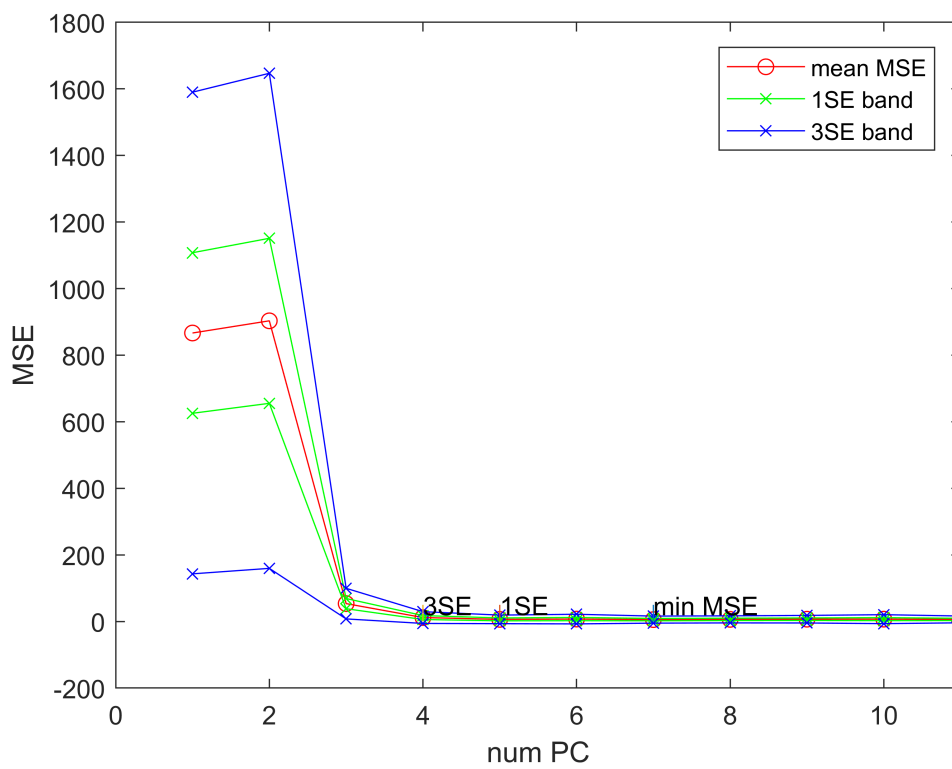
Thürlimann, C.M., Udert, K.M., Morgenroth, E., Villez, K., Comparison of four methods to obtain calibration data for online nitrite estimation by means of in-line UV-Vis spectrophotometry.

A.1 Mean squared error of cross-validation runs

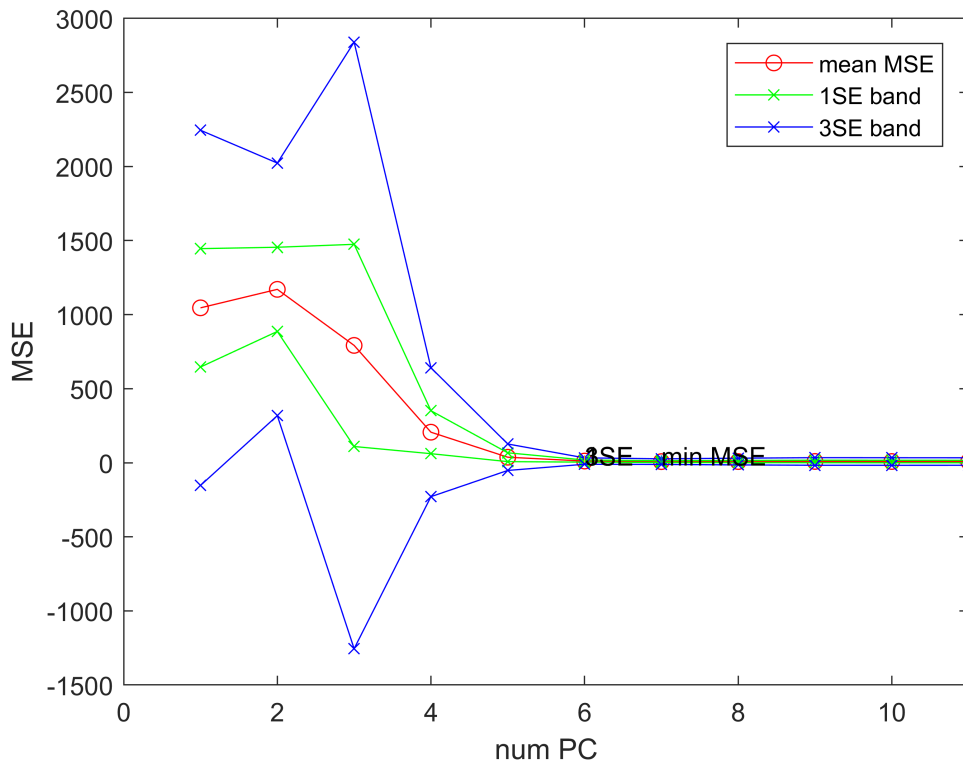
The following graphs show the mean squared error (MSE) as a function of the number of principal components obtained in the cross-validation during model calibration. They are named with the corresponding data set name and the corresponding wavelength range.



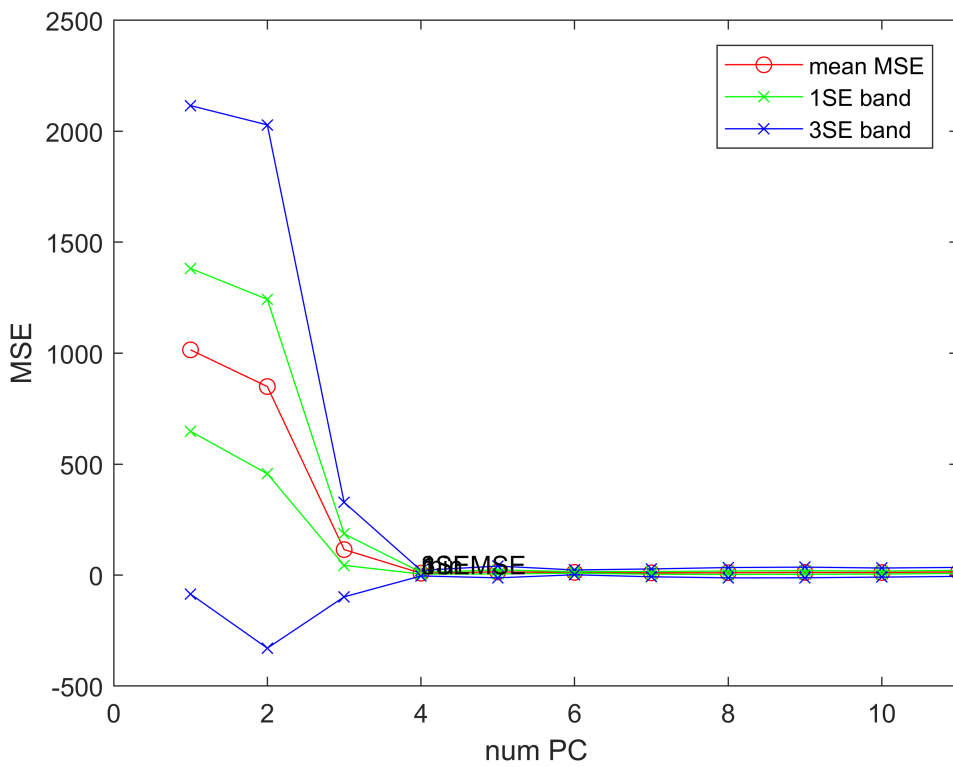
Ex-situ with biomass UV-Vis



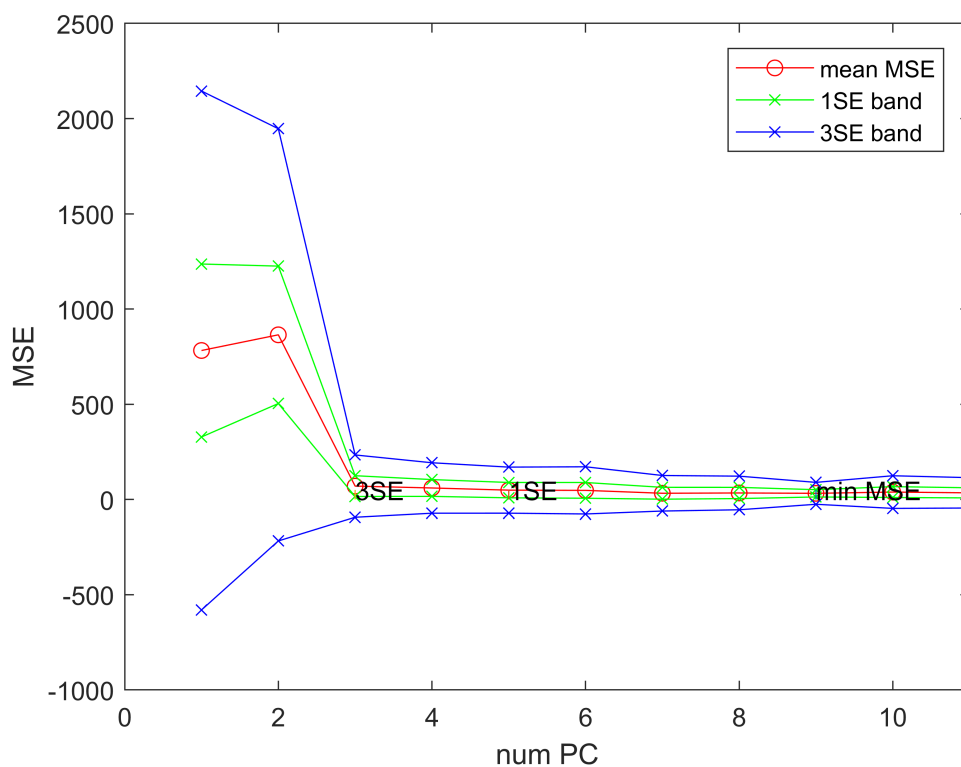
Ex-situ with biomass UV



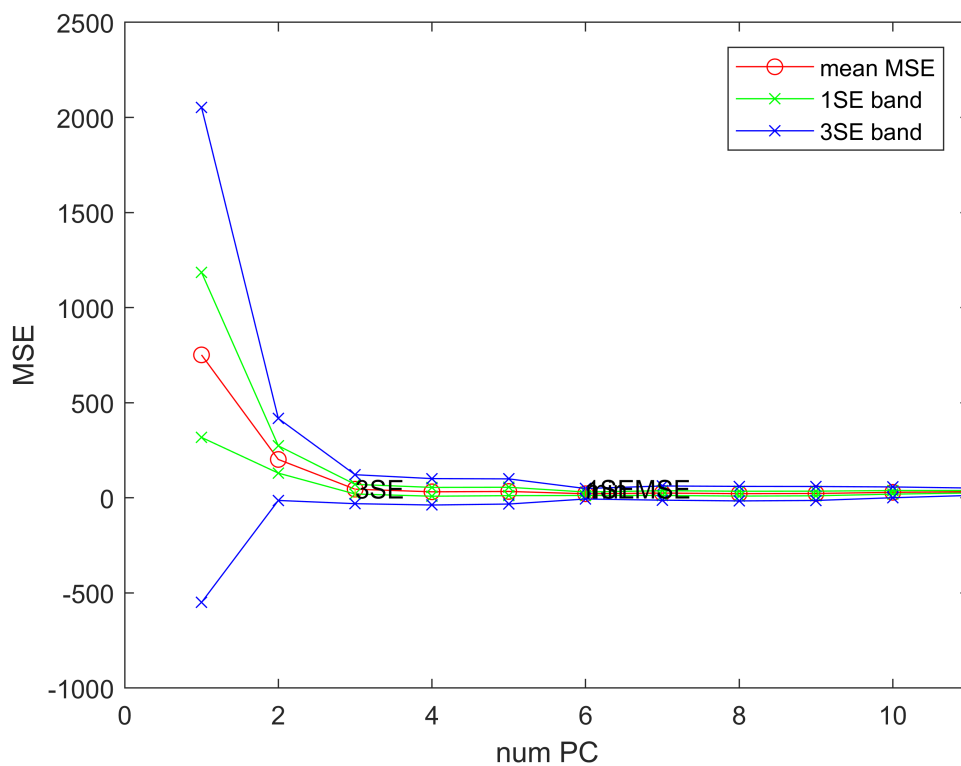
Ex-situ without biomass UV-Vis



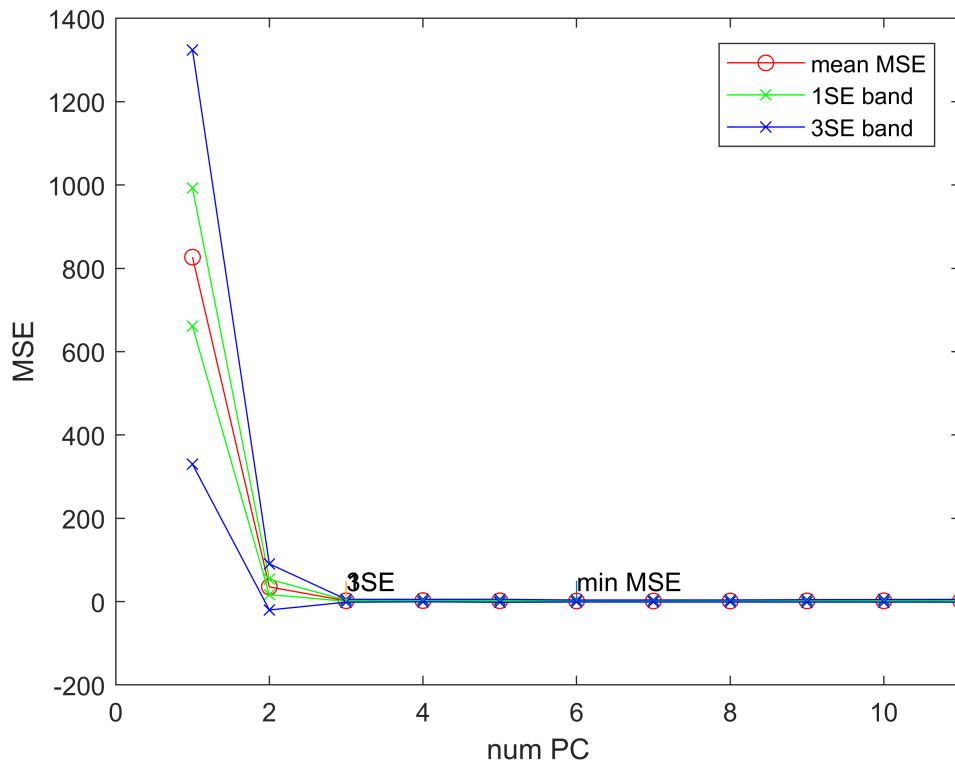
Ex-situ without biomass UV



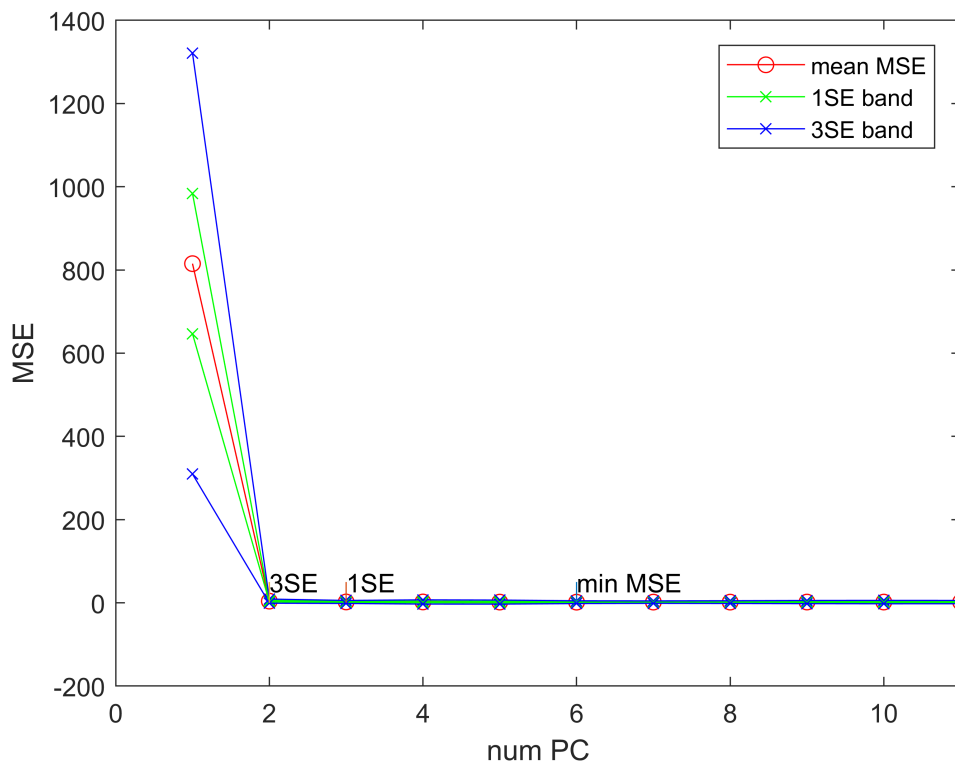
In-situ long-term UV-Vis



In-situ long-term UV



In-situ short-term UV-Vis



In-situ short-term UV

B Appendix Part II Chapter 2: Nitrite soft sensor based on OUR and PPR

B.1 Proton concentration and alkalinity consumption in a urine nitrification batch

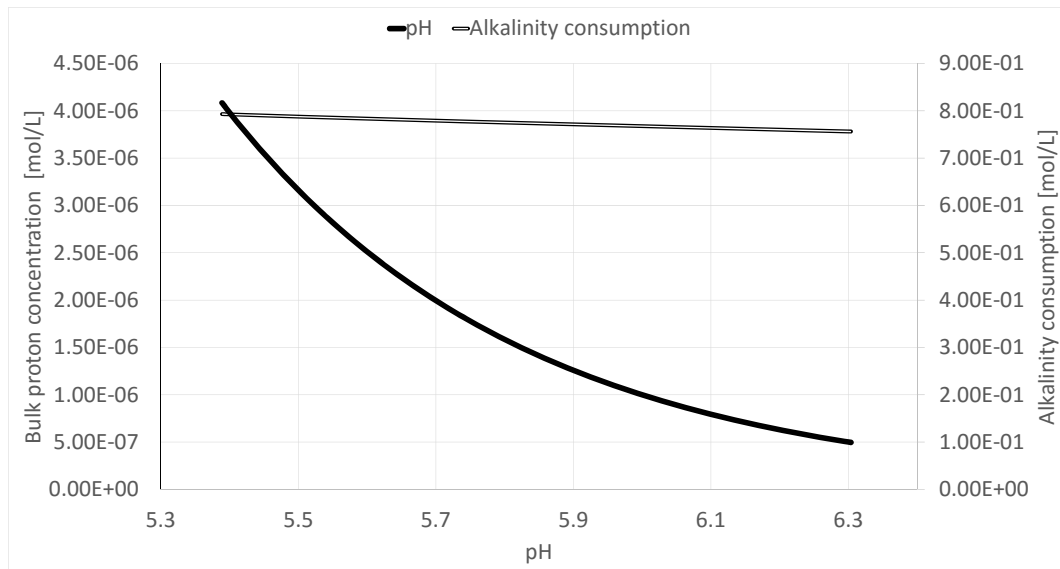


Figure B1: Alkalinity consumption by urine nitrification at different pH levels and proton concentration at different pH levels

These results were derived from a simulated urine nitrification batch process *Urine Nitrification Model V3.4*¹. The results show that the relation of proton production rate (PPR) measured in the slope of the pH signal and the alkalinity consumption can only be linearly approximated for a very limited pH range. It is safe to assume that most of the alkalinity consumption is caused by the AOB activity. Consequently, substantial pH changes, change the proportionality between PPR and alkalinity consumption and renders the resulting PPR2OUR signal useless to track the AOB activity within substantially wide pH ranges.

¹ This model has been developed at Eawag and is not published. We want to acknowledge Chris Brouckaert from the School of Chemical Engineering, University of KwaZulu-Natal, Durban, 4041, South Africa for providing a chemical speciation module for this model.

C Appendix Part II Chapter 3: Stabilizing nitrite control

This appendix is the printable part of the supplementary information of the following manuscript, submitted for publication:

Thürlimann, C.M., Udert, K.M., Morgenroth, E., Villez, K., Stabilizing control of a urine nitrification process in the presence of sensor drift.

C.1 Source-separated urine feed. Tank timeline, ammonium and chemical oxygen demand concentration.

Influent	Container number	Datum Urine	Tank filled	Date analysed	Date put in operation	Dilution	NH4 [mg NH4-N/L]	COD [mg COD/L]
Men's urine	T2_2401		24.01.2018	14.02.2018	22.02.2018	122.91	3'638	3'884
Men's urine	T3_2401		24.01.2018	14.02.2018	02.03.2018	126.86	3'653	2'778
Men's urine	T4_2401		24.01.2018	05.03.2018	09.03.2018	127.95	3'711	3'992
Men's urine	T3_0903		09.03.2018	26.03.2018	16.03.2018	130.33	3'558	3'728
Men's urine	T1_0903		09.03.2018	26.03.2018	26.03.2018	130.37	3'781	3'937
Men's urine	T2_0903		09.03.2018	06.04.2018	06.04.2018	127.28	3'908	NA
Men's urine	T4_0903		09.03.2018	16.04.2018	16.04.2018	126.74	3'637	3'105
Men's urine	T6		12.04.2018	26.04.2018	26.04.2018	128.27	3'463	2'976
Men's urine	Average						3'669	3'486
Men's urine	STD						135	514
Women's urine	T10(start)		30.04.2018	30.04.2018	04.05.2018	82.01	2'583	2'304
Women's urine	T10(end)		30.04.2018	30.04.2018	04.05.2018	81.86	2'513	2'145
Women's urine	T10.1		30.04.2018	30.04.2018	30.04.2018	82.25	2'574	2'147
Women's urine	T10.2		30.04.2018	30.04.2018	09.05.2018	83.44	2'562	2'094
Women's urine	T11(start)		30.04.2018	30.04.2018	14.05.2018	85.60	2'405	2'388
Women's urine	T11(end)		30.04.2018	30.04.2018	14.05.2018	84.28	2'655	2'014
Women's urine	Average						2'549	2'182
Women's urine	STD						84	139

D Appendix Part II Chapter 4: Ammonia aeration control

This appendix is the printable part of the supplementary information of the following journal publication: Thürlimann, C.M., Dürrenmatt, D.J., Villez, K., 2018 Soft-sensing with qualitative trend analysis for wastewater treatment plant control. *Control Engineering Practice* 70, 121–133.

D.1 Legal thresholds regarding nitrogen species

Ammonia concentration	< 1 mg N/L
Nitrite concentration (only a guideline value):	< 0.3 mg N/L
Nitrogen removal ratio $1 - \frac{\text{total kjeldahl nitrogen (raw wastewater)}}{\text{NH}_4^+\text{-N (outflow)}}$:	> 90%

D.2 Dissolved oxygen setpoints ARA Hard

Date	Advanced Control	Eco Setpoint R3/R4/R5	Normal Setpoint R3/R4/R5
		[mg O ₂ /L]	[mg O ₂ /L]
12.03.2014-28.04.2014	on	1.5/1.5/2.0	2.0/2.0/2.0
28.04.2014-19.05.2014	on	1.3/1.1/1.0	2.0/2.0/2.0
19.05.2014-22.05.2014	on	1.1/1.1/1.0	2.0/2.0/2.0
22.05.2014-23.05.2014	on	1.0/1.0/1.0	2.0/2.0/2.0
23.05.2014-02.06.2014	off	2.5/2.5/2.5	2.5/2.5/2.5
03.06.2014-08.06.2014	on	1.1/1.1/1.0	2.0/2.0/2.0
10.06.2014-12.06.2014	on	<1.1/<1.1/<1.0	2.0/2.0/2.0
13.06.2014-23.06.2014	on	1.1/1.1/1.0	2.0/2.0/2.0
23.06.2014-23.07.2014	off	2.0/2.0/2.0	2.0/2.0/2.0
23.07.2014-28.08.2014	on	1.3/1.1/1.0	2.0/2.0/2.0
28.08.2014-04.09.2014	on	1.2/1.1/1.0	2.0/2.0/2.0
04.09.2014-22.09.2014	off	2.0/2.0/2.0	2.0/2.0/2.0
22.09.2014-30.09.2014	on	1.2/1.1/1.0	2.0/2.0/2.0

D.3 Parameter set for rule-based control and QSE at the three tested plants

Parameters set WWTP Hard, Winterthur

Date / Rule	Minimal Difference EtN2	Maximal Difference NtE2	τ [min]	Control Time NtE3 [min]
12.03.2014	0.125	0.02	39	60
05.05.2014	0.125	0.04	39	60
07.05.2014	0.15	0.04	39	60
11.06.2014	0.15	0.07	39	60
06.08.2014	0.18	0.07	39	60

Parameters set WWTP PFA, Pfäffikon ZH

Rule / Date	Minimal Difference EtN2	Maximal Difference NtE2	τ [min]	Control Time NtE3 [min]
15.07.2014	0.15	0.1	39	60
16.07.2014	0.15	0.1	39	60
18.07.2014	0.15	0.125	39	60
20.07.2014	0.15	0.125	39	60
22.07.2014	0.15	0.125	39	60
19.08.2014	0.2	0.07	39	60
04.09.2014	0.13	0.04	39	60
07.09.2014	0.18	0.07	39	60

Parameters set WWTP PFU, Pfungen

Rule / Date	Minimal Difference EtN2	Maximal Difference NtE2	τ [min]	Control Time NtE3 [min]
05.05.2014	0.125	0.02	39	60
09.05.2014	0.125	0.04	39	60
06.08.2014	0.15	0.07	39	60

D.4 Summary of routine lab analysis and hydraulic loading during controller test periods (n=26) and during reference periods (n=15)

Controllor test periods (n=26)

Concentrations (volume proportional 24h composite samples)											
	NH4-N mg/L			NO2-N mg/L			CSB mg/L				
	Max	80% quantile	Average	Max	80% quantile	Average	Max	80% quantile	Average		
Eff. primary clarifier	31.9	25.6	20.9	N/A	N/A	N/A	308	258	215.7		
Eff. secondary clarifier	0.456	0.037	0.055	0.13	0.066	0.044	34.4	29.3	25.9		

Loads (volume proportional concentrations times hydraulic loading)											
	NH4-N kg/d			NO2-N kg/d			CSB kg/d			Hydraulics	
	Max	80% quantile	Average	Max	80% quantile	Average	Max	80% quantile	Average	Max	Average
Eff. primary clarifier	1343.9	1154.5	967.9	N/A	N/A	N/A	15639.2	11105	10120.2	N/A	58180
Eff. secondary clarifier	22.7	1.9	2.8	11.3	4	2.3	2229.4	1427.4	1281.2	N/A	N/A

Reference periods (n=15)

Concentrations (volume proportional 24h composite samples)											
NH4-N mg/L			NO2-N mg/L			CSB mg/L					
	Max	80% quantile	Average	Max	80% quantile	Average	Max	80% quantile	Average	Max	80% quantile
Eff. primary clarifier	33.4	26.48	20.78	N/A	N/A	N/A	271	226	193.1		
Eff. secondary clarifier	0.462	0.035	0.055	0.2	0.033	0.032	29.9	24.8	21.92		

Loads (volume proportional concentrations times hydraulic loading)											
NH4-N kg/d			NO2-N kg/d			CSB kg/d			Hydraulics Water m ³ /d		
	Max	80% quantile	Average	Max	80% quantile	Average	Max	80% quantile	Average	Max	80% quantile
Eff. primary clarifier	33.4	26.5	20.8	N/A	N/A	N/A	271	226	193.1	N/A	77176
Eff. secondary clarifier	9.4	2.5	2.6	4.8	3	1.8	2817.5	1860.1	1206.2	N/A	N/A

D.5 Additional figures

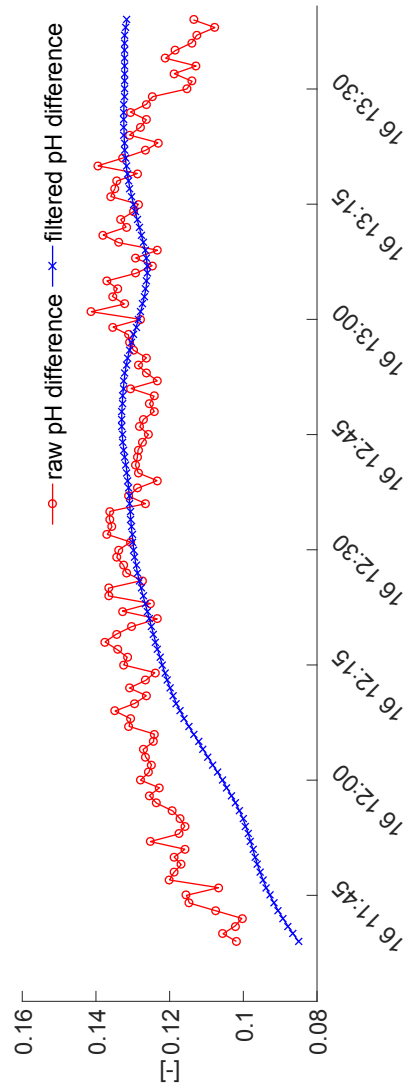


Figure A1: Raw pH difference filtered with the tri-cube kernel regression with $\tau = 39$ minutes (39 values considered in filter window).

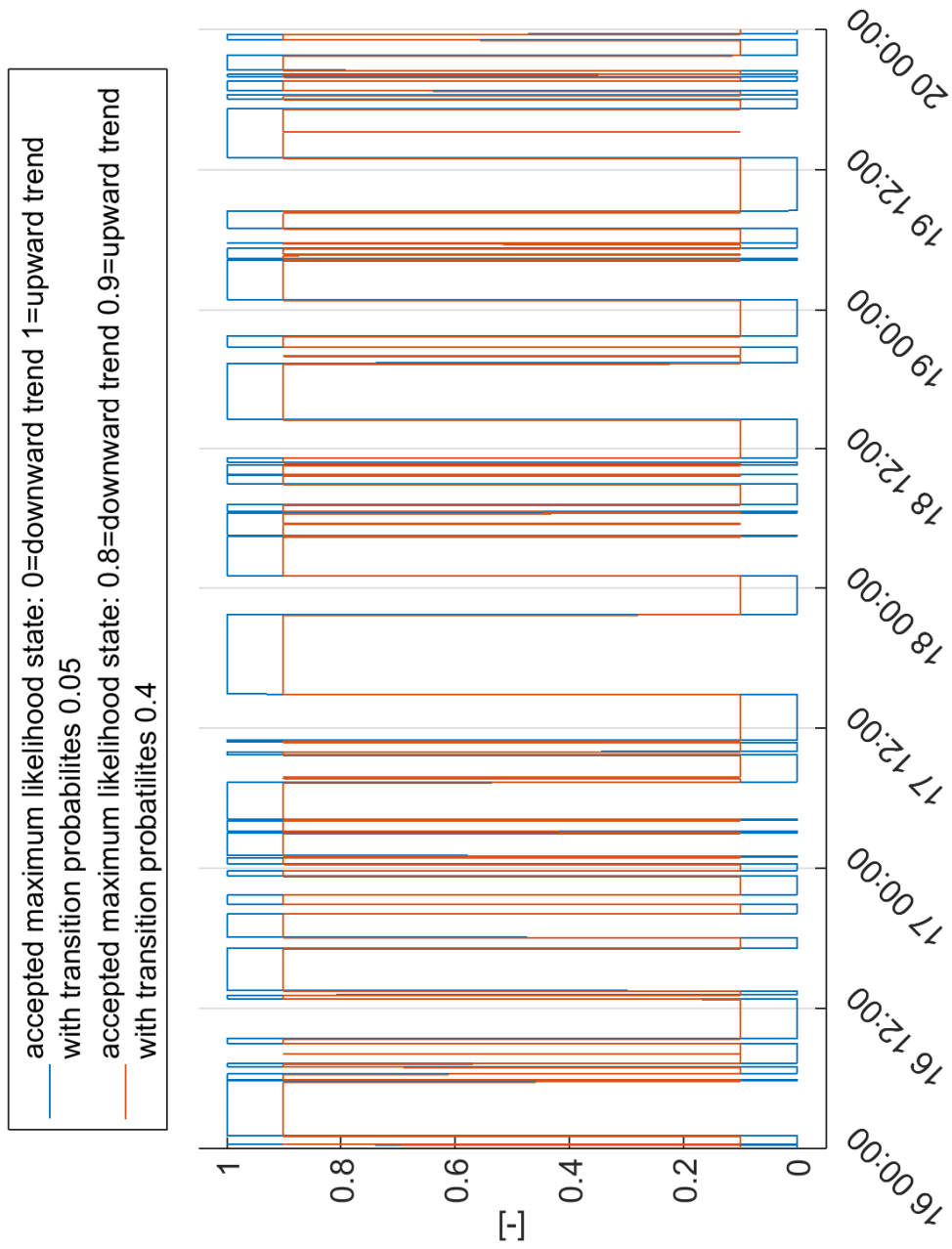


Figure A2: HMM model with same underlying signal but different transition probabilities.

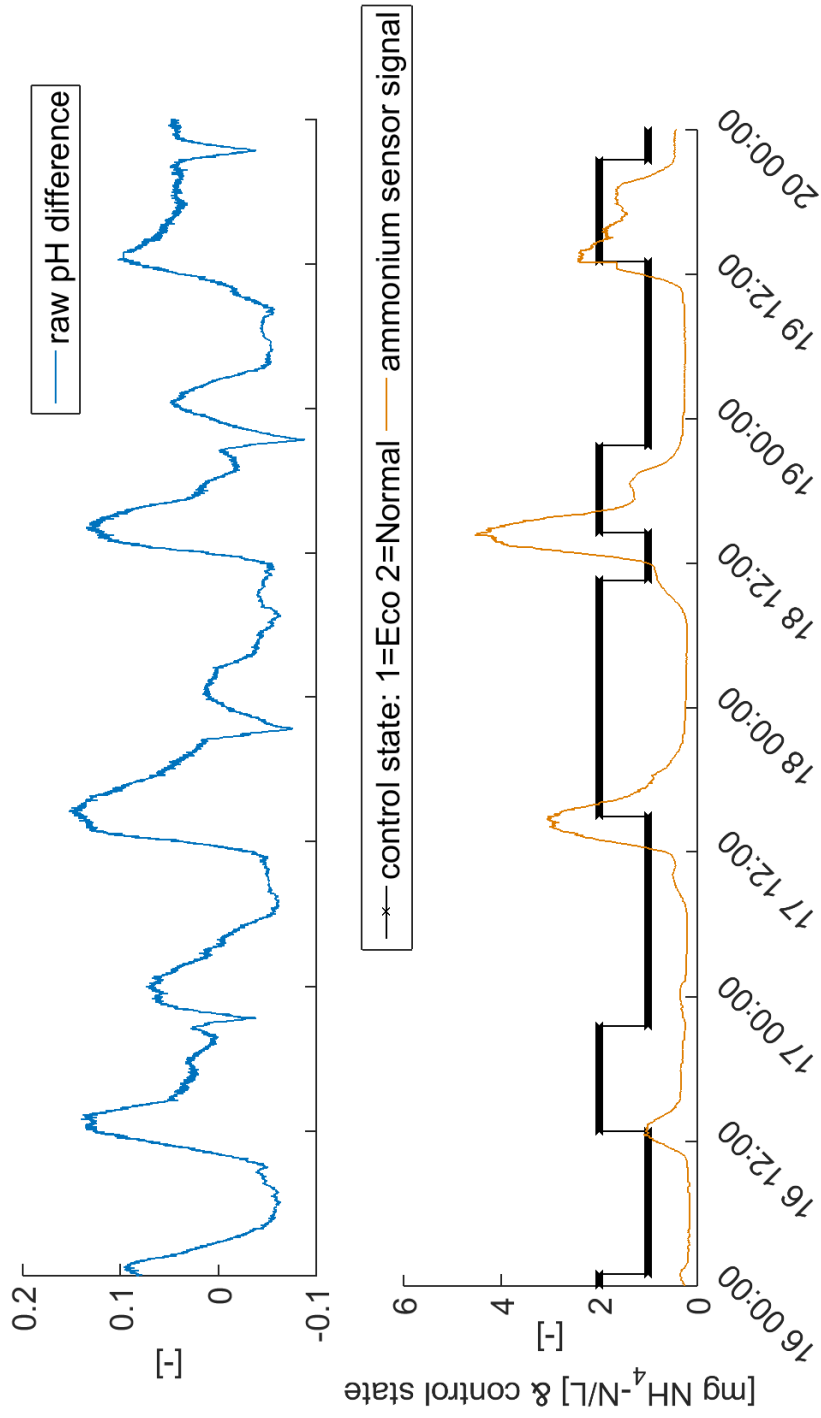


Figure A3: Same graph as Figure 9 with different HMM tuning (0.05 instead of 0.4 transition probability cf. Figure A2).

Part V

Bibliography

- Åmand, L., Olsson, G., Carlsson, B., 2013. Aeration control – a review. *Water Science and Technology* 67, 2374–2398. doi:10.2166/wst.2013.139.
- Åström, K.J., Murray, R.M., 2008. *Feedback Systems: An Introduction for Scientists and Engineers*. Princeton University Press, Princeton.
- Al-Ghusain, I., Hao, O.J., 1995. Use of pH as Control Parameter for Aerobic/Anoxic Sludge Digestion. *Journal of Environmental Engineering* 121, 225–235. doi:10.1061/(ASCE)0733-9372(1995)121:3(225).
- Andalib, M., Taher, E., Donohue, J., Ledwell, S., Andersen, M.H., Sangrey, K., 2018. Correlation between nitrous oxide (N₂O) emission and carbon to nitrogen (COD/N) ratio in denitrification process: A mitigation strategy to decrease greenhouse gas emission and cost of operation. *Water Science and Technology* 77, 426–438. doi:10.2166/wst.2017.558.
- Anderson, R.B., Morris, R.V., Clegg, S.M., Bell, J.F., Wiens, R.C., Humphries, S.D., Mertzman, S.A., Graff, T.G., McInroy, R., 2011. The influence of multivariate analysis methods and target grain size on the accuracy of remote quantitative chemical analysis of rocks using laser induced breakdown spectroscopy. *Icarus* 215, 608–627. doi:10.1016/j.icarus.2011.07.034.
- Andersson, L.G., 1980. Energy Savings at Wastewater Treatment Plants, in: Strub, A.S., Ehringer, H. (Eds.), *New Ways to Save Energy*. Springer Netherlands, Dordrecht, pp. 741–749.
- Aymerich, I., Rieger, L., Sobhani, R., Rosso, D., Corominas, L., 2015. The difference between energy consumption and energy cost: Modelling energy tariff structures for water resource recovery facilities. *Water Research* 81, 113–123. doi:10.1016/j.watres.2015.04.033.
- Baeza, J.A., Gabriel, D., Lafuente, J., 2002. In-line fast OUR (oxygen uptake rate) measurements for monitoring and control of WWTP. *Water Science and Technology* 45, 19–28. doi:10.2166/wst.2002.0541.
- Bakshi, B., Stephanopoulos, G., 1994. Representation of process trends—III. Multiscale extraction of trends from process data. *Computers and Chemical Engineering* 18, 267–302. doi:10.1016/0098-1354(94)85028-3.
- Battistoni, P., De Angelis, A., Boccadoro, R., Bolzonella, D., 2003. An Automatically Controlled Alternate Oxidic-Anoxic Process for Small Municipal Wastewater Treatment Plants. *Industrial and Engineering Chemistry Research* 42, 509–515. doi:10.1021/ie020376g.
- Benazzi, F., Gernaey, K., Jeppsson, U., Katebi, R., 2007. On-Line Estimation and Detection of Abnormal Substrate Concentrations in WWTPs Using a Software Sensor: A Benchmark Study. *Environmental Technology* 28, 871–882. doi:10.1080/09593332808618852.

- Berho, C., Pouet, M.F., Bayle, S., Azema, N., Thomas, O., 2004. Study of UV–vis responses of mineral suspensions in water. *Colloids and Surfaces A: Physicochemical and Engineering Aspects* 248, 9–16. doi:10.1016/j.colsurfa.2004.08.046.
- Blanke, M., Kinnaert, M., Lunze, J., Staroswiecki, M., 2016. *Diagnosis and Fault-Tolerant Control*. 3rd ed. 2016 ed., Springer Berlin Heidelberg, Berlin Heidelberg.
- Bocken, S.M., Braae, M., Dold, P.L., 1989. Dissolved Oxygen Control and Oxygen Utilization Rate Estimation: Extension of the Holmberg/Olsson Method. *Water Science and Technology* 21, 1197–1208. doi:10.2166/wst.1989.0319.
- Boiocchi, R., Mauricio-Iglesias, M., Vangsgaard, A.K., Gernaey, K.V., Sin, G., 2015. Aeration control by monitoring the microbiological activity using fuzzy logic diagnosis and control. Application to a complete autotrophic nitrogen removal reactor. *Journal of Process Control* 30, 22–33. doi:10.1016/j.jprocont.2014.10.011.
- Bunce, J.T., Ndam, E., Ofiteru, I.D., Moore, A., Graham, D.W., 2018. A Review of Phosphorus Removal Technologies and Their Applicability to Small-Scale Domestic Wastewater Treatment Systems. *Frontiers in Environmental Science* 6, 8–23. doi:10.3389/fenvs.2018.00008.
- Bürgmann, H., Jenni, S., Vazquez, F., Udert, K.M., 2011. Regime Shift and Microbial Dynamics in a Sequencing Batch Reactor for Nitrification and Anammox Treatment of Urine. *Applied and Environmental Microbiology* 77, 5897–5907. doi:10.1128/AEM.02986-10.
- Caniani, D., Caivano, M., Pascale, R., Bianco, G., Mancini, I., Masi, S., Mazzone, G., Firouzian, M., Rosso, D., 2019. CO₂ and N₂O from water resource recovery facilities: Evaluation of emissions from biological treatment, settling, disinfection, and receiving water body. *Science of the Total Environment* 648, 1130–1140. doi:10.1016/j.scitotenv.2018.08.150.
- Caradot, N., Sonnenberg, H., Rouault, P., Gruber, G., Hofer, T., Torres, A., Pesci, M., Bertrand-Krajewski, J.L., 2015. Influence of local calibration on the quality of online wet weather discharge monitoring: Feedback from five international case studies. *Water Science and Technology* 71, 45–51. doi:10.2166/wst.2014.465.
- Carlsson, B., Zambrano, J., 2016. Fault detection and isolation of sensors in aeration control systems. *Water Science and Technology* 73, 648–653. doi:10.2166/wst.2015.529.
- Carré, E., Pérot, J., Jauzein, V., Lin, L., Lopez-Ferber, M., 2017. Estimation of water quality by UV/Vis spectrometry in the framework of treated wastewater reuse. *Water Science and Technology* 76, 633–641. doi:10.2166/wst.2017.096.

- Cecconi, F., Reifsnnyder, S., Ito, Y., Jimenez, M., Sobhani, R., Rosso, D., 2019. ISE-ammonium sensors in WRRFs: Field assessment of their influencing factors. *Environmental Science: Water Research and Technology* doi:10.1039/C8EW00763B.
- Charbonnier, S., Gentil, S., 2007. A trend-based alarm system to improve patient monitoring in intensive care units. *Control Engineering Practice* 15, 1039–1050. doi:10.1016/j.conengprac.2006.12.005.
- Cheung, J.Y., Stephanopoulos, G., 1990. Representation of process trends-Part I. A formal representation framework. *Computers and Chemical Engineering* 14, 495–510. doi:10.1016/0098-1354(90)87023-I.
- Cornelissen, R., Van Dyck, T., Dries, J., Ockier, P., Smets, I., Van den Broeck, R., Van Hulle, S., Feyaerts, M., 2018. Application of online instrumentation in industrial wastewater treatment plants – a survey in Flanders, Belgium. *Water Science and Technology* 78, 957–967. doi:10.2166/wst.2018.375.
- Corominas, L., Garrido-Baserba, M., Villez, K., Olsson, G., Cortés, U., Poch, M., 2018. Transforming data into knowledge for improved wastewater treatment operation: A critical review of techniques. *Environmental Modelling and Software* 106, 89–103. doi:10.1016/j.envsoft.2017.11.023.
- Corominas, L., Villez, K., Aguado, D., Rieger, L., Rosén, C., Vanrolleghem, P.A., 2011. Performance evaluation of fault detection methods for wastewater treatment processes. *Biotechnology and Bioengineering* 108, 333–344. doi:10.1002/bit.22953.
- Crowley, K., O'Malley, E., Morrin, A., Smyth, M.R., Killard, A.J., 2008. An aqueous ammonia sensor based on an inkjet-printed polyaniline nanoparticle-modified electrode. *The Analyst* 133, 391. doi:10.1039/b716154a.
- Dash, S., Maurya, M.R., Venkatasubramanian, V., Rengaswamy, R., 2004. A novel interval-halving framework for automated identification of process trends. *AIChE Journal* 50, 149–162. doi:10.1002/aic.10014.
- Derlon, N., Thürlimann, C., Dürrenmatt, D., Villez, K., 2017. Batch settling curve registration via image data modeling. *Water Research* doi:10.1016/j.watres.2017.01.049.
- Diaz, R.J., Rosenberg, R., 2008. Spreading Dead Zones and Consequences for Marine Ecosystems. *Science* 321, 926–929. doi:10.1126/science.1156401.
- Dürrenmatt, D., Gujer, W., 2012. Data-driven modeling approaches to support wastewater treatment plant operation. *Environmental Modelling and Software* 30, 47–56. doi:10.1016/j.envsoft.2011.11.007.

- Dyar, M.D., Carmosino, M.L., Breves, E.A., Ozanne, M.V., Clegg, S.M., Wiens, R.C., 2012. Comparison of partial least squares and lasso regression techniques as applied to laser-induced breakdown spectroscopy of geological samples. *Spectrochimica Acta Part B: Atomic Spectroscopy* 70, 51–67. doi:10.1016/j.sab.2012.04.011.
- Ekama, G.A., 2010. The role and control of sludge age in biological nutrient removal activated sludge systems. *Water Science and Technology* 61, 1645–1652. doi:10.2166/wst.2010.972.
- Etheridge, J.R., Birgand, F., Osborne, J.A., Osburn, C.L., Burchell, M.R., Irving, J., 2014. Using in situ ultraviolet-visual spectroscopy to measure nitrogen, carbon, phosphorus, and suspended solids concentrations at a high frequency in a brackish tidal marsh. *Limnology and Oceanography: Methods* 12, 10–22. doi:10.4319/lom.2014.12.10.
- Etter, B., Tilley, E., Khadka, R., Udert, K.M., 2011. Low-cost struvite production using source-separated urine in Nepal. *Water Research* 45, 852–862. doi:10.1016/j.watres.2010.10.007.
- Feldbaum, A.A., 1960. Dual control theory I. *Automn Remote Control* 21, 874–880.
- Fowler, D., Coyle, M., Skiba, U., Sutton, M.A., Cape, J.N., Reis, S., Sheppard, L.J., Jenkins, A., Grizzetti, B., Galloway, J.N., Vitousek, P., Leach, A., Bouwman, A.F., Butterbach-Bahl, K., Dentener, F., Stevenson, D., Amann, M., Voss, M., 2013. The global nitrogen cycle in the twenty-first century. *Phil. Trans. R. Soc. B* 368, 20130164. doi:10.1098/rstb.2013.0164.
- Fu, J.M., Li, Y., Guo, J.L., 1998. Optical Behavior of Organic Pigments in Aqueous Dispersions and Its Application. *Journal of Colloid and Interface Science* 202, 450–455. doi:10.1006/jcis.1998.5464.
- Fumasoli, A., Etter, B., Sterkele, B., Morgenroth, E., Udert, K., 2016. Operating a pilot-scale nitrification/distillation plant for complete nutrient recovery from urine. *Water Science and Technology* 73, 215–222. doi:10.2166/wst.2015.485.
- Fumasoli, A., Morgenroth, E., Udert, K.M., 2015. Modeling the low pH limit of *Nitrosomonas eutropha* in high-strength nitrogen wastewaters. *Water Research* 83, 161–170. doi:10.1016/j.watres.2015.06.013.
- Fumasoli-Hug, A., 2016. Nitrification of Urine as Pretreatment for Nutrient Recovery. Doctoral Thesis. ETH Zurich. doi:10.3929/ethz-a-010612621.
- Graham, D.W., Knapp, C.W., Van Vleck, E.S., Bloor, K., Lane, T.B., Graham, C.E., 2007. Experimental demonstration of chaotic instability in biological nitrification. *The ISME Journal* 1, 385–393. doi:10.1038/ismej.2007.45.
- Gujer, W., 2008. *Systems Analysis for Water Technology*. Springer-Verlag, Berlin Heidelberg.

- Gujer, W., 2010. Nitrification and me – A subjective review. *Water Research* 44, 1–19. doi:10.1016/j.watres.2009.08.038.
- Gurden, S.P., Westerhuis, J.A., Bro, R., Smilde, A.K., 2001. A comparison of multiway regression and scaling methods. *Chemometrics and Intelligent Laboratory Systems* 59, 121–136. doi:10.1016/S0169-7439(01)00168-X.
- Haimi, H., Mulas, M., Corona, F., Vahala, R., 2013. Data-derived soft-sensors for biological wastewater treatment plants: An overview. *Environmental Modelling and Software* 47, 88–107. doi:10.1016/j.envsoft.2013.05.009.
- Hastie, T., Tibshirani, R., Friedman, J., 2009. *The Elements of Statistical Learning: Data Mining, Inference, and Prediction*, Second Edition. Springer Science & Business Media.
- Hellinga, C., Vanroileghem, P., van Loosdrecht, M.C.M., Heijnen, J.J., 1996. The potential of off-gas analyses for monitoring wastewater treatment plants. *Water Science and Technology* 33, 13–23. doi:10.1016/0273-1223(96)00155-2.
- Hernandez-Sancho, F., Sala-Garrido, R., 2008. Cost Modelling In Waste Water Treatment Processes: An Empirical Analysis For Spain, in: Hlavinek, P., Bonacci, O., Marsalek, D.J., Mahrikova, I. (Eds.), *Dangerous Pollutants (Xenobiotics) in Urban Water Cycle*. Springer Netherlands. NATO Science for Peace and Security Series, pp. 219–226.
- Höglund, C., 2001. Evaluation of Microbial Health Risks Associated with the Reuse of Source-Separated Human Urine. Phd Thesis. Tekniska högskolan i Stockholm. Stockholm.
- Ingildsen, P., 2002. Realising Full-Scale Control in Wastewater Treatment Systems Using in Situ Nutrient Sensors. Ph.D. thesis. Dept. of Industrial Electrical Engineering and Automation [Institutionen för industriell elektronik och automation], Univ.. Lund.
- ISO Central Secretary, 1994. Iso 5725:1994 accuracy (trueness and precision) of measurement methods and results.
- ISO Central Secretary, 2001. Iso 8466-2:2001 water quality - calibration and evaluation of analytical methods and estimation of performance characteristics - part 2: Calibration strategy for non-linear second-order calibration functions.
- Jaramillo, F., Orchard, M., Muñoz, C., Zamorano, M., Antileo, C., 2018. Advanced strategies to improve nitrification process in sequencing batch reactors - A review. *Journal of Environmental Management* 218, 154–164. doi:10.1016/j.jenvman.2018.04.019.

- Jiang, F., Chen, Y., Mackey, H.R., Chen, G.H., van Loosdrecht, M.C.M., 2011. Urine nitrification and sewer discharge to realize in-sewer denitrification to simplify sewage treatment in Hong Kong. *Water Science and Technology* 64, 618. doi:10.2166/wst.2011.491.
- Jin, R.C., Zhang, Q.Q., Yang, G.F., Xing, B.S., Ji, Y.X., Chen, H., 2013. Evaluating the recovery performance of the ANAMMOX process following inhibition by phenol and sulfide. *Bioresource Technology* 142, 162–170. doi:10.1016/j.biortech.2013.05.022.
- Jolliffe, I.T., Trendafilov, N.T., Uddin, M., 2003. A Modified Principal Component Technique Based on the LASSO. *Journal of Computational and Graphical Statistics* 12, 531–547. doi:10.1198/1061860032148.
- Joss, A., Derlon, N., Cyprien, C., Burger, S., Szivak, I., Traber, J., Siegrist, H., Morgenroth, E., 2011. Combined Nitritation–Anammox: Advances in Understanding Process Stability. *Environmental Science and Technology* 45, 9735–9742. doi:10.1021/es202181v.
- Joss, A., Salzgeber, D., Eugster, J., König, R., Rottermann, K., Burger, S., Fabijan, P., Leumann, S., Mohn, J., Siegrist, H., 2009. Full-Scale Nitrogen Removal from Digester Liquid with Partial Nitritation and Anammox in One SBR. *Environmental Science and Technology* 43, 5301–5306. doi:10.1021/es900107w.
- Kaelin, D., Rieger, L., Eugster, J., Rottermann, K., Bänninger, C., Siegrist, H., 2008. Potential of in-situ sensors with ion-selective electrodes for aeration control at wastewater treatment plants. *Water Science and Technology* 58, 629–637. doi:10.2166/wst.2008.433.
- Konstantinov, K.B., Yoshida, T., 1992. Real-time qualitative analysis of the temporal shapes of(bio) process variables. *AIChE Journal* 38, 1703–1715. doi:10.1002/aic.690381104.
- Kuipers, B., 1986. Qualitative simulation. *Artificial Intelligence* 29, 289–338. doi:10.1016/0004-3702(86)90073-1.
- Kuypers, M.M.M., Marchant, H.K., Kartal, B., 2018. The microbial nitrogen-cycling network. *Nature Reviews Microbiology* 16, 263–276. doi:10.1038/nrmicro.2018.9.
- Larsen, T., Broch, K., Andersen, M.R., 1998. First flush effects in an urban catchment area in Aalborg. *Water Science and Technology* 37, 251–257. doi:10.1016/S0273-1223(97)00776-2.
- Larsen, T.A., Gujer, W., 1996. Separate management of anthropogenic nutrient solutions (human urine). *Water Science and Technology* 34, 87–94. doi:10.1016/0273-1223(96)00560-4.
- Laureni, M., Falås, P., Robin, O., Wick, A., Weissbrodt, D., Nielsen, J., Ternes, T., Morgenroth, E., Joss, A., 2016. Mainstream partial nitritation and anammox: Long-term process stability and effluent quality at low temperatures. *Water Research* 101, 628–639. doi:10.1016/j.watres.2016.05.005.

- Laureni, M., Weissbrodt, D.G., Villez, K., Robin, O., de Jonge, N., Rosenthal, A., Wells, G., Nielsen, J.L., Morgenroth, E., Joss, A., 2018. Biomass segregation between biofilm and flocs improves the control of nitrite-oxidizing bacteria in mainstream partial nitrification and anammox processes. *bioRxiv* doi:10.1101/480780. [Preprint WWW Document].
- Lepot, M., Torres, A., Hofer, T., Caradot, N., Gruber, G., Aubin, J.B., Bertrand-Krajewski, J.L., 2016. Calibration of UV/Vis spectrophotometers: A review and comparison of different methods to estimate TSS and total and dissolved COD concentrations in sewers, WWTPs and rivers. *Water Research* 101, 519–534. doi:10.1016/j.watres.2016.05.070.
- Liu, S.J., Krstic, M., 2012. Stochastic Averaging and Stochastic Extremum Seeking. *Communications and Control Engineering*, Springer-Verlag, London.
- Lofrano, G., Brown, J., 2010. Wastewater management through the ages: A history of mankind. *Science of The Total Environment* 408, 5254–5264. doi:10.1016/j.scitotenv.2010.07.062.
- van Loosdrecht, M.C.M., Nielsen, P.H., Lopez-Vazquez, C.M., Brdjanovic, D. (Eds.), 2016. *Experimental Methods in Wastewater Treatment*. IWA Publishing, London.
- Lotti, T., van der Star, W.R.L., Kleerebezem, R., Lubello, C., van Loosdrecht, M.C.M., 2012. The effect of nitrite inhibition on the anammox process. *Water Research* 46, 2559–2569. doi:10.1016/j.watres.2012.02.011.
- Luttmann, R., Bracewell, D.G., Cornelissen, G., Gernaey, K.V., Glassey, J., Hass, V.C., Kaiser, C., Preusse, C., Striedner, G., Mandenius, C.F., 2012. Soft sensors in bioprocessing: A status report and recommendations. *Biotechnology Journal* 7, 1040–1048. doi:10.1002/biot.201100506.
- Martins, A.M.P., Heijnen, J.J., van Loosdrecht, M.C.M., 2003. Effect of dissolved oxygen concentration on sludge settleability. *Applied Microbiology and Biotechnology* 62, 586–593. doi:10.1007/s00253-003-1384-6.
- Mašić, A., Santos, A.T., Etter, B., Udert, K.M., Villez, K., 2015. Estimation of nitrite in source-separated nitrified urine with UV spectrophotometry. *Water Research* 85, 244–254. doi:10.1016/j.watres.2015.08.031.
- Mašić, A., Srinivasan, S., Billeter, J., Bonvin, D., Villez, K., 2017. Shape constrained splines as transparent black-box models for bioprocess modeling. *Computers and Chemical Engineering* 99, 96–105. doi:10.1016/j.compchemeng.2016.12.017.

- Mašić, A., Villez, K., 2014. Model-based observers for monitoring of a biological nitrification process for decentralized wastewater treatment - Initial results., in: 2nd IWA Specialized International Conference "Ecotechnologies for Wastewater Treatment" (EcoSTP2014), Verona, Italy. pp. 396–399.
- Maurya, M.R., Rengaswamy, R., Venkatasubramanian, V., 2007. Fault diagnosis using dynamic trend analysis: A review and recent developments. *Engineering Applications of Artificial Intelligence* 20, 133–146. doi:10.1016/j.engappai.2006.06.020.
- Mears, L., Nørregård, R., Sin, G., Gernaey, K.V., Stocks, S.M., Albaek, M.O., Villez, K., 2016. Functional unfold principal component regression methodology for analysis of industrial batch process data. *AIChE Journal* 62, 1986–1994. doi:10.1002/aic.15172.
- Mulder, A., 2003. The quest for sustainable nitrogen removal technologies. *Water Science and Technology* 48, 67–75. doi:10.2166/wst.2003.0018.
- Ohmura, K., Thürlimann, C.M., Kipf, M., Carbajal, J.P., Villez, K., 2018. Characterizing Long-term Wear and Tear of Ion-Selective pH Sensors. doi:10.31224/osf.io/mv6tz. [Preprint WWW Document].
- Olsson, G., 2012. ICA and me – A subjective review. *Water Research* 46, 1585–1624. doi:10.1016/j.watres.2011.12.054.
- Olsson, G., Andrews, J., 1978. The dissolved oxygen profile-A valuable tool for control of the activated sludge process. *Water Research* 12, 985–1004. doi:10.1016/0043-1354(78)90082-9.
- Olsson, G., Nielsen, M., Yuan, Z., Lynggaard-Jensen, A., Steyer, J.P., 2005. Instrumentation, Control and Automation in Wastewater Systems. Scientific and Technical Report No. 15, IWA Publishing.
- Park, C.W., Yoon, K.Y., Byeon, J.H., Kim, K., Hwang, J., 2012. Development of rapid assessment method to determine bacterial viability based on ultraviolet and visible (UV-Vis) spectroscopy analysis including application to bioaerosols. *Aerosol and Air Quality Research* 12, 395–404. doi:10.4209/aaqr.2011.08.0129.
- Park, S., Bae, W., 2009. Modeling kinetics of ammonium oxidation and nitrite oxidation under simultaneous inhibition by free ammonia and free nitrous acid. *Process Biochemistry* 44, 631–640. doi:10.1016/j.procbio.2009.02.002.
- Park, S., Bae, W., Chung, J., Baek, S.C., 2007. Empirical model of the pH dependence of the maximum specific nitrification rate. *Process Biochemistry* 42, 1671–1676. doi:10.1016/j.procbio.2007.09.010.
- Peng, Y.Z., Gao, J.F., Wang, S.Y., Sui, M.H., 2002. Use pH and ORP as fuzzy control parameters of denitrification in SBR process. *Water Science and Technology* 46, 131–137.

- Petri, M., 2006. Water Quality of Lake Constance, in: Knepper, T.P. (Ed.), *The Rhine*. Springer, Berlin, Heidelberg. *The Handbook of Environmental Chemistry*, pp. 127–138. doi:10.1007/698_5_018.
- Pochana, K., Keller, J., 1999. Study of factors affecting simultaneous nitrification and denitrification (SND). *Water Science and Technology* 39, 61–68. doi:10.1016/S0273-1223(99)00123-7.
- Randall, D.G., Krähenbühl, M., Köpping, I., Larsen, T.A., Udert, K.M., 2016. A novel approach for stabilizing fresh urine by calcium hydroxide addition. *Water Research* 95, 361–369. doi:10.1016/j.watres.2016.03.007.
- Rawlings, J.B., Mayne, D.Q., 2009. *Model Predictive Control Theory and Design*. Nob Hill Publishing, LLC, Madison, Wisconsin.
- Rengaswamy, R., Venkatasubramanian, V., 1995. A syntactic pattern-recognition approach for process monitoring and fault diagnosis. *Engineering Applications of Artificial Intelligence* 8, 35–51. doi:10.1016/0952-1976(94)00058-U.
- Rieger, L., Jones, R.M., Dold, P.L., Bott, C.B., 2014. Ammonia-Based Feedforward and Feedback Aeration Control in Activated Sludge Processes. *Water Environment Research* 86, 63–73. doi:10.2175/106143013X13596524516987.
- Rieger, L., Langergraber, G., Thomann, M., Fleischmann, N., Siegrist, H., 2004. Spectral in-situ analysis of NO₂, NO₃, COD, DOC and TSS in the effluent of a WWTP. *Water Science and Technology* 50, 143–152. doi:10.2166/wst.2004.0682.
- Rosen, C., Jeppsson, U., Rieger, L., Vanrolleghem, P.A., 2008. Adding realism to simulated sensors and actuators. *Water Science and Technology* 57, 337–344. doi:10.2166/wst.2008.130.
- Rosen, C., Lennox, J.A., 2001. Multivariate and multiscale monitoring of wastewater treatment operation. *Water Research* 35, 3402–3410. doi:10.1016/S0043-1354(01)00069-0.
- Rosso, D., Stenstrom, M.K., Larson, L.E., 2008. Aeration of large-scale municipal wastewater treatment plants: State of the art. *Water Science and Technology* 57, 973–978. doi:10.2166/wst.2008.218.
- Ruano, M., Ribes, J., Seco, A., Ferrer, J., 2009. Low cost-sensors as a real alternative to on-line nitrogen analysers in continuous systems. *Water Science and Technology* 60, 3261–3268. doi:10.2166/wst.2009.607.
- Ruano, M., Ribes, J., Seco, A., Ferrer, J., 2012. An advanced control strategy for biological nutrient removal in continuous systems based on pH and ORP sensors. *Chemical Engineering Journal* 183, 212–221. doi:10.1016/j.cej.2011.12.064.

- Samuelsson, O., Björk, A., Zambrano, J., Carlsson, B., 2018. Fault signatures and bias progression in dissolved oxygen sensors. *Water Science and Technology* 78, 1034–1044. doi:10.2166/wst.2018.350.
- Scali, C., Ghelardoni, C., 2008. An improved qualitative shape analysis technique for automatic detection of valve stiction in flow control loops. *Control Engineering Practice* 16, 1501–1508. doi:10.1016/j.conengprac.2008.04.009.
- Siegrist, H., Salzgeber, D., Eugster, J., Joss, A., 2008. Anammox brings WWTP closer to energy autarky due to increased biogas production and reduced aeration energy for N-removal. *Water Science and Technology* 57, 383. doi:10.2166/wst.2008.048.
- Spanjers, H., Vanrolleghem, P., 1995. Respirometry as a tool for rapid characterization of wastewater and activated sludge. *Water Science and Technology* 31, 105–114. doi:10.1016/0273-1223(95)00184-0.
- Spinelli, S., Gonzalez, S., Thomas, O., 2007. UV Spectra Library, in: Thomas, O., Burgess, C. (Eds.), *UV-Visible Spectrophotometry of Water and Wastewater*. Elsevier, Oxford, pp. 267–356.
- Steyer, J.P., Bernard, O., Batstone, D.J., Angelidaki, I., 2006. Lessons learnt from 15 years of ICA in anaerobic digesters. *Water Science and Technology* 53, 25–33. doi:10.2166/wst.2006.107.
- Steyer, J.P., Buffière, P., Rolland, D., Moletta, R., 1999. Advanced control of anaerobic digestion processes through disturbances monitoring. *Water Research* 33, 2059–2068. doi:10.1016/S0043-1354(98)00430-8.
- Strous, M., Van Gerven, E., Zheng, P., Kuenen, J.G., Jetten, M.S.M., 1997. Ammonium removal from concentrated waste streams with the anaerobic ammonium oxidation (Anammox) process in different reactor configurations. *Water Research* 31, 1955–1962. doi:10.1016/S0043-1354(97)00055-9.
- Sun, F.Y., Dong, W.Y., Shao, M.F., Li, J., Peng, L.Y., 2012. Stabilization of source-separated urine by biological nitrification process: Treatment performance and nitrite accumulation. *Water Science and Technology* 66, 1491–1497. doi:10.2166/wst.2012.337.
- Sutherland-Stacey, L., Corrie, S., Neethling, A., Johnson, I., Gutierrez, O., Dexter, R., Yuan, Z., Keller, J., Hamilton, G., 2008. Continuous measurement of dissolved sulfide in sewer systems. *Water Science and Technology* 57, 375. doi:10.2166/wst.2008.132.
- Thomann, M., Rieger, L., Frommhold, S., Siegrist, H., Gujer, W., 2002. An efficient monitoring concept with control charts for on-line sensors. *Water Science and Technology* 46, 107–116. doi:10.2166/wst.2002.0563.

- Thomas, M.F., Azema, N., Thomas, O., 2017. Chapter 6 - Physical and Aggregate Properties, in: UV-Visible Spectrophotometry of Water and Wastewater (Second Edition). Elsevier, pp. 201–224. doi:10.1016/B978-0-444-63897-7.00006-8.
- Thomas, O., Burgess, C. (Eds.), 2017. UV-Visible Spectrophotometry of Water and Wastewater. Second edition ed., Elsevier, Amsterdam, Netherlands.
- Thürlimann, C.M., Dürrenmatt, D.J., Villez, K., 2018a. Soft-sensing with qualitative trend analysis for wastewater treatment plant control. *Control Engineering Practice* 70, 121–133. doi:10.1016/j.conengprac.2017.09.015.
- Thürlimann, C.M., Udert, K.M., Morgenroth, E., Villez, K., 2017. Qualitative control for stable and efficient urine nitrification, in: 12th IWA Specialized Conference on Instrumentation, Control and Automation (ICA2017), Quebec City, QC, Canada. pp. 287–290.
- Thürlimann, C.M., Udert, K.M., Morgenroth, E., Villez, K., 2018b. Comparison of four methods to obtain calibration data for online nitrite estimation by means of in-line UV-Vis spectrophotometry Submitted.
- Tibshirani, R., 1996. Regression Shrinkage and Selection via the Lasso. *Journal of the Royal Statistical Society. Series B (Methodological)* 58, 267–288.
- Trollberg, O., Carlsson, B., Jacobsen, E.W., 2014. Extremum seeking control of the CANON process—Existence of multiple stationary solutions. *Journal of Process Control* 24, 348–356. doi:10.1016/j.jprocont.2013.11.007.
- Udert, K.M., 2002. The Fate of Nitrogen and Phosphorus in Source-Separated Urine. Ph.D. thesis. ETH Zurich. doi:10.3929/ethz-a-004541820.
- Udert, K.M., Buckley, C.A., Wächter, M., McArdell, C.S., Kohn, T., Strande, L., Zöllig, H., Hug, A., Oberson, A., Etter, B., 2014. Technologies for the treatment of source-separated urine in eThekwini. *Water SA -WISA 2014 - Water Innovations Special Edition* 41, 212–221.
- Udert, K.M., Fux, C., Münster, M., Larsen, T.A., Siegrist, H., Gujer, W., 2003. Nitrification and autotrophic denitrification of source-separated urine. *Water Science and Technology* 48, 119–130. doi:10.2166/wst.2003.0031.
- Udert, K.M., Wächter, M., 2012. Complete nutrient recovery from source-separated urine by nitrification and distillation. *Water Research* 46, 453–464. doi:10.1016/j.watres.2011.11.020.
- Van Hulle, S.W.V., Volcke, E.I., Teruel, J.L., Donckels, B., van Loosdrecht, M.C., Vanrolleghem, P.A., 2007. Influence of temperature and pH on the kinetics of the Sharon nitritation process. *Journal of Chemical Technology and Biotechnology* 82, 471–480. doi:10.1002/jctb.1692.

- Vanrolleghem, P., Lee, D., 2003. On-line monitoring equipment for wastewater treatment processes: State of the art. *Water Science and Technology* 47, 1–34. doi:10.2166/wst.2003.0074.
- Venkatasubramanian, V., Rengaswamy, R., Yin, K., Kavuri, S.N., 2003. A review of process fault detection and diagnosis: Part I: Quantitative model-based methods. *Computers and Chemical engineering* 27, 293–311. doi:10.1016/S0098-1354(02)00160-6.
- Villez, K., 2015. Qualitative path estimation: A fast and reliable algorithm for qualitative trend analysis. *AIChE Journal* 61, 1535–1546. doi:10.1002/aic.14736.
- Villez, K., Billeter, J., Bonvin, D., 2019. Incremental parameter estimation under rank-deficient measurement conditions. *Processes* 7. doi:10.3390/pr7020075.
- Villez, K., Habermacher, J., 2016. Shape anomaly detection for process monitoring of a sequencing batch reactor. *Computers and Chemical Engineering* 91, 365–379. doi:10.1016/j.compchemeng.2016.04.012.
- Villez, K., Rengaswamy, R., 2013. A generative approach to qualitative trend analysis for batch process fault diagnosis, in: *European Control Conference, Zurich*. pp. 1958 – 1963.
- Villez, K., Rosén, C., Anctil, F., Duchesne, C., Vanrolleghem, P.A., 2008. Qualitative representation of trends: An alternative approach to process diagnosis and control. *Water Science and Technology* 57, 1525. doi:10.2166/wst.2008.141.
- Villez, K., Rosén, C., Anctil, F., Duchesne, C., Vanrolleghem, P.A., 2013. Qualitative Representation of Trends (QRT): Extended method for identification of consecutive inflection points. *Computers and Chemical Engineering* 48, 187–199. doi:10.1016/j.compchemeng.2012.08.010.
- Villez, K., Rosén, C., D’hooge, E., Vanrolleghem, P.A., 2010. Online Phase Length Optimization for a Sequencing Batch Reactor by Means of the Hotelling’s T^2 Statistic. *Industrial and Engineering Chemistry Research* 49, 180–188. doi:10.1021/ie801907n.
- Villez, K., Vanrolleghem, P.A., Corominas, L., 2016. Optimal flow sensor placement on wastewater treatment plants. *Water Research* 101, 75 – 83. doi:10.1016/j.watres.2016.05.068.
- Viterbi, A., 1967. Error bounds for convolutional codes and an asymptotically optimum decoding algorithm. *IEEE Transactions on Information Theory* 13, 260–269. doi:10.1109/TIT.1967.1054010.
- Wagner, M., Loy, A., Nogueira, R., Purkhold, U., Lee, N., Daims, H., 2002. Microbial community composition and function in wastewater treatment plants. *Antonie van Leeuwenhoek* 81, 665–680. doi:10.1023/A:1020586312170.

- Wang, Q., Ye, L., Jiang, G., Hu, S., Yuan, Z., 2014. Side-stream sludge treatment using free nitrous acid selectively eliminates nitrite oxidizing bacteria and achieves the nitrite pathway. *Water Research* 55, 245–255. doi:10.1016/j.watres.2014.02.029.
- Wentzell, P.D., Andrews, D.T., Hamilton, D.C., Faber, K., Kowalski, B.R., 1997. Maximum likelihood principal component analysis. *Journal of Chemometrics* 11, 339–366. doi:10.1002/(SICI)1099-128X(199707)11:4<339::AID-CEM476>3.0.CO;2-L.
- Wett, B., Hell, M., Nyhuis, G., Puempel, T., Takacs, I., Murthy, S., 2010. Syntrophy of aerobic and anaerobic ammonia oxidisers. *Water Science and Technology* 61, 1915–1922. doi:10.2166/wst.2010.969.
- Wilsenach, J.A., van Bragt, W.P.M., de Been, P., van Loosdrecht, M.C.M., 2005. Evaluation of separate urine collection and treatment to augment existing wastewater treatment works. *Water Science and Technology* 52, 71–80. doi:10.2166/wst.2005.0089.
- Winkler, S., Rieger, L., Saracevic, E., Pressl, A., Gruber, G., 2004. Application of ion-sensitive sensors in water quality monitoring. *Water Science and Technology* 50, 105–114. doi:10.2166/wst.2004.0678.
- Won, S.G., Ra, C.S., 2011. Biological nitrogen removal with a real-time control strategy using moving slope changes of pH(mV)- and ORP-time profiles. *Water Research* 45, 171–178. doi:10.1016/j.watres.2010.08.030.
- Wunderlin, P., Mohn, J., Joss, A., Emmenegger, L., Siegrist, H., 2012. Mechanisms of N₂O production in biological wastewater treatment under nitrifying and denitrifying conditions. *Water Research* 46, 1027–1037. doi:10.1016/j.watres.2011.11.080.
- Wunderlin, P., Siegrist, H., Joss, A., 2013. Online N₂O Measurement: The Next Standard for Controlling Biological Ammonia Oxidation? *Environmental Science and Technology* 47, 9567–9568. doi:10.1021/es402971p.
- Zanetti, L., Frison, N., Nota, E., Tomizioli, M., Bolzonella, D., Fatone, F., 2012. Progress in real-time control applied to biological nitrogen removal from wastewater. A short-review. *Desalination* 286, 1–7. doi:10.1016/j.desal.2011.11.056.
- Zeng, R.J., Lemaire, R., Yuan, Z., Keller, J., 2004. A novel wastewater treatment process: Simultaneous nitrification, denitrification and phosphorus removal. *Water Science and Technology* 50, 163–170. doi:10.2166/wst.2004.0635.
- Zhou, Y., Oehmen, A., Lim, M., Vadivelu, V., Ng, W.J., 2011. The role of nitrite and free nitrous acid (FNA) in wastewater treatment plants. *Water Research* 45, 4672–4682. doi:10.1016/j.watres.2011.06.025.

Zou, H., Hastie, T., Tibshirani, R., 2006. Sparse Principal Component Analysis. *Journal of Computational and Graphical Statistics* 15, 265–286. doi:10.1198/106186006X113430.

Part VI

Curriculum Vitae

Curriculum Vitae

Personal details

Name: Christian Marc Thürlimann
Date of Birth: January, 24 1987
Place of Birth: Zürich, Switzerland
Nationality: Swiss

Education

01/2015 – 04/2019 Doctoral Student at Institute for Environmental Engineering, Swiss Federal Institute of Technology (ETH) Zurich, Switzerland and Department of Process Engineering, Swiss Federal Institute of Aquatic Science and Technology (Eawag) Dübendorf, Switzerland
Supervisors: Prof. Dr. Eberhard Morgenroth and Dr. Kris Villez

09/2010 – 08/2012 Master of Science ETH in Environmental Engineering
Swiss Federal Institute of Technology (ETH) Zurich, Switzerland

10/2006 – 09/2009 Bachelor of Science ETH in Environmental Science
Swiss Federal Institute of Technology (ETH) Zurich, Switzerland

08/2001 – 08/2005 Swiss Matura with Focus Chemistry and Biology
Kantonsschule am Burggraben, St. Gallen, Switzerland